POLITECNICO DI MILANO
ENERGY DEPARTMENT
DOCTORAL PROGRAMME IN ELECTRICAL ENGINEERING, XXIX-CYCLE

OPTIMAL PLANNING OF ENERGY STORAGE SYSTEMS CONSIDERING UNCERTAINTY

Doctoral Dissertation of:
Nhi Thi Ai Nguyen

Supervisor:
Prof. Alberto Berizzi

Tutor:
Prof. Cristian Bovo

The Chair of the Doctoral Program:
Prof. Gabriele D'Antona

2016 – XXIX

Abstract

Renewable energy has been increasingly integrated into power systems as a result of the effort to reduce CO_2 emissions and build a future power grid economically feasible and environmentally sustainable. Particularly, according to the Blue Map scenario for power supply, electricity generation from renewable energy provides a share of 22% of global electricity generation in 2050, which grows almost threefold compared to the Baseline scenario [1]. Along with this growing share of renewable technologies, greater interest has been attracted to the use of Energy Storage Systems (ESSs) due to the variable nature of most renewable energy sources. ESSs can accommodate renewable generation in time-shifting its energy to match demand and avoid power curtailment. They can also be used to mitigate transmission congestion and hedge forecast errors, etc. In this context, appropriate siting and sizing of storage systems is of importance not only for power system operation but also for economic consideration. The integration of wind energy into power systems creates challenges for system planning concerning the variable and uncertain nature of wind. Deterministic approaches can not explicitly capture this uncertainty source, hence can not provide the right decision. In this work, the planning problem of ESSs under uncertainty is investigated.

Two approaches, namely combined Genetic Algorithm (GA) and cumulant-based probabilistic approach and two-stage stochastic approach, for incorporating wind and load uncertainty into ESS planning problems are proposed. In the first approach, optimal siting and sizing of ESSs is carried out based on a 2-step algorithm: first, ESS locations and expected value of ESS capacities are determined based on the combined GA and deterministic Optimal Power Flow (OPF) model; then in the second step, probabilistic assessment is performed on the obtained ESS locations and capacities. In the second approach, a two-stage stochastic OPF model is formulated with the goal of minimizing ESS capital cost in the first stage and system operational cost in the second stage. A multi-period AC OPF model is adopted for both approaches. The full AC OPF model can capture realistic physical power flows of the system better than a DC OPF; it is also more accurate and reliable when issues such as congestion and voltage

constraints are concerned. Also, the multi-period formulation can explicitly take into account inter-temporal constraints relevant to the storage devices.

A methodology to identify candidate ESS locations is also proposed. The best candidate locations for ESSs is determined based on the Lagrangian multipliers, a byproduct of the OPF. A sensitivity analysis is performed, using this methodology, to assess the impacts of ESS locations on system operation parameters such as production cost, wind curtailment and marginal prices. In this case, two applications of the ESSs are considered, including time-shifting wind generation and mitigating transmission congestion.

A final procedure for optimal siting and sizing of ESSs under uncertainty is then proposed. The first and necessary step in this procedure is preliminarily identifying candidate ESS locations. This helps reduce system size and make the planning problems tractable. Then, either the combined GA and Probabilistic Optimal Power Flow (POPF) approach or two-stage stochastic programming approach can be adopted for optimal planning of the ESSs considering wind and load uncertainties. Applicability of this procedure is demonstrated with a case study and a complete comparison on solutions of the combined GA and cumulant-based POPF approach and the two-stage stochastic programming approach is provided.

Acknowledgements

First and foremost I would like to express my sincerest gratitude and appreciation to my supervisor, Prof. Alberto Berizzi, for the continuous guidance and support, for his kindness, patience, motivation, immense knowledge and understanding throughout the whole PhD study.

Special thanks go to my tutor, Prof. Cristian Bovo, for his advices, enthusiasm and insightful discussions during my study.

I also wish to thank my friends and colleagues at the Electrical Engineering section of the Department of Energy, Politecnico di Milano for their support along the journey and for making the working environment more enjoyable.

Last but not least, from the bottom of my heart I wish to thank my family for their endless love and encouragement. Special thanks to my husband and my little newborn daughter for their faithful support and understanding during my last year PhD.

Contents

List of Figures

List of Tables

List of Acronyms

BES	:	Battery Energy Storage
CAES	:	Compressed Air Energy Storage
CDF	:	Cumulative Distribution Function
ESS	:	Energy Storage System
FES	:	Flywheel Energy Storage
GA	:	Genetic Algorithm
LMP	:	Locational Marginal Price
NiCd	:	Nickel-Cadmium
OPF	:	Optimal Power Flow
PCA	:	Principal Component Analysis
PDF	:	Probability Density Function
POPF	:	Probabilistic Optimal Power Flow
PHS	:	Pumped Hydroelectric Storage
PCS	:	Power Conversion System
RES	:	Renewable Energy Sources
SMES	:	Superconducting Magnetic Energy Storage
SP	:	Stochastic Programming
TES	:	Thermal Energy Storage

Notation

θ_i^t	:	Voltage angle of bus *i* in period *t*
θ_k^t	:	Voltage angle of bus *k* in period *t*
η_{ch_i}	:	Charging efficiency of ESS at bus *i*
η_{d_i}	:	Discharging efficiency of ESS at bus *i*
λp_i^t	:	Lagrangian multiplier associated to the real power flow equation at bus *i* in period *t*
nb	:	Total number of system buses
ng	:	Total number of generating units
ns	:	Total number of ESSs
B_{ik}	:	Imaginary part of the ik^{th} element of the bus admittance matrix
G_{ik}	:	Real part of the ik^{th} element of the bus admittance matrix
B_i^0	:	Initial energy level of the ESS at bus *i*
B_i^t	:	Energy level of ESS at bus *i* in hour *t*
B_i^{min}	:	Lower limit of energy level of ESS at bus *i*
B_i^{max}	:	Upper limit of energy level of ESS at bus *i*
I_{ij}^t	:	Magnitude of the current flowing from bus *i* to bus *j*
I_{ji}^t	:	Magnitude of the current flowing from bus *j* to bus *i*
I_{ij}^{max}	:	Upper limit of current flow from bus *i* to bus *j*
I_{ji}^{max}	:	Upper limit of current flow from bus *j* to bus *i*
PC^t	:	Production cost at period *t*
$P_{ch_i}^t$	:	Real charging power of ESS at bus *i* in hour *t*
$P_{ch_i}^{min}$	:	Lower limit of charging power of ESS at bus *i*
$P_{ch_i}^{max}$	:	Upper limit of charging power of ESS at bus *i*
$P_{d_i}^t$	:	Real discharging power of ESS at bus *i* in hour *t*
$P_{d_i}^{min}$	:	Lower limit of discharging power of ESS at bus *i*
$P_{d_i}^{max}$	:	Upper limit of discharging power of ESS at bus *i*
$P_{G_i}^t$	:	Real generation power at bus *i* in period *t*
$P_{G_i}^{min}$	:	Lower limits of real generation power at bus *i*
$P_{G_i}^{max}$	:	Upper limits of real generation power at bus *i*
$P_{L_i}^t$	:	Real power of load at bus *i* in period *t*
$Q_{ch_i}^t$	:	Reactive charging power of ESS at bus *i* in hour *t*

$Q_{ch_i}^{min}$	:	Lower limit of reactive charging power of ESS at bus *i*
$Q_{ch_i}^{max}$	:	Lower limit of reactive charging power of ESS at bus *i*
$Q_{d_i}^{t}$	:	Reactive discharging power of ESS at bus *i* in hour *t*
$Q_{d_i}^{min}$	:	Lower limit of reactive discharging power of ESS at bus *i*
$Q_{d_i}^{max}$	:	Lower limit of reactive discharging power of ESS at bus *i*
$Q_{G_i}^{t}$	:	Reactive generation power at bus *i* in period *t*
$Q_{G_i}^{min}$	:	Lower limits of reactive generation power at bus *i*
$Q_{G_i}^{max}$	:	Upper limits of reactive generation power at bus *i*
$Q_{L_i}^{t}$	:	Reactive power of load at bus *i* in period *t*
T	:	Optimization horizon
V_i^t	:	Voltage magnitude of bus *i* in period *t*
V_i^{min}	:	Lower limit of voltage magnitude at bus *i*
V_i^{max}	:	Upper limit of voltage magnitude at bus *i*
V_k^t	:	Voltage magnitude of bus *k* in period *t*

CHAPTER 1

Introduction

1.1 Background and motivation

Over the past 40 years, along with the increase in the world's population, electricity generation has been growing by more than 40%. This electricity generation will continue to grow and is forecasted to grow by 70%, from 22126 TWh in 2011 to 37000 TWh in 2030 [2]. However, traditional ways of electricity production using fossil fuels have posed threat to the environment as well as human being health. Burning of these fossil fuels is considered to be the largest contributing factor of greenhouse gas emissions into the atmosphere, which is considered one of the causes of global warming. The impact of global warming on the environment is extensive and affects many areas. Consequently, increasing worldwide efforts are prompted to reduce emissions from fossil fuels. The deployment of Renewable Energy Sources (RES) has been one of the solutions. It is important for renewable energy to not only keep up with the increasing population growth, but also gradually replace fossil fuels if we are to meet future energy demands. With renewable portfolio standards calling for more renewable generation and advances in wind power systems, wind generation has become the fastest growing generation source in the world. Specifically, this fast growing of wind generation is the result of a combination of the following factors [3]:

- Strong political support for renewable energy for its environmental advantages as well as national energy security advantages. Government subsidies are also provided, which typically compensate the initial costs, gives price support or a credit for wind power generation.

- Ratepayers are willing to pay a premium for "green power" through green pricing programs to share the goals of facilitating renewable energy integration and reducing green house gas emissions.

- Improved wind generation technology, including increasing power ratings, larger manufacturing operations and improved performance capabilities of wind turbine systems. Such improvement has led many utilities to view wind generation as a hedge against the increasing volatility in natural gas prices.

- Governments at all levels are increasingly implementing Renewable Portfolio Standards (RPS), which is a regulatory mandate to increase production of energy from renewable sources such as wind, solar, biomass and other alternatives to fossil and nuclear electric generation. In general, the RPS sets a target for the share of electricity to be supplied from designated renewable energy resources by a certain year.

Wind generation does not function in a similar manner as conventional generation resources. Wind exhibits both variability and uncertainty. Its power output can not be fully controlled, and can not be reliably predicted. The uncertainty and variability of wind can pose challenges for grid operators. This variability of wind generation impacts all time horizons of power system operation, including short-term variability (order of seconds to hours) and long-term variability (order of months to years). Short-term variability of wind is caused by occasional gusts and stills of wind and the geographical spreading of wind power plants. The small and fast variations (seconds to minutes) of aggregated wind power output (as a consequence of turbulence or transient events) are quite small and do not significantly impact power grids. Variations of longer periods (hourly variations) are much more important for power systems, considering in relation to load fluctuations. These variations in wind generation might require additional actions to balance the system and higher system flexibility is necessary to accommodate the mismatch between generation and load. Long-term variations of wind power, on the other hand, include seasonal variations and the inter-annual variations, resulting from diurnal wind speed variations and shifting weather patterns. These variations are not very important for daily operation of the system and management of the grid, but they play an important role in long-term system planning [4].

The impacts of wind variability and uncertainty on power systems depend basically on wind penetration level, which is the ratio between installed wind capacity and peak load. In most cases, at small penetration levels, typically less than 15% to 20%, the integration of wind power is not a big issue assuming there is no grid capacity or stability constraints. At higher penetration levels, i.e., more than 20%, wind needs to be curtailed during the low consumption periods to ensure grid stability (frequency, voltage, reactive power) [3, 5] (See Figure 1.1 for a summary on problems in renewable energy integration and possible solutions). ESSs are one of the greatest potentials to solve such wind integration issues. ESSs can be added into power systems to provide all or some portion of the additional regulation control and reserves. In addition, due to its variable nature, wind can be negatively correlated with load and electricity price. Wind might blow at periods of low load, low electricity price and fail to blow at periods of high load, high price, which makes it difficult to exploit the full potential of wind resource. In this case, ESSs can be employed to firm and shape a portion of wind power to accommodate wind generation and improve overall system economics. For example, ESSs can be used to store the strong wind at night when load is low and release it at peak load periods during the day. Also, when wind power exceeds the minimum load at night and has to be curtailed to avoid grid stability problem, ESSs can serve to charge this otherwise curtailed amount of wind power and discharge it during the day to supply loads.

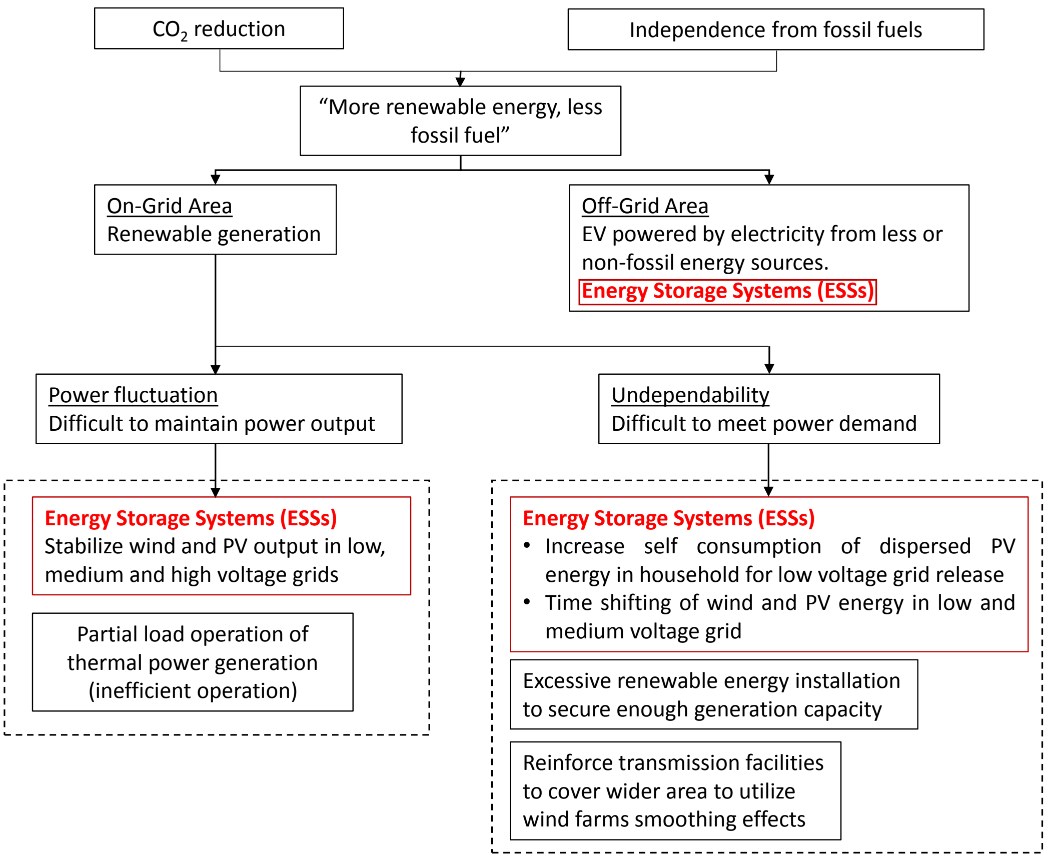

Figure 1.1: *Problems with renewable integration and possible solutions [6]*

The integration of wind resource also introduces transmission congestion into power networks since the grid was not initially built for transmitting such high amount of energy. Consequently, in order to accommodate increasing penetration levels of wind, a solution has to be found such that transmission congestion is mitigated while maintaining minimum impacts on system reliability as well as system capital and operational costs, otherwise wind power has to be curtailed. Grid expansion to avoid these congestions will take long time. Energy storage devices, however, can be an option to solve this problem. They could be used to store the excess wind power during congestions and dispatch it later, when the transmission capacity is available. This would help reduce wind curtailment and also defer or avoid transmission upgrades.

In cases when wind generation is bid to electricity market based on forecast wind data, storage devices can also be used to hedge forecast uncertainties and hence optimize wind generation revenues by shifting wind power from higher than forecast deliveries to avoid penalties associated with lower than forecast deliveries [3].

A basic question arisen is who might be interested in the investment into ESSs. Seemingly, it appears this is an investment to wind plant owners based on the benefits they receive from this device. However, in reality, grid operators might have more incentive to install storage devices due to the rules from some regulators. For instance, some regulators have the rule that integration issues are the responsibility of grid operators, and that wind owners should not be penalized for the lack of transmission capacity, which means that wind developers are paid for wind generation no matter how wind power has to be curtailed, and that installing energy storage for curtailment reduction are not necessary for them. In this case, grid operators would have incentive to invest on storage devices to recover the energy for which they are paying. Transmission and distribution utilities can also take advantage of some benefit streams with energy storage such as load shifting for asset deferral or ancillary services, which would help to offset the cost of the system while wind developers do not gain any benefit from such application. For these reasons, investment in energy storage systems is more likely to make sense to utilities than to wind owners. Perhaps, a multi-party agreement involving both utilities and wind owners could be made early in the wind development process to bring benefits to both sides [7].

In general, ESSs can be a possibility to solve wind integration issues by providing more flexibility and balancing to wind generation, improving overall system economics and security. They will play a key role in enabling a low-carbon electricity system with increasing penetration of renewables. The history of stationary ESSs dates back to the 20^{th} century, when power stations were often shut down overnight, with lead-acid accumulators supplying residual loads on the direct current networks. Utility companies gradually recognized the importance of energy storage devices in providing flexibility in power systems and the first central station for energy storage, a Pumped Hydroelectric Storage (PHS), was put to use in 1929. The subsequent development of electricity supply industry with their complementary and extensive transmission and distribution networks, has essentially drawn interest in using this energy storage technology until recent years. Up to 2005, more than 200 PHS systems were in use all over the world, providing a total of more than 100 GW of generation capacity. However, pressures from deregulation and environmental concerns have led to the decrease in major investment in PHS facilities, and interest in the applications of other forms of ESSs is growing, due to some primary drivers including changes in utility regulatory environment, an increasing reliance on electricity in industry, commerce and the home, power quality/quality-of-supply issues, the growth of renewable as a major new source of electricity supply, and environmental requirements. These factors, combined with the rapidly accelerating rate of technological development in many of the emerging ESSs, with unit cost reductions, now make their practical applications attractive on future timescales of only a few years [8].

1.2 Research Objectives

As the use of ESSs for wind penetration increases, decision on their sizes and locations becomes important for both security of operation and economy of the system. The goal is to place a minimum capacity of ESSs at appropriate sites where their applications will be most exploited. The addition of ESSs introduces time correlation characteristic into the planning problem, which is a major difference between ESS planning and conventional system planning. Moreover, the integration of wind generation resource into power systems creates challenges for system planning, concerning the high uncertainty in wind power production. Deterministic approaches can not explicitly capture the stochastic nature of wind and hence can not help to make the right decision. Consequently, it is crucial to develop probabilistic techniques for solving the uncertainty issue associated with wind generation. This research aims at answering several questions related to the planning of ESSs in power systems with high wind penetration:

1. Given available data of wind power and load, how to decide optimal locations and size for the ESSs to be installed?
2. What is the optimal operational schedule of the ESSs to support wind generation?
3. How to incorporate wind and load uncertainties into the planning of ESSs in its combined operation with wind power?

1.3 Main Contributions

The main contributions of the thesis is summarized as follows:

1. A multi-period AC OPF formulation with ESSs is proposed, in which ESSs are employed to time-shift wind generation. The full AC OPF formulation is used to better capture realistic physical power flows of the system, opposite to most of the available models, which are based on the linear DC model. It is much more accurate and reliable when issues such as congestion and voltage constraints are concerned. This formulation is implemented into multi-period model, which takes into account time inter-dependence, i.e., the problem is solved simultaneously for all periods of the optimization horizon.

In this way, the inter-temporal constraints relevant to storage devices can be suitably included.

2. Two approaches, namely probabilistic and stochastic approach, to include wind and load uncertainties in the planning of ESSs are studied. In the probabilistic approach, a GA-based probabilistic OPF (POPF) model to optimally place and size ESSs in a transmission grid is proposed. For the POPF, a cumulant-based multi-period AC OPF with ESSs is introduced. In the stochastic approach, a two-stage stochastic model is proposed to determine the optimal capacity of ESSs in time-shifting wind generation considering the stochastic behavior of wind and load.

1.4 Outline of the Thesis

The thesis is organized as follows:

Chapter 1: Introduction
This chapter contains the background and motivation of the thesis. It continues with research objectives and main contributions of the thesis and ends up with the outline of the thesis and list of publications.

Chapter 2: Energy Storage Systems: Applications and Technologies
This chapter provides an overview on possible applications of ESSs to support wind generation. It also provides a description of storage technologies applicable for different grid connected wind power applications.

Chapter 3: Deterministic Multi-period AC Optimal Power Flow with Energy Storage Systems
This chapter describes in detail the mathematical formulation of the multi-period AC OPF model with ESS integration. A methodology to define candidate ESS locations is also presented.

Chapter 4: Optimization under Uncertainty
This chapter presents theory and methodology of the approaches that will be adopted in the planning problems with ESSs in the next chapter, including cumulant-based probabilistic approach and the classical recourse-based stochastic programming approach.

Chapter 5: Energy Storage System Planning Considering Uncertainty
This chapter explicitly describes methodologies of two approaches for including uncertainty into ESS planning problems, i.e., the combined GA and cumulant-based probabilistic approach and the two-stage stochastic programming approach. All tests and results are presented and discussed.

Chapter 6: Conclusions and Recommendations

In this chapter, the conclusions of the thesis and recommendations for future work are provided.

1.5 List of publications

1. N. T. A. Nguyen, D. D. Le, G. G. Moshi, C. Bovo, and A. Berizzi, "Sensitivity analysis on locations of Energy Storage in power systems with wind integration," *IEEE Transactions on Industry Applications*, vol. 52, no. 6, pp. 5185-5193, Nov-Dec. 2016. (ISSN: 0093-9994)

2. D. D. Le, N. T. A. Nguyen, V. D. Ngo, and A. Berizzi, "Advanced probabilistic power flow methodology for power systems with renewable resources," *Turk J Elec Eng & Comp Sci*, 2016. (ISI/SCIE, SCOPUS indexed journal; ISSN: 1300-0632) (*Accepted*)

3. N. T. A. Nguyen, D. D. Le, G. G. Moshi, C. Bovo, and A. Berizzi, "Energy Storage Operation in Power Systems Considering Correlation Between Wind Farms," *IEEE* 16^{th} *International Conference on Environment and Electrical Engineering (EEEIC)*, Florence, 2016.

4. N. T. A. Nguyen, D. D. Le, C. Bovo, and A. Berizzi, "Optimal Power Flow with energy storage systems: Single-period model vs. multi-period model," *PowerTech, 2015 IEEE Eindhoven*, Eindhoven, 2015, pp. 1-6.

5. N. T. A. Nguyen, D. D. Le, G. G. Moshi, C. Bovo, and A. Berizzi, "Sensitivity analysis on locations of Energy Storage in power systems with wind integration," *IEEE* 15^{th} *International Conference on Environment and Electrical Engineering (EEEIC)*, Rome, 2015, pp. 1115-1119.

6. N. T. A. Nguyen, D. D. Le, G. G. Moshi, C. Bovo, and A. Berizzi, "Two-step procedure to Site and Size ESS considering Uncertainties," *to be submitted to a journal*.

7. N. T. A. Nguyen, D. D. Le, C. Bovo, and A. Berizzi, "Stochastic Sizing of Energy Storage Systems for Wind Integration," *to be submitted to a journal*.

CHAPTER 2

Energy Storage Systems: Applications and Technologies

2.1 Introduction

The challenges associated with meeting demand variations while providing reliable services has historically motivated the use of energy storage devices while recent interest in energy storage has been motivated by at least five factors: advances in storage technologies, increase in fossil fuel prices, development of deregulated energy markets including markets for high-value ancillary services, challenges to siting new transmission and distribution facilities, and increasing penetration of variable renewable generation [9]. Much of the current attention for ESSs is based on its potential applications with renewable energy sources, specifically wind energy resource.

This chapter provides an overview on potential applications of storage devices to support wind generation. The main ESS technologies currently available and under development are also explicitly described. Technical and economic characteristics of each storage technology, including power rating, typical discharge times, investment and operation costs, efficiency, response time and life time are also presented.

2.2 ESS applications

The role of ESSs is to provide flexibility to wind generation due to the variability and uncertainty behavior of wind. Accordingly, wind energy becomes controllable and dispatchable to meet system loads and meet energy bid in an electricity market. Also, it can be controlled to efficiently utilize available transmission capacity. The roles of ESSs can be described by the number of uses (cycles) and the duration of operation, as shown in Figure 2.1. For power quality application, ESSs with high cycle stability and short duration of operation is required; for time shifting application, on the contrary, longer storage duration and fewer cycles are necessary [6]. In this section, different ESS applications are described in details.

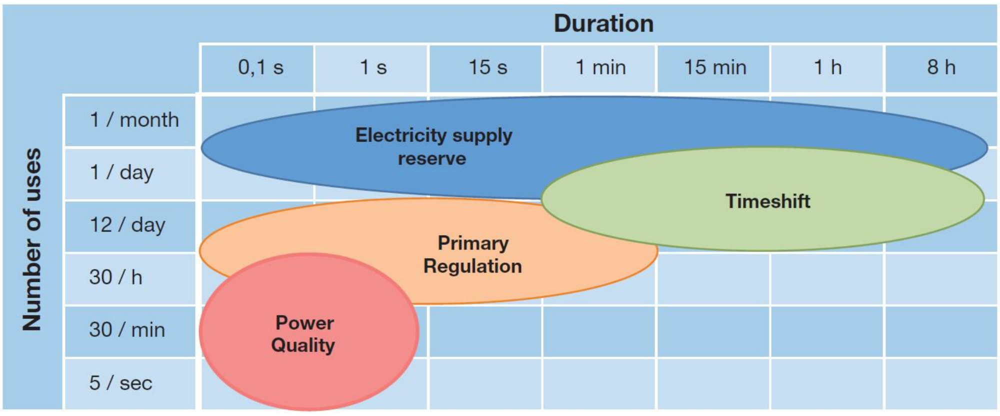

Figure 2.1: *Different uses of ESSs depending on frequency and duration of use [6]*

2.2.1 Time-shifting

Due to its variable and weather-dependent nature, wind energy might be high at periods of low demand and low electricity price and it might be low when demand is high, which might result in wind curtailment. In this case, ESSs can be employed to store the wind energy generated during low demand periods and sale it later at a higher price during periods of high demand. Since this operation of the ESSs effectively shift wind energy in time, this application is called *time-shifting* (Fig. 2.2).

The benefit of using ESSs is expected to be higher with a larger gap between peak and off-peak of demand. For this application, ESSs are required to have large energy capacity with a long charging/discharging duration (from hours to days). In addition, their efficiency is another important factor to consider when choosing ESSs for this application, since a significant amount of power will be lost in an inefficient storage device [7, 10].

2.2.2 Forecast hedging

In an electricity market, where buyers and sellers have to enter into negotiated contracts for power supply, the variability of wind becomes especially challenging. Since wind forecasts

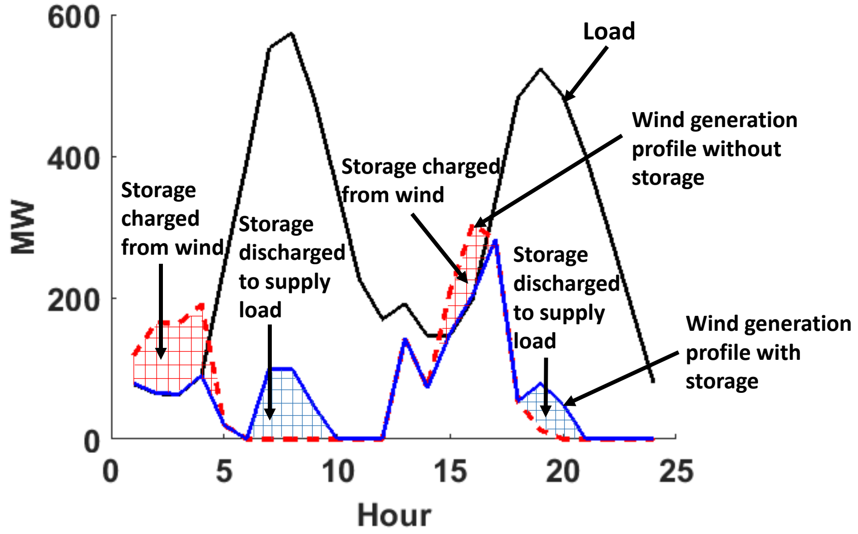

Figure 2.2: *ESS for time-shifting wind energy*

can not precisely provide prediction on the amount of wind power output during the contracted period, there might be a risk that the real wind generation will be higher or less than the bid amount and a shortfall in wind generation will result in penalties for wind generators. Energy storage devices can be used to store the wind energy in excess of bid amounts and supplement wind generation less than bid amounts with stored energy on a real-time basis, which helps to reduce the risk of paying penalties due to forecast errors. This application of the ESSs is called forecast hedging.

A forecast hedging application requires an ESS with several hours of charging/discharging duration, since the contracts typically last several hours. High round-trip efficiency is not as critical as for time-shifting application but must be reasonably favorable for good economics [7].

2.2.3 Transmission Curtailment Reduction

Wind resources are often located in far from population centers and installation of wind farm sites might require an extension of transmission capacity to transfer wind power to supply loads otherwise wind has to be curtailed when there is transmission congestion. To mitigate constraints imposed by insufficient transmission capacity on the utilization of wind generation, wind energy has to be stored during periods of insufficient transmission capacity and then released when capacity becomes available. An ESS located close to wind generators can capture the excess wind energy at these periods to avoid wind curtailment and deliver it later when there is sufficient capacity, which allows the sale of wind power that would otherwise be lost. Similarly, an ESS located close to load centers (the other side of the congested transmission lines) would be used to charge the wind energy when there is no congestion. This energy can be used later, when congestion occurs.

The curtailment reduction application requires an energy storage device of large energy capacity, i.e., charging/discharging duration in the order of hours to days. Besides, since energy stored during a curtailment period would be lost anyway, the round-trip efficiency of the storage device in this application is not as critical as in other applications.

2.2.4 Fluctuation Suppression

The inherently variable nature of wind could cause fluctuations in frequency and voltage. In this fluctuation suppression application, ESSs would be used to stabilize wind farm generation frequency by absorbing the excess energy during output spikes and releasing energy during output drops. This application is typically at the wind farm in order to make wind power compliant with stability criteria imposed by transmission operators. Hence, this is a special case within the otherwise grid based applications of energy storage. Ramping capability of the ESSs is relatively important for this application [7, 10].

2.2.5 Grid frequency support

This application provides short duration power necessary to maintain grid frequency within a nominal range following a severe system disturbance caused by a significant imbalance between generation and load. In power systems with a high penetration of wind, a sudden reduction in wind can cause such a disturbance. While such disturbances are usually addressed by conventional spinning reserve, these “clean” markets are subject to minimize the use of conventional generation. As a result, storage devices can be a solution to support the grid until alternative strategies can be implemented (e.g., dispatchable loads). The ESSs must detect the disturbance and respond within 20 milliseconds by injecting real power for up to 30 minutes [7, 11].

2.2.6 Energy arbitrage

Another application of ESSs is energy arbitrage, in which the ESSs are capable of "buy low sell high". Specifically, they can be used to purchase electricity at times when market prices are low and sale the electricity back to wholesale market when the prices are higher (e.g., during peak load periods). The variability of renewable generation, especially wind generation, increases wholesale market price volatility, i.e., prices get dropped when renewable energy is generated at high levels, and get recovered when renewable generation decreases. This higher volatility provides opportunity to enhance the value of energy storage devices [12]. In this application, the ESSs are required to have a response time of minutes to hours and a discharge duration of hours [9].

2.2.7 Combined applications

Energy storage is currently still a relatively expensive solution to wind integration related issues. Ideally, an ESS should provide multiple applications, even applications not related to wind generation. For instance, an ESS used for time-shifting application might also be used for frequency regulation when time-shifting is not necessary. It is important for a storage device in this case that the applications are not conflicting with each other. In some cases, the technical requirements for operation make it difficult for the ESS to be used simultaneously in two applications. Even when multiple applications are already incorporated into a storage device, trying to achieve all benefits simultaneously is also difficult, and may not be economical. For example, the use of an ESS for frequency regulation may make it unavailable for forecast hedging, as the frequency regulation application may require the energy storage to operate at 50% state of charge while forecast hedging requires it to be fully charged. Also, using a system for frequency regulation may cause the battery to get aged prematurely and require early replacement [7].

2.3 ESS technologies

There are two aspects of electricity important for understanding technology and applications of storage, i.e., power and energy. Energy can be thought of as a volume, which can be a kilowatt-hour or a megawatt-hour, while power is known as a rate of flow, which is a kilowatt or megawatt. Some applications such as time-shifting or forecast hedging require a large volume of storage capacity while others such as grid frequency support require a large responsive power capacity. It is, therefore, important to distinguish between storage technologies best suited for power applications and those best suited for energy applications. Power applications require high power output, usually for relatively short periods of time (a few seconds to a few minutes). Storage used for power applications usually has capacity to store quite small amounts of energy per kW of rated power output. Energy applications require relatively large amounts of energy, often with discharge duration of hours to days. Storage devices used for energy applications must have a much larger energy capacity than those used for power applications [13, 14].

Other factors that influence the choice of ESS technology for a particular application includes response time, discharge frequency, depth of discharge, efficiency, service life and system costs.

This section provides a description of ESS configuration, ESS technical economic parameters, along with performance characteristics of major energy storage technologies in support of wind generation.

2.3.1 ESS configurations

In most applications, an ESS consists of a storage unit and a Power Conversion System (PCS) which interfaces the storage unit to the grid or the load. The PCS is used to convert from AC to DC current and vice versa for storage units, except mechanical ones. The PCS, therefore, performs as a rectifier while the ESS is charged (AC to DC) and as an inverter when it is discharged (DC to AC). The PCS also conditions the power during conversion to make sure there is no damage to the storage device. This component of the ESS usually costs from 33% to 50% of the storage system [8]. A conventional configuration of ESS is shown in Figure 2.3.

In this configuration, the storage unit is interfaced to the grid through a PCS which operates in both discharging and charging modes. For end-use application, the ESS can be connected to the bus which feeds such load as a machine or industrial processing unit. In this case, the storage unit is only activated when grid power is interrupted [15].

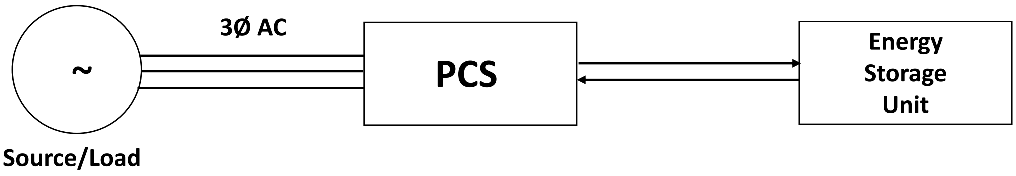

Figure 2.3: *Energy storage unit connected directly to the grid [15]*

2.3.2 Technical-economic characteristics of ESSs

2.3.2.1 Power and Energy Capacity

Power capacity is the rate of discharge of the storage devices. It is measured in kilowatt (kW) or megawatt (MW). The power capacity of an ESS is actually its nameplate power rating under normal operating conditions. That power rating also represents the storage device maximum power output under normal operating conditions. Some types of ESS can discharge at a relatively higher rate (e.g., 1.5 to 2 times their nominal rating) for relatively short periods of time (e.g., several minutes to as much as 30 minutes). This feature is often referred to as the storage peak power rating or pulse power rating, which is usually several times the normal power rating. This power rating is necessary for circumstances involving an urgent need for relatively high power output within quite short durations. However, discharging at higher rate will make storage efficiency gradually reduced (relative to efficiency during discharge at the nominal discharge rate), and the storage device itself will get lost of life more easily (compared to damage incurred at the normal discharge rate) [7, 8].

Another important characteristic of storage systems is discharge duration, expressed in units of time, ranging from seconds to hours. Discharge duration is the amount of time that the storage plant can discharge at its rated power without being recharged. This characteristic is also represented by energy capacity of the ESSs, where energy capacity, measured in kilowatt-hours (kWh) or megawatt-hours (MWh), is defined as the power capacity times discharge duration. For example, an ESS with power capacity of 1 MW and energy capacity of 5 MWh is able to deliver 1 MW in 5 hours when fully charged [13].

2.3.2.2 Power and Energy Density

Power density is the amount of power that can be delivered from an ESS with a given volume or mass. Similarly, energy density is the amount of energy that can be stored in a storage device that has a given volume or mass. These criteria are important in situations when space is limited and/or when weight is important [8].

2.3.2.3 Depth of Discharge, Frequency of Discharge, and Response Time

Depth of discharge is the percentage of power discharged relative to full capacity before the storage is recharged. Some technologies are sensitive to depth of discharge. Deep discharge of some electrochemical batteries reduces their life expectation and may cause physical damage to the battery cells. Other technologies operate best under full or 100% depth of discharge.

Frequency of discharge is how often power will be discharged from a storage technology. Some applications only require infrequent discharge (spinning reserve, for example) while others are cycled continuously.

Response time is how quickly a storage technology can be brought online and start discharging its energy. Most storage technologies have a response time of several seconds or less.

2.3.2.4 Ramp Rate

An important storage system characteristic for some applications is the ramp rate that is the rate at which power output can change. Generally, storage ramp rates are rapid, i.e., output can change quite rapidly). Storage devices with a slow response time tend also to have a slow ramp rate.

2.3.2.5 Service Life

Life cycle is the approximate number of charge and discharge cycles that a particular energy storage device can undergo before failure. For many energy storage devices, cycling introduces structural, mechanical and thermal stresses which form the life-limiting factor for the device. For some energy storage technologies such as electrochemical batteries, cycle life depends on how deeply the battery is discharged from full charge. The deeper the average discharge, the more the battery is exercised and the shorter the life [7].

2.3.2.6 Round-trip Efficiency

There are several ways to measure the efficiency of an energy storage device, but in the utility industry the most commonly used is the AC round-trip efficiency. AC round-trip efficiency is determined as the AC energy input to the AC energy output ratio. Self-discharge loss during the storage operation is not included. For example, a 10 MW/50 MWh battery system may require a 60 MWh energy input to fully charge the empty storage device. The system can then be discharged to deliver 50 MWh. The efficiency of this system would be 50MWh/60 MWh or 83.3%.

Generally, ESSs can be divided into three groups based on the round-trip efficiency [8]:

- Very high efficiency: the ESSs have a very high efficiency, i.e., more than 90%. Some examples of this group include Superconducting Magnetic Energy Storage (SMES), flywheel, super-capacitor and Li-ion battery.

- High efficiency: the ESSs have an efficiency of 60-90%. For example, Pumped Hydro Storage, Compressed Air Energy Storage, batteries (except for Li-ion), flow batteries and conventional capacitors.

- Low efficiency: the ESSs have an efficiency lower than 60%. Hydrogen, Metal-Air, solar fuel, and Thermal Energy Storage belong to this group.

There may be a trade-off between capital cost and round-trip efficiency when choosing a storage technology. For instance, a storage technology with a low capital cost but a low round-trip efficiency may be competitive with a high cost, high round-trip efficiency technology.

The efficiency of ESSs is affected by a number of different factors. For most energy storage technologies, energy is lost during the process of charging and discharging. Energy may also be lost while the device is not in use, and these losses are called standby losses. Standby losses are a measure of efficiency that compares how much of energy used to charge a storage device is lost before discharging. Moreover, if the storage system does not operate at the same voltage as the system, losses arise since a transformer must be used. ESSs that store only DC power must include a charger and an inverter to convert AC power to DC power for storage, and then back again for delivery; these power electronics also generate losses. Some technologies have other intrinsic losses, such as the thermodynamic losses in batteries. Efficiency can also be affected by ambient conditions such as temperature. Some technologies require ancillary devices, which require power, to connect them to the grid. These “parasitic” loads reduce efficiency much like standby losses [7, 13].

2.3.2.7 System Cost

The cost of an ESS follows two metrics, i.e., *cost per unit power* (€/kW) and *cost per unit energy* (€/kWh). Cost per unit power is used in a manner similar to the way other capital investment in the utility industry are usually described. It is defined as the *cost per unit of rated power*, and can be used with equipment cost (cost of the installed device), installation cost, or life cycle cost. Cost per unit energy, €/kWh, describes the *cost per unit of energy storage capacity*.

To calculate the investment costs required to install a storage unit, it is important to consider not only the storage device itself but also the PCS and the Balance of Plant (BoP). The PCS consists of all equipment necessary to supply energy from the utility grid to the ESS and to discharge stored energy to the grid. BoP consists of the costs for project engineering and construction management, grid connection (including transformers), land, access, and services; and any additional assets and services required (e.g., foundations, buildings, aspects of system integration, etc.) [16]. System cost is the cost of an integrated energy storage system, including the storage device, PCS and BoP [15]:

$$cost_{total} = cost_{PCS} + cost_{storage} + cost_{BoP} \quad [€] \tag{2.1}$$

where, $cost_{PCS}$ is the cost of the PCS, $cost_{storage}$ is the cost of the storage unit, and $cost_{BoP}$ is the cost of BoP.

For most systems, the cost of the PCS is proportional to the power rating R[kW] of the ESS:

$$cost_{PCS} = UnitCost_{PCS} R \tag{2.2}$$

where, $UnitCost_{PCS}$ [€/kW] is the cost per unit power of the PCS.

The cost of the storage unit is proportional to its energy rating B[kWh]:

$$cost_{storage} = UnitCost_{storage} B \tag{2.3}$$

where, $UnitCost_{storage}$ [€/kW] is the cost per unit energy of the storage unit.

The balance-of-plant costs, $Cost_{BoP}$, are typically proportional to energy capacity, but in some cases are fixed costs or proportional to power rating.

In Figure 2.4, capital costs per unit energy and per unit power of different ESS technologies are provided.

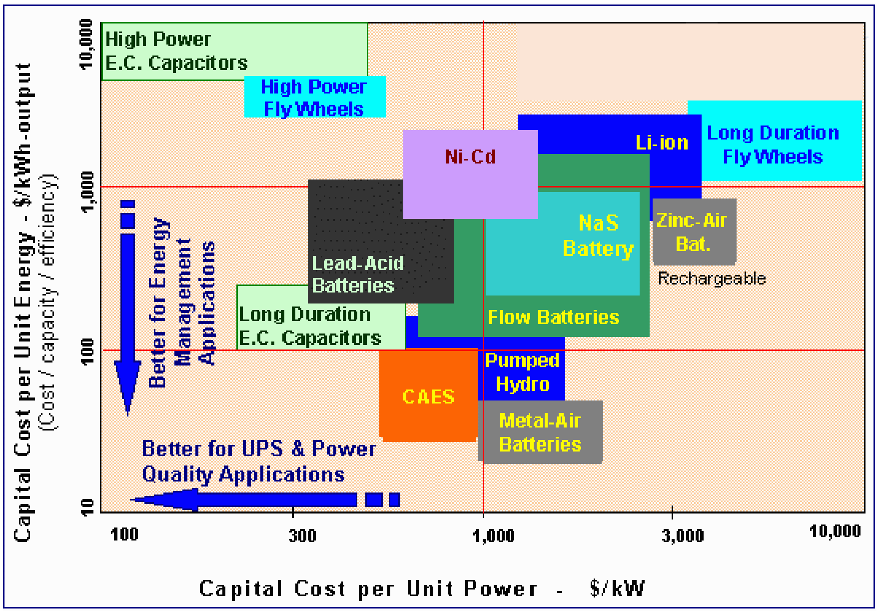

Figure 2.4: *ESS capital costs [17]*

Details about capital costs of bulk ESS technologies are presented in Table A.1 in Appendix A.

2.3.3 ESS Technologies

ESS technologies can be categorized according to two criteria, i.e., function and form. In terms of function, they can be categorized into technologies used for power applications such as power quality and reliability, and energy applications such as time-shifting and forecast hedging. Capacitor/supercapacitors, Superconducting Magnetic Energy Storage (SMES), Flywheel Energy Storage (FES) and batteries are in the category of power applications whereas Pumped Hydro Storage (PHS), Compressed Air Energy Storage (CAES), Thermal Energy Storage (TES), large-scale batteries, flow batteries, fuel cells and solar fuel fall into the category of energy applications. However, this simple classification does not reflect the wide range of technical parameters of storage devices. Since electrical energy can be stored in different forms of energy such as mechanical, thermal, chemical, electromagnetic, and electrochemical, etc, storage technologies can also be classified by the form of storage into mechanical, thermal, chemical, electromagnetic, and electrochemical storage devices. The classification of energy storage technologies according to the form of stored energy is presented in Fig. 2.5 [8, 10, 12].

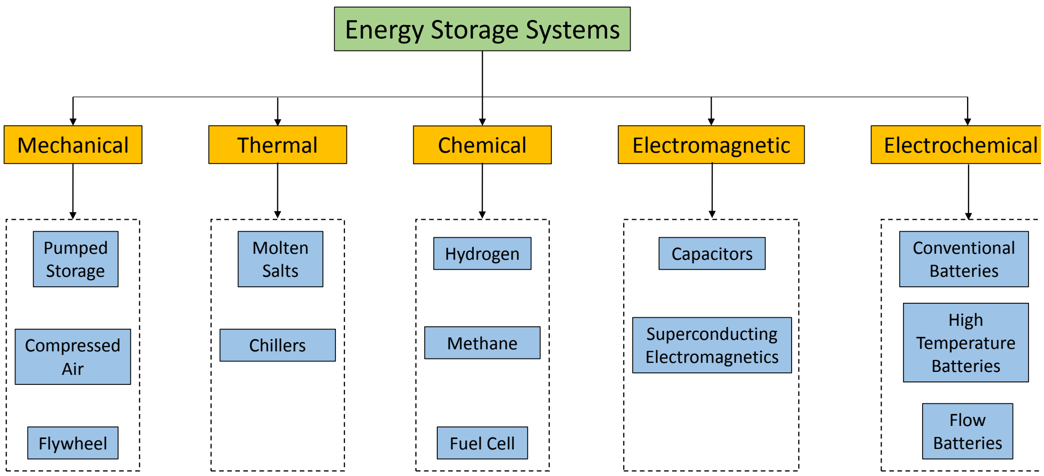

Figure 2.5: *Classification of ESS Technologies*

Below is a brief description of the energy storage technologies that are already commercially used or have a great potential in utility applications, focusing specifically on applications with wind generation.

2.3.3.1 Mechanical ESS

2.3.3.2 Pumped Hydro Storage

PHS is the largest and most mature energy storage technology available with more than 120 GW installed capacity, accounting for nearly 99% of the worldwide installed storage capacity [8, 10].

A conventional PHS system (Fig. 2.6) consists of two large water reservoirs, electric machine (motor/generator) and reversible pump-turbine group or pump and turbine separated. During off-peak hours, water is pumped from the lower reservoir to store in the upper one, considered as a charging process. During discharging process at peak hours, or more in general, when needed, water from the upper reservoir is released and flows through hydro turbines which are connected to generators to produce electrical energy.

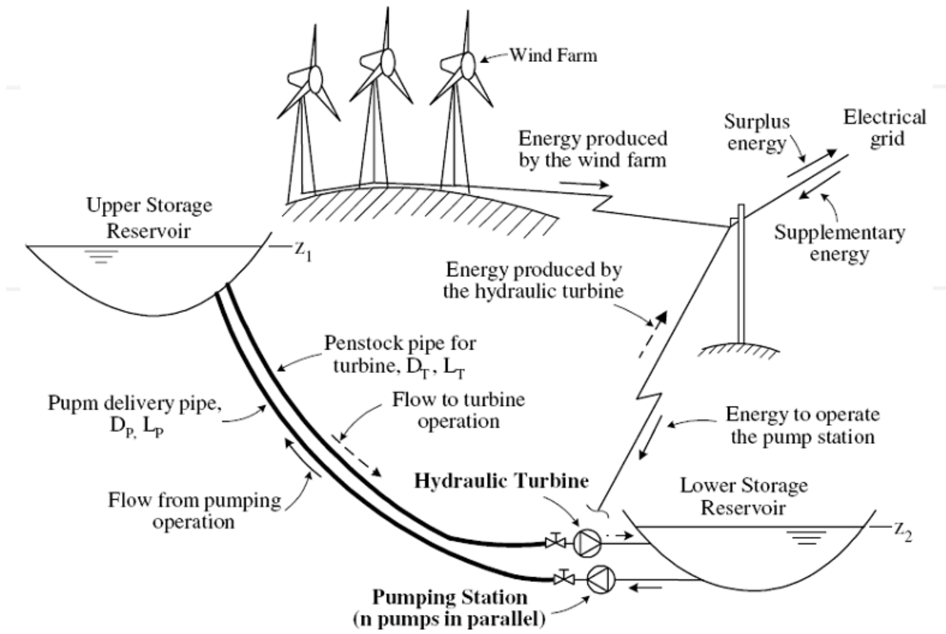

Figure 2.6: *Pumped Hydro Storage System [8]*

PHS has several technical advantages over other storage technologies. It uses familiar technology and has simple principle of operation, which allowed the installation of large-scale PHS facilities. Another advantage of PHS is the ability to size the facility independently for power and energy. The power capacity of a pumped hydro facility depends on the size and number of turbines generating power while energy capacity depends on the water volume and height of the reservoirs. As a result, the energy capacity of a pumped hydro facility is independent of its discharge rate.

PHS also has some disadvantages. It has a relatively low energy density, thus it is best implemented at large scales. The cost of such projects can be enormous and impacts on the environment can be significant. Besides, locations for such projects are limited by geographical conditions. Therefore, the flexibility of its application is low.

PHS has large power and energy rating, long lifetime, high efficiency and very small discharge losses. The main applications of PHS with wind integration include time-shifting, frequency control and non-spinning reserve supply. Due to its slow response time, PHS is not suitable for suppressing wind fluctuations.

2.3.3.3 Compressed Air Energy Storage

CAES is a technology known and used since the 20^{th} century for many industrial applications. The first commercial CAES was a 290 MW unit built in Hundorf, Germany in 1978. The second commercial CAES was a 110 MW unit built in McIntosh in Alabama, USA in 1991.

The third one, the largest ever, is a 2700 MW plant that is planned for construction in Norton in Ohio, USA [10, 16].

In a CAES system (Fig. 2.7), electrical energy is stored by compressing a large volume of air and storing it in either an underground structure (salt cavern, abandon mines, rock structures) or an above-ground system of vessels or pipes. Underground storage can be less expensive, but it depends on the availability of geographical locations. The electrical energy is released by feeding the stored compressed air into the inlet of a combustion turbine.

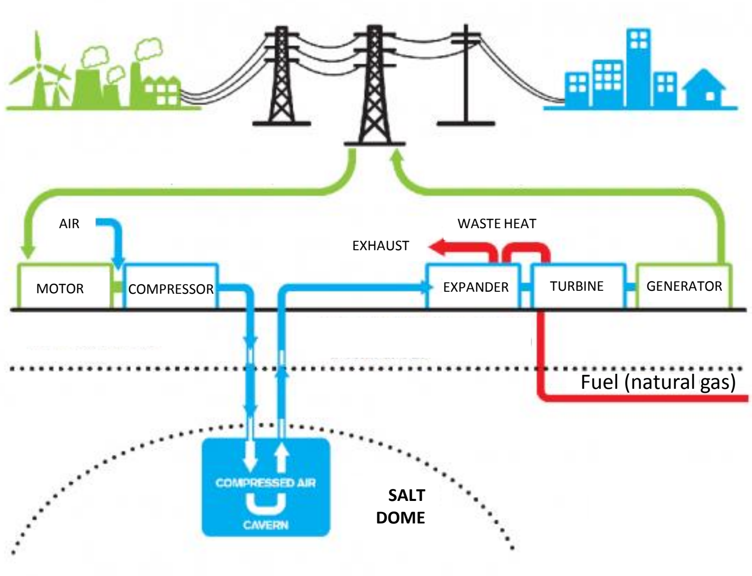

Figure 2.7: *CAES System [18]*

Similar to PHS, power and energy capacity of a CAES system are independent. Its input power rating depends on the size of the compressor and output power rating depends on the size of the turbine-generator. The energy capacity depends on the size and pressure rating of the cavern or other air storage system. With such large scale, capital costs in \$/kW and \$/kWh of this storage technology is usually cheaper than others (with the possible exception of PHS) provided a suitable location is found. This makes CAES highly attractive for large wind power applications.

With the high power and energy capacity, CAES system is another choice for energy applications with wind power generation, as similar to PHS system. However, this technology has quite low efficiency and its installation is also limited by topographical conditions.

2.3.3.4 Flywheel Energy Storage (FES)

The first FES generation, which uses a large steel rotating body on mechanical bearings, was available since 1970s. A FES is a mass rotating about an axis, which can store energy mechanically in the form of kinetic energy. Typically, rotating masses rest on a very low friction bearings (e.g., magnetic) in evacuated chambers designed to reduce friction as much as possible.

These rotating masses are coupled with a motor-generator, set inside a housing at very low pressure to reduce self-discharge losses [8, 10, 12, 16].

During charging process, inertial masses are accelerated to a very high speed which can reach from 20,000 to over 50,000 rpm. The energy is stored in the flywheel by keeping the rotating body at a constant speed. During the discharging process, the flywheel releases energy and drives the machine as a generator.

The main advantages of FES are the excellent cycle stability, low maintenance cost, high power density and high efficiency. FES are generally considered short discharge duration devices with instantaneous response time, making it a choice for power quality applications such as suppressing fast wind power fluctuation, providing ride-through of interruptions of several seconds or bridging the shift between two sources. Since frequent cycling and continuous operation wear down mechanical components, life expectancy of this storage device is a concern. FES have an expected life cycle of 100,000 charge-discharge cycles, limited by mechanical wear [10, 12].

2.3.3.5 Electromagnetic ESS

Electrical energy is really difficult to be stored in the form of electricity, hence most storage technologies seek to store electrical energy by first converting it into other forms of energy. However, there are two technologies storing electrical energy as electricity, i.e., capacitors and superconducting electromagnets [12].

2.3.3.6 Capacitors and Super-Capacitors

The most direct and literal way of storing electrical energy is with a capacitor. In its simplest form, a capacitor consists of two metal plates separated by a non-conducting material called a dielectric. When one plate is charged with electricity from a direct-current source, the other plate will induce in it charges of the opposite sign. Energy is stored in the electrical field between the two plates. The main problem associated with conventional capacitors is the low energy density. If a large capacity is required, the area of the dielectric must be very large and the use of large capacitors is relatively uneconomical [12, 16].

Recent progress in electrochemical capacitors, also called double layer, super-capacitors or ultra-capacitors, leads to capacitors with much higher energy density than conventional ones, thus enabling much more compact designs. In super-capacitors, electrical energy is stored by means of an electrolyte solution between two solid conductors rather than the solid dielectric between electrodes as in conventional capacitors. The electrodes are often made from porous carbon or another high surface area material. Since the surface area of activated carbons is very high and since the distance between the plates is extremely small (less than 1 nm), very large capacitances and stored energy are possible using super-capacitors. Some double layer capacitors have a voltage rating at or above 600 V, which makes them suitable for power quality and intermittent renewable fluctuation suppression applications. Their disadvantages include interdependence of the cells, sensitivity to cell voltage imbalances and maximum voltage thresholds, and safety issues, including electrical, fire, chemical, and explosion hazards. Their main advantages are long life cycle and short charge/discharge time [12, 16].

2.3.3.7 Superconducting Magnetic Energy Storage (SMES)

In SMES, electrical energy is stored in a magnetic field created by the flow of direct current in a coil of cryogenically cooled, superconducting material. Once the superconducting coil is charged, the current will not deteriorate and the magnetic energy can be stored indefinitely. The stored energy is then released by discharging the coil. Cryogenic refrigeration is required to keep the device cold enough to maintain superconducting properties. SMES units have fast response time (under 100 ms), life expectancy independent of duty cycle, high efficiency (above 95%) and reliability, and "permanent" storage which allows the energy to be held indefinitely with no standby losses due to heat dissipation, evaporation, etc. This makes SMES an excellent choice for Uninterrupted Power Supplies (UPS) and power quality applications.

2.3.3.8 Electrochemical ESS (Batteries)

Electrochemical energy storage technologies, also called Battery Energy Storage (BES) technology, store electricity in electrochemical form. This technology has a history even longer than that of PHS technology. It is the oldest and widely used form of electrical energy storage, which was first developed in the early nineteenth century and played an important role in early investigations into electricity. BES can be divided into three main categories, i.e., conventional, high temperature, and flow. BES technology has limited cycling times due mainly to electrode fouling and electrolyte degradation. Major focus has been drawn into developing advanced batteries using advances in materials and designs.

2.3.3.9 Conventional BES Technology

A conventional BES is made up of one or more electrochemical cells. Each cell consists of an anode and a cathode, separated by an electrolyte (liquid, paste or solid). During charging process, the battery is charged by an internal chemical reaction under a potential applied across both electrodes while during discharging process, the reaction is reversible and let the battery release the absorbed energy. The most commonly used BES for utility scale applications include Lead-Acid (LA) battery, Nickel-Cadmium (NiCd) battery and Lithium-Ion (Li-ion) battery.

- ***Lead-Acid Batteries*** LA is the oldest and most technologically mature battery technology. A lead-acid cell is composed of a lead negative electrode and a lead oxide positive electrode in a common sulfuric acid electrolyte. This technology remains widely used in most new applications due to its low cost and ready availability, despite of many disadvantages such as low specific energy and power, short life cycle, high maintenance requirements and environmental hazards associated with lead and sulfuric acid. However, with the improvements in chemistry, mechanical and electrical design, and operational and manufacturing techniques, many of these disadvantages have been mitigated, and lead-acid remains the most popular energy storage technology for large-scale applications [7, 12].

Lead-acid battery is generally best suited to power quality applications. For applications with wind generation, it is mostly suitable for grid frequency support application. Lead-acid batteries are categorized in several ways, i.e., method of electrolyte management (flooded vs. valve-regulated), grid alloys (lead-antimony vs. lead-calcium), and application (cranking vs. deep-cycle). The performance can vary greatly between different types, hence it is important to choose the right type of LA batteries for a given application. The round trip efficiency of this technology is between 75 and 85% and the life time, depending on technology, is between 3-10 years [3, 7, 12].

- ***Nickel-Cadmium Batteries***

  Like LA batteries, NiCd battery is a relatively mature technology, and can easily be built into relatively large systems. NiCd batteries has an operating principle similar to that of LA batteries but their construction is slightly different from that of LA batteries, with nickel oxyhydroxide and cadmium electrodes in a common potassium hydroxide electrolyte. This technology has relatively low round trip efficiency, between 60 and 70%, and cadmium is highly toxic. Nevertheless, it is more expensive than LA battery, it is still an attractive technology since it is technologically mature and offer a longer life span than LA battery of around 10-15 years. The most suitable application with wind generation of this technology is also grid frequency support [3, 7, 12].

- ***Lithium-Ion Batteries***

  Lithium-Ion technology is extensively used in consumer electronics due to their high energy density, low standby losses and tolerance to cycling. They are mostly employed in electric vehicles market and are also being considered for utility applications. This technology still faces significant cost barriers and some versions do not tolerate deep cycling well. Nevertheless, it has demonstrated the ability to provide a very wide range of grid benefits. It has a round trip efficiency of between 85 and 95% with a lifetime of 10 to 15 years. Since it is still a relatively young technology for grid applications, cost estimates vary widely. In addition, the high capital cost limits the large-scale use of this technology for wind power integration support [12].

2.3.3.10 High Temperature Battery Technology

High temperature batteries, or molten salt batteries, are similar to conventional ones, but are based on electrochemical reactions which only occur at high temperatures. The most common batteries of this technology are sodium sulfur (NaS) and sodium nickel chloride, among which NaS is much more common [12].

Originally, NaS battery was developed for electric vehicle applications. Later, it was used for the utility market by the Tokyo Electric Power Company (TEPCO) and NGK Insulators, Ltd., both based in Japan. By the late 1990s, NGK and TEPCO deployed a series of large-scale demonstration systems, including two 6 MW, 48 MWh installations at TEPCO substations. In 2002, TEPCO and NGK announced full commercialization of their NaS battery line under the trade name NaS, for power quality and load shifting applications. Also in 2002, the first NaS battery was installed in the U.S. at an American Electric Power (AEP) laboratory at Gahanna, Ohio. NaS batteries have also been tested for wind applications, including mitigating wind power fluctuations and time-shifting wind power [7].

NaS battery is most suited for energy and/or power applications, including load leveling, energy arbitrage, and renewables output smoothing, although their fast response time (1 ms) and the ability to provide pulse power make them suitable for a very wide range of applications.

NaS battery is still in the early stages of commercialization, especially on the grid scale. Its round trip efficiency is generally high (70 to 90%), although the parasitic energy required to maintain the batteries in a molten state may reduce this somewhat. Energy outputs range up to tens of MWh, with discharge capacities from 50 kW to 100 MW. The main barrier to its deployment is the high cost and similar to many other battery technologies, is contains toxic materials which lead to an ecological problem for disposal. There are also safety concerns due to high operating temperatures and explosive nature of sodium when exposed to water [12].

2.3.3.11 Flow Battery Technology

Flow battery is electrochemical battery in which the active materials are contained in the electrolyte rather than in the solid electrodes. These electrolytes are stored in external tanks and pumped through reaction stacks which convert the chemical energy into electrical energy during discharge cycles, and vice-versa during charge cycles [7].

The most important advantage of a flow battery is the independent sizing for energy and power. Its energy rating depends on the volume of electrolyte while power rating depends on the size of the reaction stacks. The nature of flow battery makes it particularly suitable to large-scale systems. The electrolyte does not wear out, thus a relatively long service life is expected. In addition, the flowing electrolyte simplifies thermal management as well as some aspects of maintenance. However, flow battery is a complex system with pumps, plumbing, and other ancillary components, which increases the cost of maintenance and leakage losses than conventional ones. Flow battery is a relatively immature technology and has not yet been tested widely [7, 12].

Flow battery is most suited for energy applications such as peaking and spinning reserve. Its full power discharge ranges from four to ten hours. Life expectancy is 10 to 15 years, although refurbishment can extend the lifetime to 20 years. Efficiency is in the range of 60 to 70% with nearly instantaneous response times for the battery itself (0.35 ms). Although the pumps and power electronics have a slower response time, the overall expected response time is several milliseconds [12].

There are two types of flow batteries: hybrid and redox. Hybrid flow batteries use electro-active components deposited as a solid layer. The battery cell contains one battery electrode and one fuel cell electrode, with the energy limited by the size of the battery electrode. Redox flow batteries are a reversible fuel cell with the electro-active components dissolved in the electrolyte. The energy is related to electrolyte volume and power is related to the electrode area in the cells. Common redox flow battery chemistries are zinc bromine and vanadium [12].

Vanadium redox batteries have demonstrated their applications with PV and wind generation, load leveling, and power quality and reliability, including spinning reserve. To support wind generation, they can be used for time shifting as well as forecast hedging applications. Zinc bromide batteries are still in the early stages of development, but have the potential for low cost and high energy density. However the zinc builds up unevenly on the electrodes and as a result the battery must be fully discharged every 5 to 10 cycles. Bromine is extremely corrosive, which is potentially a human and environmental hazard. Zinc bromine batteries are best suited for applications requiring high energy density instead of high power density such as bulk energy storage [12].

In Figure 2.8, system power ratings and discharge time of different ESS technologies are provided. As shown in the figure, CAES and PHS have discharge time in tens of hours and

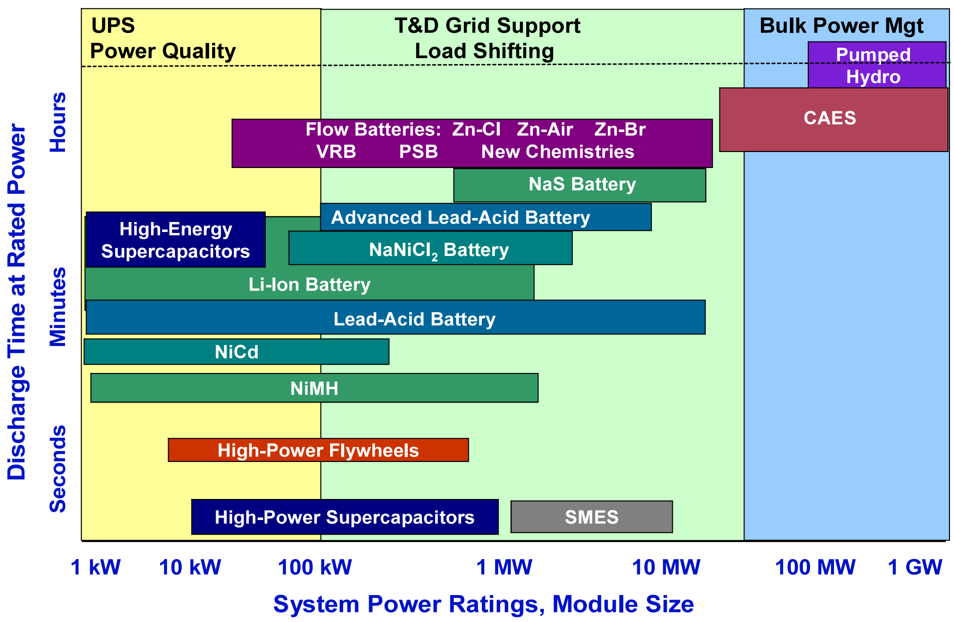

Figure 2.8: *ESS ratings [19]*

their corresponding power capacities reach as high as 1000 MW. On the contrary, various electrochemical batteries and flywheels are positioned around lower power ratings and shorter discharge times.

More information on advantages and disadvantages of different ESS technologies for wind power integration can be found in Table A.2 in Appendix A.

2.4 Summary

This chapter has presented possible applications of ESSs to support wind generation. ESSs can be used for either time-shifting wind energy, hedging wind forecast errors, mitigating wind curtailment due to limited transmission capacity, stabilizing output frequency of wind farms, or maintaining grid frequency within a nominal range in case of imbalance between generation and load. An ESS could be used for multiple applications but these applications should not conflict with each other and bring higher benefits compared to the case with a single application.

Parameters characterizing an ESS such as power and energy capacity, round-trip efficiency, power and energy density, depth of discharge, frequency of discharge, response time, ramp rate, service life and system cost have also been described. A brief description of ESS technologies for wind applications that are already commercially used or have a great potential in utility applications has also been provided. There are some technologies suitable for energy applications such as PHS and CAES while others are more suited for power applications such as flywheels, capacitors and batteries.

CHAPTER 3

Deterministic Multi-period Optimal Power Flow with Energy Storage Systems

3.1 Introduction

The OPF problem was first formulated by Carpentier in 1962 and has become a predominant method for security and economic analysis in support of power system operation and control. An OPF problem finds the optimal solution to an objective function subject to the power flow constraints and other operational constraints such as generator minimum and maximum output constraints, transmission stability and voltage constraints, and limits on switching mechanical equipment. There are a variety of OPF formulations with different constraints, different objective functions, and different solution methods. Formulations that use the exact AC power flow equations are known as AC OPF. Simpler versions which assume all voltage magnitudes are fixed and all voltage angles are close to zero are known as DC OPF. DC stands for direct current, but it might cause confusion: DC OPF is a linearized form of a full AC OPF, not a power flow solution for a direct current network. AC OPF problems refer to either a full AC OPF which simultaneously optimizes real and reactive power or a decoupled AC OPF which separately optimize real and reactive power and iterate between the two to reach an optimal solution [20]. In this research work, only real power are optimized, voltage and reactive power are assumed constant.

DC OPF is a linear approximation of the OPF problem. In a DC OPF model, power losses and reactive power are implicitly ignored, which results in the negligibility of transmission losses. AC OPF model, on the other hand, is based on the natural power flow characteristics of the network, in which transmission losses and reactive power are fully considered. Consequently, the AC OPF model can capture realistic physical power flows of the system better than the DC one. It is also much more accurate and reliable when issues such as congestion and voltage constraints are concerned. In this work, an AC OPF model is used for operation and planning study of storage devices.

This chapter presents a general review on the conventional deterministic AC OPF problem, including its mathematical formulation and applications. The model of ESSs is then introduced and included in the OPF problem, resulting in two OPF models, namely single-period and multi-period OPF. Finally, a methodology to define candidate buses for ESS installation based on Lagrangian multipliers, a byproduct of the OPF solution, is presented.

3.2 Deterministic AC Optimal Power Flow model

Generally, an OPF problem has the form [21]:

$$\begin{aligned} Min \quad & f(x,u) \\ s.t. \quad & g_1(x,u) = 0 \\ & g_2(x,u) \leq 0 \end{aligned} \tag{3.1}$$

The objective function *f(x, u)* represents the optimization goal which might be minimization of generation cost, minimization of active power losses, minimization of reactive power losses, or maximization of social benefit, depending on specific applications; $g_1(x,u)$ and $g_2(x,u)$ are system equality and inequality constraints, respectively; vector *x* includes state variables such as bus voltage magnitude and angle, branch currents, generator reactive power output, etc; vector *u* contains control variables such as real and reactive power generation, generator voltage control settings, transformer tap settings, etc. Depending on the selection of f, g, and h, the OPF problem may become a linear, mixed integer-linear, nonlinear (e.g., non-convex), or mixed integer-nonlinear programming problem.

3.2.1 Objective function

In this work, the objective function minimizes the total cost of generation. Generation cost of each generating unit is modeled as a quadratic function of its real output power, i.e., $C_i(P_{G_i})$. The objective function of the OPF problem is, therefore:

$$Min \quad \sum_{t=1}^{T}\sum_{i=1}^{ng}(c_{2_i}P_{G_i}^{t2} + c_{1_i}P_{G_i}^{t} + c_{0_i}) = Min \quad \sum_{t=1}^{T}(PC^t) \tag{3.2}$$

where, T is the optimization horizon considered, *ng* is the total number of generating units; c_{0_i}, c_{1_i}, and c_{2_i} are cost coefficients describing the quadratic cost curve of generating unit at bus *i*; $P_{G_i}^t$ is real generation power at bus *i* and time period *t*. The real generation power $P_{G_i}^t$ is a control variable of the OPF problem.

3.2.2 Equality constraints

Equality constraints mainly involve active and reactive power balance equations at each node *i* in each period *t*:

$$P_i^t = P_{G_i}^t - P_{L_i}^t = V_i^t \sum_{k=1}^{nb} V_k^t [G_{ik} \cos(\theta_i^t - \theta_k^t) + B_{ik} \sin(\theta_i^t - \theta_k^t)] + G_{ii} V_i^2 \tag{3.3}$$

$$Q_i^t = Q_{G_i}^t - Q_{L_i}^t = V_i^t \sum_{k=1}^{nb} V_k^t [G_{ik} \sin(\theta_i^t - \theta_k^t) - B_{ik} \cos(\theta_i^t - \theta_k^t)] - B_{ii} V_i^2 \tag{3.4}$$

where, *nb* is the total number of system buses; $P_{G_i}^t$ and $Q_{G_i}^t$ are real and reactive generation power at bus *i* in period *t*, respectively; $P_{L_i}^t$ and $Q_{L_i}^t$ is real and reactive power of load at bus *i* in period *t*; V_i^t and V_k^t are voltage magnitude of bus *i* and *k* in period *t*, respectively; θ_i^t and θ_k^t are voltage angle of bus *i* and *k* in period *t*, respectively; G_{ik} and B_{ik} are the real and imaginary part of the ik^{th} element of the bus admittance matrix.

3.2.3 Inequality constraints

Inequality constraints include minimum and maximum limits on control and state variables such as real and reactive generation power, bus voltage and line current magnitudes, generator ramp-up and ramp-down.

Real and reactive generation power at bus *i* in hour *t* are limited by (3.5) and (3.6):

$$P_{G_i}^{min} \leq P_{G_i}^t \leq P_{G_i}^{max} \tag{3.5}$$

$$Q_{G_i}^{min} \leq Q_{G_i}^t \leq Q_{G_i}^{max} \tag{3.6}$$

where, $P_{G_i}^{min}$ and $P_{G_i}^{max}$ are lower and upper limits of real generation power at bus *i*; $Q_{G_i}^{min}$ and $Q_{G_i}^{max}$ are lower and upper limit of reactive generation power at bus *i*.

Minimum and maximum limits on voltage magnitude of each bus *i* are represented by equation (3.7). These limits are often given by very strict standards since too high or too low voltages could lead to power system instability.

$$V_i^{min} \leq V_i^t \leq V_i^{max} \tag{3.7}$$

where, V_i^{min} and V_i^{max} are lower and upper limits of voltage magnitude at bus *i*.

The currents flowing on each branch are limited by equations (3.8) and (3.9), which represent the thermal limits of transmission lines. To make the mathematics less complex (by avoiding the square root in the calculation of current magnitude), limits are enforced on the square of current magnitude instead of the current magnitude only.

$$(I_{ij}^t)^2 \leq (I_{ij}^{max})^2 \tag{3.8}$$

$$(I_{ji}^t)^2 \leq (I_{ji}^{max})^2 \tag{3.9}$$

where, I_{ij}^t and I_{ji}^t are magnitude of the current flowing from bus *i* to bus *j* and from bus *j* to bus *i* in period *t* respectively; I_{ij}^{max} = I_{ji}^{max} is the upper limit of current flow from bus *i* to bus *j* or from bus *j* to bus *i* respectively.

Ramp-up and ramp-down limits on each generating unit are imposed by equations (3.10) and (3.11):

$$P_{G_i}^t - P_{G_i}^{t-1} \leq R_{U_i} \tag{3.10}$$

$$P_{G_i}^{t-1} - P_{G_i}^t \leq R_{D_i} \tag{3.11}$$

where, R_{U_i} and R_{D_i} are respectively ramp-up and ramp-down limits of generating unit at bus *i*.

This AC OPF formulation is a nonlinear programming (NLP) problem. The presence of non-linearity and non-convexity in the objective function and constraints makes the OPF problem computationally challenging. However, the main advantage of NLP formulations for the OPF problem is that they accurately capture system behavior.

3.3 Energy Storage System model

A storage device is characterized by its rated energy, rated charging/discharging power, and efficiencies. In this model, the ESS is used to time-shift electric energy from wind generation. The storage device is charged from wind energy in excess of load or transmission capacity and then discharged when necessary. The storage charging and discharging capabilities are modeled with two separate variables, i.e., charging power P_{ch} and discharging power P_d, with corresponding charging and discharging efficiencies, η_{ch} and η_d. Operation of the ESS is modeled using the energy balance equation (3.12).

$$B_i^t = B_i^{t-1} + (\eta_{ch_i} P_{ch_i}^t - P_{d_i}^t / \eta_{d_i}) \Delta t \tag{3.12}$$

where, B_i^t and B_i^{t-1} are energy level of ESS at bus *i* in period *t* and hour *t-1*, respectively; $P_{ch_i}^t$ and $P_{d_i}^t$ are real charging power and discharging power of ESS at bus *i* in period *t*, respectively; η_{ch_i} and η_{d_i} are respectively charging and discharging efficiency of ESS at bus *i*; Δt is the time interval between two consecutive periods.

After a cycle of time, the model assumes that the storage device must return to the initial status for the next cycle. Consequently, the energy continuity constraint (3.13) is enforced to make sure energy level of the ESS at the end of the simulation period is equal to its initial energy.

$$B_i^{t=T} = B_i^0 \tag{3.13}$$

where, T is the optimization period considered; B_i^0 is the initial energy level of the ESS at bus i; $B_i^{t=T}$ is the energy level of the ESS at the end of the simulation period.

Following are limits on ESS charging and discharging power, and ESS energy level:

$$P_{ch_i}^{min} \leq P_{ch_i}^t \leq P_{ch_i}^{max} \tag{3.14}$$

where, $P_{ch_i}^{min}$ and $P_{ch_i}^{max}$ are lower and upper limits of charging power of ESS at bus i.

$$P_{d_i}^{min} \leq P_{d_i}^t \leq P_{d_i}^{max} \tag{3.15}$$

where, $P_{d_i}^{min}$ and $P_{d_i}^{max}$ are lower and upper limits of discharging power of ESS at bus i.

$$B_i^{min} \leq B_i^t \leq B_i^{max} \tag{3.16}$$

where, B_i^{min} and B_i^{max} are lower and upper limits of energy level of ESS at bus i.

Equations (3.14) and (3.15) show that the charging and discharging rates of the ESS are limited to its rated charging/discharging power. Equation (3.16) indicates that energy level of the ESS at each period is limited to its available energy capacity or to the space to store energy in this device.

The ramp-up and ramp-down limits of charging and discharging power of the storage device are enforced by constraints (3.17) and (3.18):

$$(P_{d_i}^t - P_{d_i}^{t-1}) - (P_{ch_i}^t - P_{ch_i}^{t-1}) \leq R_{Us_i} \tag{3.17}$$

$$(P_{d_i}^{t-1} - P_{d_i}^t) - (P_{ch_i}^{t-1} - P_{ch_i}^t) \leq R_{Ds_i} \tag{3.18}$$

where, $P_{d_i}^{t-1}$ and $P_{ch_i}^{t-1}$ are discharging and charging power of the ESS at bus i in period *t-1*, R_{Us_i} and R_{Ds_i} are respectively ramp up and ramp down limits of ESS at bus i.

Here, the ESS is assumed to be interfaced with the grid using a power electronic converter. Hence, in an AC network, it also absorbs or generates reactive power while charging and discharging active power. This generation or absorption of reactive power from the ESS does not affect its energy level. The generation or absorption of reactive power are limited by constraints (3.19) and (3.20).

$$Q_{ch_i}^{min} \leq Q_{ch_i}^t \leq Q_{ch_i}^{max} \tag{3.19}$$

where, $Q_{ch_i}^t$ is the reactive charging power of ESS at bus i in period t, $Q_{ch_i}^{min}$ and $Q_{ch_i}^{max}$ are lower and upper limits of reactive charging power of ESS at bus *i*.

$$Q_{d_i}^{min} \leq Q_{d_i}^{t} \leq Q_{d_i}^{max} \tag{3.20}$$

where, $Q_{d_i}^t$ is the reactive discharging power of ESS at bus i in period t, $Q_{d_i}^{min}$ and $Q_{d_i}^{max}$ are lower and upper limits of reactive discharging power of ESS at bus i.

3.4 Multi-period Optimal Power Flow model with Energy Storage Systems

The traditional OPF problem without storage deals with static optimization, in which there is no correlation across time and the optimal solution is independently solved at each period considered (e.g., one hour). The addition of ESSs into an OPF model introduces time interdependence, i.e., ESS can be decided to charge at periods of high wind or low electricity price and discharge at periods of low wind or high electricity price. Besides, the amount of charging/discharging power of ESSs at the current period is partly dependent on its energy level at the previous period. Thus, the optimization problem in each period become coupled, yielding an optimization problem across time.

An OPF problem with ESS integration can be formulated into single-period and multi-period models. In single-period model, the problem is formulated to run independently for each period while in multi-period one, it is run once for the whole optimization period. The link between period *t* and *t+1* in single-period model is performed through the energy balance equation (3.12) of the ESSs. The objective function for both models are presented in equations (3.21) and (3.22).

- For single-period model: The objective function is to minimize the hourly generation cost of all generating units:

$$Min \quad \sum_{i=1}^{ng}(c_{0_i} + c_{1_i}P_{G_i}^t + c_{2_i}P_{G_i}^{t^2}) = Min \quad PC^t \tag{3.21}$$

- For multi-period model: The objective function is to minimize the total generation cost of all generating units:

$$Min \quad \sum_{t=1}^{T}[\sum_{i=1}^{ng}(c_{0_i} + c_{1_i}P_{G_i}^t + c_{2_i}P_{G_i}^{t^2})] = Min \quad \sum_{t=1}^{T} PC^t \tag{3.22}$$

With the addition of ESSs, the objective functions (3.21) and (3.22) become:

- For single-period model:

$$Min \quad \sum_{i=1}^{ng}(c_{0_i} + c_{1_i}P_{G_i}^t + c_{2_i}P_{G_i}^{t^2}) + \sum_{j=1}^{ns}(c_{d_j}P_{d_j}^t - c_{ch_j}P_{ch_j}^t) \tag{3.23}$$

- For multi-period model:

$$Min \quad \sum_{t=1}^{T}[\sum_{i=1}^{ng}(c_{0_i} + c_{1_i}P_{G_i}^t + c_{2_i}P_{G_i}^{t^2}) + \sum_{j=1}^{ns}(c_{d_j}P_{d_j}^t - c_{ch_j}P_{ch_j}^t)] \tag{3.24}$$

The complementary condition which requires that the ESS is not charged and discharged simultaneously is enforced based on the Locational Marginal Price (LMP) λp. For energy storage capacity at bus *i*, if λp_i^t is strictly positive then $P_{ch_i}^t$ and $P_{d_i}^t$ are never simultaneously nonzero, i.e. simultaneous charging and discharging will not occur. Negative LMPs are common in power markets and may result from negative offer curves or binding line flow constraints. A negative LMP implies that an ESS would be paid to charge and pay to discharge at the same time. This can result in a simultaneous charging and discharging of the ESS [22]. Accordingly, complementary constraints are managed by applying suitable fictitious charging and discharging costs (c_{ch} and c_d) for the ESS. When charging, the ESS is treated as a normal load. Therefore, the operational cost of charging is the LMP at the ESS bus, thus the charging cost c_{ch} is set to zero. To prevent simultaneous charging and discharging, the operational cost of discharging c_d is set to a very small quantity, i.e., $c_d = 10^{-2}$.

The objective function in both models has to fulfill equality and inequality constraints in each period. Equality constraints include active and reactive power balance equations (3.25), the energy balance equations (3.12) and the energy continuity equations (3.13) of the ESS.

$$P_i^t = P_{G_i}^t - P_{L_i}^t + P_{d_i}^t - P_{ch_i}^t = V_i^t \sum_{k=1}^{nb} V_k^t [G_{ik}\cos(\theta_i^t - \theta_k^t) + B_{ik}\sin(\theta_i^t - \theta_k^t)] \tag{3.25}$$

$$Q_i^t = Q_{G_i}^t - Q_{L_i}^t + Q_{d_i}^t - Q_{ch_i}^t = V_i^t \sum_{k=1}^{nb} V_k^t [G_{ik}\sin(\theta_i^t - \theta_k^t) - B_{ik}\cos(\theta_i^t - \theta_k^t)] \tag{3.26}$$

Inequality constraints include network inequality constraints (3.5) - (3.11), and ESS inequality constraints (3.15) - (3.20).

The Lagrangian function at each period *t* of the OPF problem can be written as:

$$\begin{aligned} L^t = & PC^t + \sum_{i=1}^{nb} \lambda p_i^t \{P_i^t - \sum_{k=1}^{nb} V_i^t V_k^t [G_{ik}\cos(\theta_i^t - \theta_k^t) + B_{ik}\sin(\theta_i^t - \theta_k^t)] - G_{ii}V_i^2\} \\ & + \sum_{k=1}^{nb} \lambda q_i^t \{Q_i^t - \sum_{k=1}^{nb} V_i^t V_k^t [G_{ik}\sin(\theta_i^t - \theta_k^t) - B_{ik}\cos(\theta_i^t - \theta_k^t)] + G_{ii}V_i^2\} \end{aligned}$$

$$+\sum_{i=1}^{ng}\mu p_{i,max}^{t}(P_i^{max}-P_i^t)+\sum_{i=1}^{ng}\mu p_{i,min}^{t}(P_i^t-P_i^{min})+\sum_{i=1}^{ng}\mu q_{i,max}^{t}(Q_i^{max}-Q_i^t)$$
$$+\sum_{i=1}^{ng}\mu q_{i,min}^{t}(Q_i^t-Q_i^{min})+\sum_{i=1}^{nb}\gamma_{i,max}^{t}(V_i^{max}-V_i^t)+\sum_{i=1}^{n}\gamma_{i,min}^{t}(V_i^t-V_i^{min})$$
$$+\sum_{i=1}^{nbr}\zeta_{i,max}^{t}((I_i^{max})^2-(I_i^t)^2)+\sum_{i=1}^{nbr}\zeta_{i,min}^{t}((I_i^t)^2-(I_i^{min})^2)+\sum_{i=1}^{ns}\psi p_{i,max}^{t}(P_{d_i}^{max}-P_{d_i}^t)$$
$$+\sum_{i=1}^{ns}\psi p_{i,min}^{t}(P_{d_i}^t-P_{d_i}^{min})+\sum_{i=1}^{ns}\psi q_{i,max}^{t}(Q_{d_i}^{max}-Q_{d_i}^t)+\sum_{i=1}^{ns}\psi q_{i,min}^{t}(Q_{d_i}^t-Q_{d_i}^{min})$$
$$+\sum_{i=1}^{ns}\phi p_{i,max}^{t}(P_{ch_i}^{max}-P_{ch_i}^t)+\sum_{i=1}^{ns}\phi p_{i,min}^{t}(P_{ch_i}^t-P_{ch_i}^{min})+\sum_{i=1}^{ns}\phi q_{i,max}^{t}(Q_{ch_i}^{max}-Q_{ch_i}^t)$$
$$+\sum_{i=1}^{ns}\phi q_{i,min}^{t}(Q_{ch_i}^t-Q_{ch_i}^{min}) \tag{3.27}$$

where, *nbr* is the number of branches of the system; λp_i^t, λq_i^t, $\mu p_{i,max}^t$, $\mu p_{i,min}^t$, $\mu q_{i,max}^t$, $\mu q_{i,min}^t$, $\gamma_{i,max}^t$, $\gamma_{i,min}^t$, $\zeta_{i,max}^t$, $\zeta_{i,min}^t$, $\psi p_{i,max}^t$, $\psi p_{i,min}^t$, $\psi q_{i,max}^t$, $\psi q_{i,min}^t$, $\phi p_{i,max}^t$, $\phi p_{i,min}^t$, $\phi q_{i,max}^t$, and $\phi q_{i,min}^t$ are Lagrangian multipliers.

At the optimal solution, the following Karush-Kuhn-Tucker (KKT) condition must be satisfied [23]:

$$\frac{\partial L^t}{\partial P_i^t}=\frac{\partial PC^t}{\partial P_i^t}+\lambda p_i^t-\mu p_{i,max}^t+\mu p_{i,min}^t-\psi p_{i,max}^t+\psi p_{i,min}^t+\phi p_{i,max}^t-\phi p_{i,min}^t=0 \tag{3.28}$$

The LMP of real power at each node *i* in each period *t*, which is the marginal cost of serving the next incremental demand at that bus, is defined as:

$$LMP_i^t=\lambda p_i^t=-\frac{\partial PC^t}{\partial P_i^t}+\mu p_{i,max}^t-\mu p_{i,min}^t+\psi p_{i,max}^t-\psi p_{i,min}^t-\phi p_{i,max}^t+\phi p_{i,min}^t \tag{3.29}$$

3.5 Methodology to define candidate ESS locations

In this section, the methodology to define the most suitable candidate locations for ESSs is described. It is performed on a daily basis, employing the OPF model described in 3.4. The best candidate locations of ESSs are then defined based on the Lagrangian multipliers.

The OPF problem is formulated as a sparse and complete model, hence, the Lagrangian multiplier λp_i^t associated to the real power flow equation at bus *i* in period *t* represents the variation of the total production cost with respect to the variation of real injected power at the same bus, i.e., it is the Locational Marginal Price (LMP) at bus *i* in period *t*:

$$\lambda p_i^t=LMP_i^t=-\frac{\partial PC^t}{\partial P_i^t} \tag{3.30}$$

According to the formulation of the OPF model, λp_i^t includes the effects of both real losses and congestions.

From the information provided by the Lagrangian multiplier λp_i^t above, best candidate buses and worst candidate buses for installing ESSs are identified. Indeed, buses with the highest Lagrangian multipliers are selected as the best candidate buses, where any variation of real injected power has greater impact on the production cost than other buses. As a result, if the ESSs are installed at the best candidate buses, their operation will have higher influence on the production cost. In particular, the procedure is described as below:

- Firstly, a base case OPF (without ESS installed) is solved. In this way, the Lagrangian multiplier λp_i^t is determined for each bus *i* at each hour *t*. At this step, constraints on ESSs, including equations (3.12) and (3.15)-(3.16) are removed from the OPF problem. Next, the following parameter df_i is computed for each bus *i*:

  $$df_i = \sum_{t=1}^{T} |\lambda p_i^t| \tag{3.31}$$

  This parameter allows to take into account the effect of the ESSs not only for a specific period, but considering the whole time horizon. It is then sorted: the highest values indicate the most suitable buses for the installation of ESSs. The lowest values, on the other hand, indicate the less sensitive candidates.

- Secondly, based on the total number of ESSs available, they are connected to the system at the best candidate buses and the OPF problem, with all constraints included, is solved.

3.6 Summary

This chapter presents OPF models with ESS integration. The models are formulated to minimize system production cost. The ESSs are used to support wind generation by shifting wind from periods of high wind or low electricity price to periods of low wind or high electricity price. The addition of ESSs into OPF models has introduced time correlation behavior, which results in an optimization problem coupled across time. Consequently, the OPF problems with ESS can be formulated into single-period model which runs independently for each period or multi-period model which runs once for the whole optimization period. Mathematically, multi-period model is a more proper optimization approach to deal with such time-coupled device as ESSs. A methodology to determine candidate buses for ESS installation is also presented. It is based on the Lagrangian multipliers, a byproduct of the OPF model.

CHAPTER 4

Optimization under Uncertainty

4.1 Introduction

A large number of problems in power system planning require that decisions to be made in the presence of uncertainties. Uncertainties, for example, governs equipment failures, electricity demand, and renewable generation, etc. These uncertainty sources can be categorized into two types. The first is configuration uncertainty which relates to transmission line, generator or other equipment failures, in other words, contingencies. The second category is input uncertainty which relates to the limited knowledge on future values of such parameters as electricity demand or generation. Probability distributions and scenario techniques are the common representations of uncertainty. The selection of uncertainty representation depends on the goal of the analysis, the level of underlying uncertainty and knowledge of the underlying uncertainty [24, 25]. In this work, the second category of uncertainty source, i.e., uncertainty in load and wind generation, will be examined. Considering uncertainties in power system planning is becoming more critical as renewable energy technologies, especially wind energy, play an increasing role in the portfolio mix of electricity generation. A key difficulty in optimization under uncertainty is to deal with an uncertainty space, which is usually huge and might lead to very large and computationally intractable optimization models. Consequently, proper techniques for modeling random variables have to be applied.

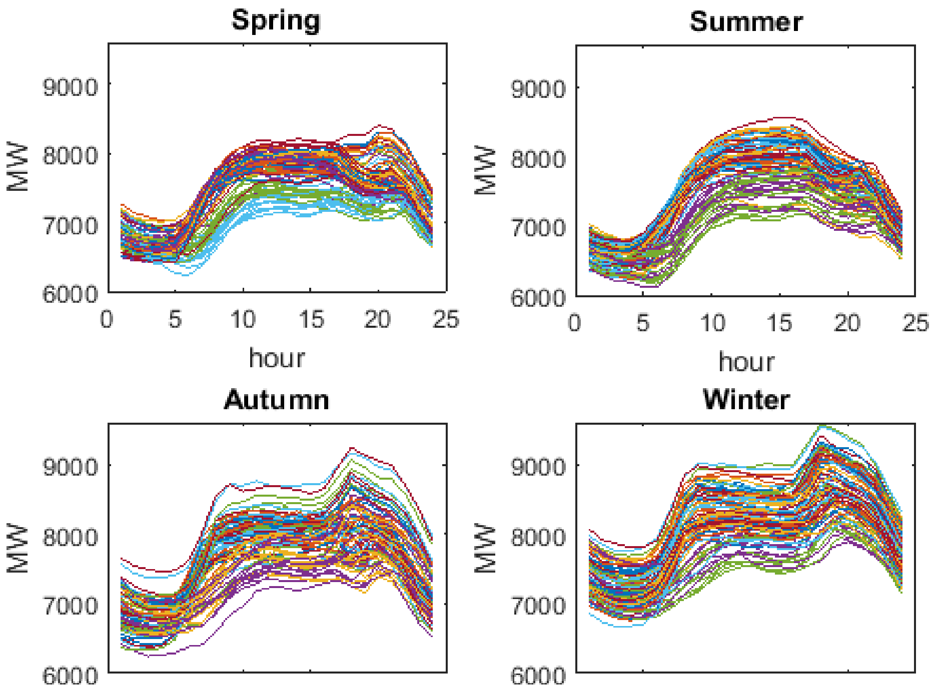

Figure 4.1: *Daily load profiles in 4 seasons*

There has been a variety of approaches developed to cope with the complexity of optimization problems under uncertainty [26–45]. This chapter discusses the approaches that will be adopted in the planning problems with ESSs in the next chapter, including cumulant-based probabilistic approach and the classical recourse-based stochastic programming approach. Theory and methodology of these approaches will be presented.

4.2 Load and wind variability

4.2.1 Load variability

In Figure 4.1, the daily load profiles in 4 seasons of a year is presented [46]. Basically, short-term variations of load (order of seconds to hours) are generally small. In longer term (order of days to years), changes in load tend to be more predictable. The load follows predictable daily, weekly (weekdays and weekends), and seasonal patterns. For example, there is a clear diurnal pattern of morning hour up variations, late afternoon variations, and evening down variations. The seasonal change of daylight and changes in the residential use of electricity as the daylight varies with the season can be observed in the load profiles in different seasons, which results in seasonal variations of the load. The load in each time period can be modeled by superimposing a random noise to the mean load, which has been the basic load modeling method in power system analysis. For the whole period considered, the usual practice in modeling the variability of load is to use a normal distribution.

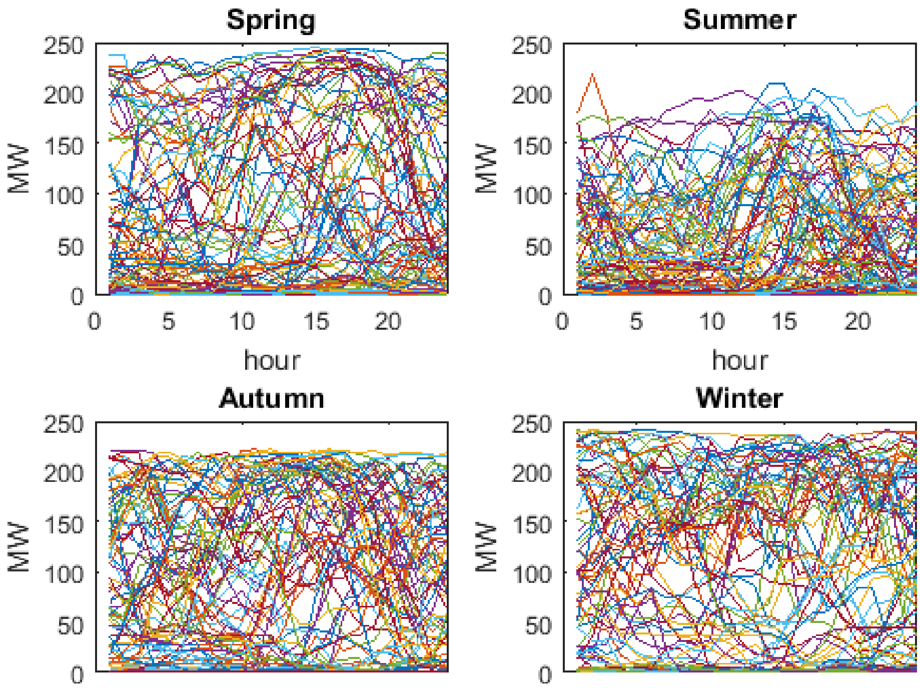

Figure 4.2: *Daily wind profiles in 4 seasons*

4.2.2 Wind variability

In Figure 4.2, the daily wind profiles in 4 seasons of a year is presented [46]. The key difference is that load variations are better understood than wind variations. As can be observed, wind power output is completely different from hour to hour and from day to day, which may vary between zero and the maximum value for any time period. Wind power might be very high in a windy day while pretty low in a non-windy day. On other days, it might be high during night and low during daylight or vice versa. There is no clear pattern of the daily, monthly, weekly or seasonal wind power. With this high variability of wind power, information from the daily mean value or a normal distribution is insufficient to represent its stochasticity.

4.3 Probability representation of uncertainty

Different probability distributions are used to describe different kinds of uncertainty. The following is description of two Probability Density Functions (PDFs), i.e., normal and beta distribution, to be used in this research in the following chapters.

4.3.1 Normal distribution

General formula for the PDF of normal distribution, also called Gaussian distribution, for a random variable $\widetilde{X}$ is [47]:

$$f(x) = \frac{1}{\sigma\sqrt{2\pi}} e^{\frac{(x-\mu)^2}{2\sigma^2}} \tag{4.1}$$

$$-\infty \leq x \leq \infty \tag{4.2}$$

$$\sigma > 0 \tag{4.3}$$

where, μ is mean value of the random variable, which is also called the location parameter; σ is standard deviation of the random variable, which is also called the scale parameter.

The shape of a normal PDF can be seen in Figure 4.3.

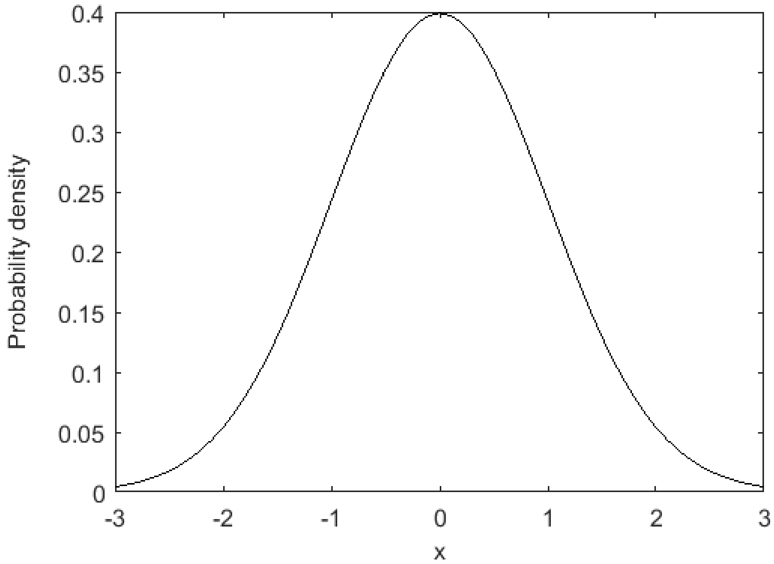

Figure 4.3: *PDF of a normal distribution*

4.3.2 Beta distribution

General formula for the PDF of beta distribution for a random variable $\widetilde{X}$ is [47]:

$$f(x) = \frac{(x-b)^{\alpha-1}(a-x)^{\beta-1}}{B(\alpha,\beta)(a-b)^{\alpha+\beta-1}} \tag{4.4}$$

$$b \leq x \leq a \tag{4.5}$$

$$a > 0 \tag{4.6}$$

$$b > 0 \tag{4.7}$$

where, a and b are upper and lower bounds of the random variable; α and β are the shape parameters; B(α, β) is beta function and:

$$B(\alpha,\beta) = \frac{\Gamma(\alpha)\Gamma(\beta)}{\Gamma(\alpha+\beta)} \tag{4.8}$$

Figure 4.4 is an example of beta PDF for four different values of the shape parameters α and β.

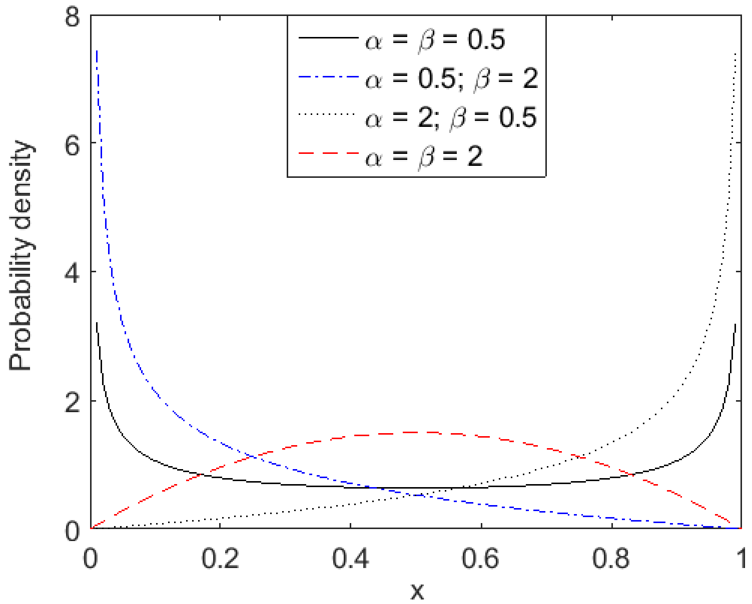

Figure 4.4: *PDF of beta distribution*

4.4 Cumulant-based probabilistic approach

4.4.1 Mathematical background

In this section, fundamental concepts in probability theory and statistics are presented.

4.4.1.1 Functions of random variables

A random variable $\widetilde{X}$ is a function that assigns a value to each of an experiment outcomes. There are two types of random variables, i.e., discrete and continuous. A continuous random variable can take on any value in its sample space. On the contrary, a discrete variable is a variable that can only take a countable number of distinct values.

Cumulative Distribution Function (CDF) $F_{\widetilde{X}}(x)$ of a random variable $\widetilde{X}$ is a function giving the probability that $\widetilde{X}$ is less than or equal to x, for every value x:

$$F_{\widetilde{X}}(x) = \mathbb{P}\{\widetilde{X} \leq x\} \tag{4.9}$$

where $\mathbb{P}\{\cdot\}$ denotes probability.

CDF of a continuous random variable can be defined in terms of its PDF $f_{\widetilde{X}}(x)$:

$$F_{\widetilde{X}}(x) = \int_{-\infty}^{x} f_{\widetilde{X}}(x)dx \tag{4.10}$$

CDF of a discrete random variable can be formed as follows:

$$F_{\widetilde{X}}(x) = \sum_{x_i \leq x} p_i \tag{4.11}$$

where p_i is the probability corresponding to possible values x_i of discrete random variable $\widetilde{X}$.

For a discrete random variable, Probability Mass Function (PMF) is used instead of PDF:

$$f_{\widetilde{X}}(x) = \begin{cases} \mathbb{P}\{\widetilde{X} = x_i\} & \text{if } x = x_i \\ 0 & \text{if } x \neq x_i \end{cases} \tag{4.12}$$

Characteristic function $\psi_{\widetilde{X}}(t)$ of a random variable $\widetilde{X}$ is defined as follows [48]:

$$\psi_{\widetilde{X}}(t) = \mathbb{E}(e^{jt\widetilde{X}}) = \int_{-\infty}^{+\infty} e^{jtx} dF_{\widetilde{X}}(x) \tag{4.13}$$

where, j is the imaginary unit; t is a real variable; and $\mathbb{E}(\cdot)$ is the mathematical expectation operator.

4.4.1.2 Moments and cumulants

- *Moments*

  For a continuous random variable $\widetilde{X}$, the r^{th} ($r \in \{1, 2, 3, \dots\}$) order moment is [48]:

$$m_{\widetilde{X}^r} = \mathbb{E}(\widetilde{X}^r) = \int_{-\infty}^{+\infty} x^r f_{\widetilde{X}}(x) dx \tag{4.14}$$

  The first order moment ($r = 1$) is called mean or expected value of $\widetilde{X}$:

$$m_{\widetilde{X}} = m_{\widetilde{X}^1} = \mathbb{E}(\widetilde{X}) = \int_{-\infty}^{+\infty} x f_{\widetilde{X}}(x) dx \tag{4.15}$$

  A moment of a probability distribution of a random variable about its mean is called central moment. The r^{th} order central moment is as follows:

$$\mu_{\widetilde{X}^r} = \mathbb{E}[(\widetilde{X} - m_{\widetilde{X}})^r] = \int_{-\infty}^{+\infty} (x - m_{\widetilde{X}})^r f_{\widetilde{X}}(x) dx \tag{4.16}$$

  The second central moment ($r = 2$) is called variance, denoted as $\sigma^2_{\widetilde{X}}$, where $\sigma_{\widetilde{X}}$ is the standard deviation of $\widetilde{X}$.

For a discrete random variable $\widetilde{X}$, the r^{th} order moment is calculated:

$$m_{\widetilde{X}^r} = \mathbb{E}(\widetilde{X}^r) = \sum_{i=1}^{\xi} p_i x_i^r \tag{4.17}$$

where ξ is possible values and p_i is the probability corresponding to value x_i of $\widetilde{X}$.

Its mean is:

$$m_{\widetilde{X}} = m_{\widetilde{X}^1} = \mathbb{E}(\widetilde{X}) = \sum_{i=1}^{\xi} p_i x_i \tag{4.18}$$

The r^{th} order central moment is as follows:

$$\mu_{\widetilde{X}^r} = \sum_{i=1}^{\xi} p_i (x_i - m_{\widetilde{X}})^r \tag{4.19}$$

- *Cumulants*

  The cumulants of a probability distribution are a set of quantities that provide an alternative to the moments of the distribution [48].

  Applying a logarithm operator to $\psi_{\widetilde{X}}(t)$ in (4.13) and expanding by a McLaurin's series, the result is:

$$\ln \psi_{\widetilde{X}}(t) = \sum_{r=1}^{n} \frac{k_{\widetilde{X}^r}}{r!} (jt)^r + e_n \tag{4.20}$$

  where $k_{\widetilde{X}^r}$ is defined as the r^{th} ($r \in \{1, 2, 3, \dots\}$) order cumulant of $\widetilde{X}$, e_n is the error of the expansion.

  Cumulants can be obtained from moments and vice versa [49, 50]:

$$\begin{cases} k_{\widetilde{X}^1} = m_{\widetilde{X}^1} \\ k_{\widetilde{X}^{r+1}} = m_{\widetilde{X}^{r+1}} - \sum\limits_{i=1}^{r} C_r^i m_{\widetilde{X}^i} k_{\widetilde{X}^{r-i+1}} \end{cases} \tag{4.21}$$

  and

$$\begin{cases} m_{\widetilde{X}^1} = k_{\widetilde{X}^1} \\ m_{\widetilde{X}^{r+1}} = k_{\widetilde{X}^{r+1}} + \sum\limits_{i=1}^{r} C_r^i m_{\widetilde{X}^i} k_{\widetilde{X}^{r-i+1}} \end{cases} \tag{4.22}$$

  where C_r^i are the binomial coefficients.

- *Joint moments and joint cumulants*

  When random variables are dependent, their joint moments and joint cumulants, so joint PDF and joint characteristic function, are needed to express their relationship. In probability theory and statistics, random variables are independent [1] if the realization of one

[1] Note that "independent" and "uncorrelated" are not the same. Two random variables $\widetilde{X_1}$ and $\widetilde{X_2}$ are uncorrelated

variable does not affect the probability distributions of the others; otherwise, they are dependent.

N *continuous* random variables $\widetilde{X}_i$ (i = 1, 2, ...,N) are jointly continuous if there is a function $f_{\widetilde{X}_1,\widetilde{X}_2,\ ...,\widetilde{X}_N}(x_1, x_2,\ ..., x_N)$, called the joint PDF, such that:

$$\begin{aligned}&\mathbb{P}\{\widetilde{X}_1 \leq t_1, \widetilde{X}_2 \leq t_2, ..., \widetilde{X}_N \leq t_N\}\\ &= \int_{-\infty}^{t_1}\int_{-\infty}^{t_2} ... \int_{-\infty}^{t_N} f_{\widetilde{X}_1,\widetilde{X}_2,\ ...,\widetilde{X}_N}(x_1, x_2,\ ..., x_N)\ dx_1 dx_2 ... dx_N\end{aligned} \tag{4.23}$$

The joint PDF must satisfy:

- $f_{\widetilde{X}_1,\widetilde{X}_2,\ ...,\widetilde{X}_N}(x_1, x_2,\ ..., x_N)\ dx_1 dx_2 ... dx_N \geq 0$
- $\int\limits_{-\infty}^{+\infty}\int\limits_{-\infty}^{+\infty} ... \int\limits_{-\infty}^{+\infty} f_{\widetilde{X}_1,\widetilde{X}_2,\ ...,\widetilde{X}_N}(x_1, x_2,\ ..., x_N)\ dx_1 dx_2 ... dx_N = 1$

For N *discrete* random variables, we define the joint PDF as follows

$$\mathbb{P}\{\widetilde{X}_1 = x_1, \widetilde{X}_2 = x_2, ..., \widetilde{X}_N = x_N\} = f_{\widetilde{X}_1,\widetilde{X}_2,\ ...,\widetilde{X}_N}(x_1, x_2,\ ..., x_N)\ dx_1 dx_2 ... dx_N \tag{4.24}$$

Analogously, the above joint PDF must satisfy:

- $f_{\widetilde{X}_1,\widetilde{X}_2,\ ...,\widetilde{X}_N}(x_1, x_2,\ ..., x_N)\ dx_1 dx_2 ... dx_N \geq 0$
- $\sum\limits_{x_1}\sum\limits_{x_2} ... \sum\limits_{x_N} f_{\widetilde{X}_1,\widetilde{X}_2,\ ...,\widetilde{X}_N}(x_1, x_2,\ ..., x_N) = 1$

The joint characteristic function $\psi_{\widetilde{X}_1,\widetilde{X}_2,\ ...,\widetilde{X}_N}(t_1, t_2,\ ..., t_N)$ of N random variables $\widetilde{X}_i$ (i = 1, 2, ...,N) is defined as follows [51]:

$$\begin{aligned}&\psi_{\widetilde{X}_1,\widetilde{X}_2,\ ...,\widetilde{X}_N}(t_1, t_2,\ ..., t_N) = E(e^{j\boldsymbol{t}^T\widetilde{\boldsymbol{X}}})\\ &= \overbrace{\int_{-\infty}^{+\infty}\int_{-\infty}^{+\infty} ... \int_{-\infty}^{+\infty}}^{N\ times} e^{j\boldsymbol{t}^T\boldsymbol{x}}\ f_{\widetilde{X}_1,\widetilde{X}_2,\ ...,\widetilde{X}_N}(x_1, x_2,\ ..., x_N)\ dx_1 dx_2 ... dx_N\end{aligned} \tag{4.25}$$

where, $\boldsymbol{t} = [t_1, t_2,\ ..., t_N]^T$ and $\boldsymbol{x} = [x_1, x_2,\ ..., x_N]^T$.

when their covariance $Cov(\widetilde{X_1}, \widetilde{X_2})$ is zero: $Cov(\widetilde{X_1}, \widetilde{X_2}) = \mathbb{E}(\widetilde{X_1}\widetilde{X_2}) - \mathbb{E}(\widetilde{X_1})\mathbb{E}(\widetilde{X_2})$ = 0. If two random variables are uncorrelated, there is no linear relationship between them. If two random variables are independent, they are also uncorrelated; however, the converse is not always true since they can still be dependent. The key point here is that correlation is only a measure of linear dependence. The only case in which lack of correlation implies independence is when the joint distribution of two random variables is Gaussian.

The r^{th} order joint moment can be obtained as [51]:

$$\begin{aligned} m_{\widetilde{X}_1^{r_1},\widetilde{X}_2^{r_2},\,...,\widetilde{X}_N^{r_N}} &= \mathbb{E}(\widetilde{X}_1^{r_1}\widetilde{X}_2^{r_2}...\widetilde{X}_N^{r_N}) \\ &= \overbrace{\int_{-\infty}^{+\infty}\int_{-\infty}^{+\infty}...\int_{-\infty}^{+\infty}}^{N\ times} x_1^{r_1}x_2^{r_2}...x_N^{r_N}\ f_{\widetilde{X}_1,\widetilde{X}_2,\,...,\widetilde{X}_N}(x_1,x_2,\ ...,x_N)\ dx_1dx_2...dx_N \end{aligned} \tag{4.26}$$

where, $r_1 + r_2 + \cdots + r_N = r$.

Similarly as in (4.20), expanding $\ln\psi_{\widetilde{X}_1,\widetilde{X}_2,\,...,\widetilde{X}_N}(t_1,t_2,\ ...,t_N)$ using McLaurin's series [51], the result is:

$$\ln\psi_{\widetilde{X}_1,\widetilde{X}_2,\,...,\widetilde{X}_N}(t_1,t_2,\ ...,t_N) = \sum_{r_1,r_2,\ ...,r_N=0}^{\infty} k_{\widetilde{X}_1^{r_1},\widetilde{X}_2^{r_2},...,\widetilde{X}_N^{r_N}} \frac{(jt_1)^{r_1}}{r_1!}\frac{(jt_2)^{r_2}}{r_2!}\cdots\frac{(jt_N)^{r_N}}{r_N!} \tag{4.27}$$

where $k_{\widetilde{X}_1^{r_1},\widetilde{X}_2^{r_2},...,\widetilde{X}_N^{r_N}}$ is the r^{th} order joint cumulant of the N random variables.

Suppose that $\widetilde{Z}$ is a random variable, linearly combined by N random variables $\widetilde{X}_i$ (i = 1, 2, ...,N):

$$\widetilde{Z} = a_1\widetilde{X}_1 + a_2\widetilde{X}_2 + \cdots + a_N\widetilde{X}_N \tag{4.28}$$

If the N random variables $\widetilde{X}_i$ are independent, the r^{th} order cumulant of $\widetilde{Z}$ is calculated as follows [51]:

$$k_{\widetilde{Z}^r} = a_1^r k_{\widetilde{X}_1^r} + a_2^r k_{\widetilde{X}_2^r} + \cdots + a_N^r k_{\widetilde{X}_N^r} \tag{4.29}$$

In contrast, $k_{\widetilde{Z}^r}$ is calculated by using some formulas [51, 52] as in (4.30) where the first three cumulants are given:

$$\begin{aligned} k_{\widetilde{Z}^1} &= \mathbb{E}(\sum_{i=1}^{N} a_i\widetilde{X}_i) = \sum_{i=1}^{N} a_i k_{\widetilde{X}_i^1} \\ k_{\widetilde{Z}^2} &= \mathbb{E}[(\sum_{i=1}^{N} a_i\widetilde{X}_i)^2] - [\mathbb{E}(\sum_{i=1}^{N} a_i\widetilde{X}_i)]^2 \\ &= \sum_{i=1}^{N} a_i^2 k_{\widetilde{X}_i^2} + 2\sum_{i=1,i<j}^{N} a_i a_j k_{\widetilde{X}_i,\widetilde{X}_j} \\ k_{\widetilde{Z}^3} &= \mathbb{E}[(\sum_{i=1}^{N} a_i\widetilde{X}_i)^3] - 3\mathbb{E}(\sum_{i=1}^{N} a_i\widetilde{X}_i)\mathbb{E}[(\sum_{i=1}^{N} a_i\widetilde{X}_i)^2] + 2[\mathbb{E}(\sum_{i=1}^{N} a_i\widetilde{X}_i)]^3 \\ &= \sum_{i=1}^{N} a_i^3 k_{\widetilde{X}_i^3} + 3\sum_{i=1,i\neq j}^{N} a_i^2 a_j k_{\widetilde{X}_i^2,\widetilde{X}_j} + 6\sum_{i=1,i<j<l}^{N} a_i a_j a_l k_{\widetilde{X}_i,\widetilde{X}_j,\widetilde{X}_l}\cdots \end{aligned} \tag{4.30}$$

4.4.2 Constructing probability distributions for random variables

For cumulant-based approaches, series expansions (e.g., Gram-Charlier, Edgeworth, etc.) are widely used to estimate distribution functions of desired random variables from their cumulants or moments. These expansions give an approximation of a PDF and/or a CDF of a random variable around the Gaussian distribution: they are expected to give a good approximation if the considered distribution is nearly Gaussian. However, if non-Gaussian distributions (e.g., Beta, Weibull, discrete distributions) are taken into account, such input distributions will make output distributions far from Gaussian distribution, and hence the accuracy of these approximations could be significantly affected.

In this research, a technique is developed to enhance cumulant-based probabilistic optimization approach for taking into account different types of input probability distributions of practical interest and building distributions of output random variables. It effectively combines Von Mises method and Gram-Charlier expansion [53]. This makes the proposed approach more interesting from the practical point of view.

Von Mises method [50, 54, 55] allows to define a discrete distribution characterized by ν impulses using the first (2ν-1) moments m_0, m_1, ..., $m_{2\nu-2}$. The steps to obtain the discrete distribution are presented in the following, while theoretical rationale for the following formulas can be found in [54, 56]

Determinants $D_0, D_1, ..., D_{\nu-1}$ are first defined as follows:

$$D_0 = |m_0| \tag{4.31}$$

$$D_1 = \begin{vmatrix} m_0 & m_1 \\ m_1 & m_2 \end{vmatrix} \tag{4.32}$$

$$D_{\nu-1} = \begin{vmatrix} m_0 & m_1 & \cdots & m_{\nu-1} \\ m_1 & m_2 & \cdots & m_\nu \\ \vdots & \vdots & \ddots & \vdots \\ m_{\nu-1} & m_\nu & \cdots & m_{2\nu-2} \end{vmatrix} \tag{4.33}$$

If D_0 to $D_{\nu-1}$ are positive, there exists a distribution with not less than ν impulses.

Next, the vector $\boldsymbol{m}$ is built:

$$\boldsymbol{m} = -\left[m_\nu, m_{\nu+1}, ..., m_{2\nu-1}\right]^T \tag{4.34}$$

and (4.35) is solved to obtain $\boldsymbol{c}$:

$$[\boldsymbol{D}_{\nu-1}]\boldsymbol{c} = \boldsymbol{m} \tag{4.35}$$

where $[\boldsymbol{D}_{\nu-1}]$ is the matrix corresponding to determinant $D_{\nu-1}$.

$\boldsymbol{c}$ is substituted in (4.36), solved to obtain $\boldsymbol{x}$:

$$x^{\nu} + c_{\nu-1}x^{\nu-1} + \cdots + c_1 x + c_0 = 0 \tag{4.36}$$

Solution $\boldsymbol{x}$ is used to solve (4.37) for probabilities p_i (corresponding to x_i) and, eventually, PDF and CDF can be obtained.

$$\begin{bmatrix} 1 & 1 & \cdots & 1 \\ x_1 & x_2 & \cdots & x_\nu \\ x_1^2 & x_2^2 & \cdots & x_\nu^2 \\ \vdots & \vdots & \ddots & \vdots \\ x_1^{\nu-1} & x_2^{\nu-1} & \cdots & x_\nu^{\nu-1} \end{bmatrix} \begin{bmatrix} p_1 \\ p_2 \\ p_3 \\ \vdots \\ p_\nu \end{bmatrix} = \begin{bmatrix} m_0 \\ m_1 \\ m_2 \\ \vdots \\ m_{\nu-1} \end{bmatrix} \tag{4.37}$$

The desired discrete distribution is characterized by ν impulses with abscissas x_i and corresponding probabilities p_i.

Based on Von Mises method, an approximated approach was developed to obtain probability distribution for an output random variable [54], in which the continuous and discrete distributions of input random variables are treated separately.

Assume that an output random variable $\widetilde{Z}_i$ is the sum of two components:

$$\widetilde{Z}_i = \widetilde{Z_{i_c}} + \widetilde{Z_{i_d}} \tag{4.38}$$

where, $\widetilde{Z_{i_c}}$ and $\widetilde{Z_{i_d}}$ are continuous and discrete parts, respectively.

In cumulant-based approaches, each output random variable is represented by a linear combination of input random variables. When applying cumulant-based approaches in power system, discrete distributions are usually used to represent input random variables such as random branch outages, unscheduled generating unit outages, etc., while continuous distributions are used for describing input random variables like load. Continuous part $\widetilde{Z_{i_c}}$ and discrete part $\widetilde{Z_{i_d}}$ are formed by continuous and discrete distributions of input random variables, respectively.

The approximated approach was originally proposed and tested by the authors of [54], assuming that continuous part has Gaussian distribution. In this case, the PDF of $\widetilde{Z}_i$ is:

$$f_{\widetilde{Z}_i}(x) = \sum_{i=1}^{\nu} p_i f_{\widetilde{Z_{i_c}}}(x - x_i) \tag{4.39}$$

where ν, x_i, and p_i are the number of impulses considered, abscissas, and corresponding probabilities of $\widetilde{Z_{i_d}}$, and $f_{\widetilde{Z_{i_c}}}(\cdot)$ is the PDF of the normally distributed $\widetilde{Z_{i_c}}$ [50]:

$$f_{\widetilde{Z_{i_c}}}(x) = \frac{1}{\sqrt{2\pi}\sigma_{\widetilde{Z_{i_c}}}} \exp(-\frac{(x - m_{\widetilde{Z_{i_c}}})^2}{2\sigma^2_{\widetilde{Z_{i_c}}}}) \tag{4.40}$$

where $m_{\widetilde{Z_{i_c}}}$ and $\sigma_{\widetilde{Z_{i_c}}}$ are the mean and standard deviation of $\widetilde{Z_{i_c}}$, respectively.

The CDF of $\widetilde{Z_i}$ is as follows:

$$F_{\widetilde{Z_i}}(x) = \sum_{i=1}^{\nu} p_i F_{\widetilde{Z_{i_c}}}(\frac{x - x_i - m_{\widetilde{Z_{i_c}}}}{\sigma_{\widetilde{Z_{i_c}}}}) \tag{4.41}$$

where $F_{\widetilde{Z_{i_c}}}(\cdot)$ is the CDF of $\widetilde{Z_{i_c}}$:

$$F_{\widetilde{Z_{i_c}}}(x) = \frac{1}{\sqrt{2\pi}} \int_{-\infty}^{x} \exp(-\frac{t^2}{2})dt \tag{4.42}$$

However, for a practical application in power systems, various non-Gaussian distributions need to be taken into account [53]. In this section, continuous part, that may be a non-Gaussian distribution, is first approximated by Gram-Charlier expansion [57], then PDF and CDF of random variable $\widetilde{Z_i}$ are obtained by combining the discrete and continuous contributions:

$$f_{\widetilde{Z_i}}(x) = \sum_{i=1}^{\nu} p_i[\phi(x_{_{Ni}}) + \phi(x_{_{Ni}}) \sum_{l=1}^{\infty} c_l H_l(x_{_{Ni}})] \tag{4.43}$$

$$F_{\widetilde{Z_i}}(x) = \sum_{i=1}^{\nu} p_i[\Phi(x_{_{Ni}}) + \phi(x_{_{Ni}}) \sum_{l=1}^{\infty} c_l H_{l-1}(x_{_{Ni}})] \tag{4.44}$$

where, ν is the number of impulses considered; $x_{_{Ni}} = (x - x_i - m_{\widetilde{Z_{i_c}}})/\sigma_{\widetilde{Z_{i_c}}}$; x_i and p_i are abscissas and probabilities corresponding to ν impulses of $\widetilde{Z_{i_d}}$, respectively; $m_{\widetilde{Z_{i_c}}}$ and $\sigma_{\widetilde{Z_{i_c}}}$ are the mean and standard deviation of $\widetilde{Z_{i_c}}$; c_l is a coefficient that can be obtained from cumulants of $\widetilde{Z_{i_c}}$; $H_l(\cdot)$ is the l^{th} order of the so-called Hermite polynominal; formulas for calculation of c_l and $H_l(\cdot)$ can be found in [58]; $\phi(x_{_{Ni}})$ and $\Phi(x_{_{Ni}})$ are the PDF and CDF of standard normal distribution:

$$\phi(x_{_{Ni}}) = \frac{1}{\sqrt{2\pi}} e^{\frac{-x^2}{2}} \tag{4.45}$$

$$\Phi(x_{_{Ni}}) = \int_{-\infty}^{x_{_{Ni}}} \frac{1}{\sqrt{2\pi}} e^{\frac{-t^2}{2}} dt \tag{4.46}$$

It is worth noticing that for the technique to construct probability distributions for random variables presented in this section a suitable value of the order of cumulants to be adopted in the computations should be selected, as it determines the maximum number of impulses that can be considered in the resulting discrete distributions. The accuracy can be increased by using moments of higher order (higher number of impulses ν used); however, since increasing the number of impulses makes the method more cumbersome, accuracy and computational intensity should be balanced [55].

4.4.3 Application of cumulants to Probabilistic Optimal Power Flow

The general model for OPF is presented in detail in Section 3.2. The relationship between vectors of output and input variables is generally formulated as follows:

$$\boldsymbol{z} = h(\boldsymbol{x}) \tag{4.47}$$

where, $\boldsymbol{x}$ is the vector of input variables; $\boldsymbol{z}$ is the vector of output variables; $h(\cdot)$ is a multivariate nonlinear function mapping between input and output.

Cumulant-based POPF relies on the behavior of random variables when they are combined in a linearized fashion [59] around the solution of a deterministic OPF. In the following, the formation of output random variables from a linear combination of input random variables and the steps to calculate cumulants and form probability distributions of desired output random variables are presented.

At first, a deterministic OPF is solved. At the optimum, KKT optimality conditions must be fulfilled [59].

Incorporating variables into the first-order KKT conditions, then:

$$F(\boldsymbol{z}, \boldsymbol{x}) = 0 \tag{4.48}$$

where, $F(\cdot)$ is set of nonlinear equations determining the first-order KKT conditions.

The relationship between $\boldsymbol{z}$ and $\boldsymbol{x}$ is formed by taking full derivative of (4.48):

$$\mathbf{H}_{\mathcal{L}} \Delta \boldsymbol{z} + \Delta \boldsymbol{x} = 0 \tag{4.49}$$

where, $\Delta \boldsymbol{z}$ and $\Delta \boldsymbol{x}$ are changes of vectors of output and input variables, respectively; $\mathbf{H}_{\mathcal{L}}$ is the Hessian matrix of the Lagrangian function with respect to $\boldsymbol{z}$.

Equation (4.49) is arranged as:

$$\Delta \boldsymbol{z} = -\mathbf{H}_{\mathcal{L}}^{-1} \Delta \boldsymbol{x} \tag{4.50}$$

When the input variables of the OPF problem are uncertain, the problem is defined as a POPF problem. Each element x_ℓ ($\ell = 1, 2, ..., N$) of vector $\boldsymbol{x}$ in (4.47) is considered as the realization of a random variable $\widetilde{X_\ell}$. From relationships in (4.50), each element z_ℓ of $\boldsymbol{z}$ is, therefore, the realization of corresponding random variable $\widetilde{Z_\ell}$. Consequently, we have the relationship between output and input random variables as follows:

$$\begin{bmatrix} \widetilde{Z_1} \\ \widetilde{Z_2} \\ \vdots \\ \widetilde{Z_N} \end{bmatrix} = \mathbf{M} \begin{bmatrix} \widetilde{X_1} \\ \widetilde{X_2} \\ \vdots \\ \widetilde{X_N} \end{bmatrix} \tag{4.51}$$

where, $\mathbf{M} = -\mathbf{H}_{\mathcal{L}}^{-1}$.

$\mathbf{M}$ can be written in the following form

$$\mathbf{M} = \begin{bmatrix} a_{1,1} & a_{1,2} & \cdots & a_{1,N} \\ a_{2,1} & a_{2,2} & \cdots & a_{2,N} \\ \vdots & \vdots & \ddots & \vdots \\ a_{N,1} & a_{N,2} & \cdots & a_{N,N} \end{bmatrix} \tag{4.52}$$

then each output random variable $\widetilde{Z_\ell}$ is a linear combination of input random variables $\widetilde{X_1}$, $\widetilde{X_2}$, ..., $\widetilde{X_N}$ as follows:

$$\begin{aligned} \widetilde{Z_1} &= a_{1,1}\widetilde{X_1} + a_{1,2}\widetilde{X_2} + \cdots + a_{1,N}\widetilde{X_N} \\ \widetilde{Z_2} &= a_{2,1}\widetilde{X_1} + a_{2,2}\widetilde{X_2} + \cdots + a_{2,N}\widetilde{X_N} \\ &\vdots \\ \widetilde{Z_N} &= a_{N,1}\widetilde{X_1} + a_{N,2}\widetilde{X_2} + \cdots + a_{N,N}\widetilde{X_N} \end{aligned} \tag{4.53}$$

When N input random variables $\widetilde{X}_\ell$ are independent, (4.29) is used to calculate cumulants of output random variables. The r^{th} order cumulant of ℓ^{th} output random variable $\widetilde{Z_\ell}$ is:

$$k_{\widetilde{Z_\ell}^r} = a_{\ell,1}^r k_{\widetilde{X}_1^r} + a_{\ell,2}^r k_{\widetilde{X}_2^r} + \cdots + a_{\ell,N}^r k_{\widetilde{X}_N^r} \tag{4.54}$$

On the contrary, (4.30) is used and $k_{\widetilde{Z_\ell}^r}$ is obtained as follows:

$$k_{\widetilde{Z_\ell}^1} = \mathbb{E}(\sum_{i=1}^{N} a_{\ell,i}\widetilde{X}_i) = \sum_{i=1}^{N} a_{\ell,i} k_{\widetilde{X}_i^1} \tag{4.55}$$

$$k_{\widetilde{Z_\ell}^2} = \mathbb{E}[(\sum_{i=1}^{N} a_{\ell,i}\widetilde{X}_i)^2] - [\mathbb{E}(\sum_{i=1}^{N} a_{\ell,i}\widetilde{X}_i)]^2 \tag{4.56}$$

$$= \sum_{i=1}^{N} a_{\ell,i}^2 k_{\widetilde{X}_i^2} + 2 \sum_{i=1,i<j}^{N} a_{\ell,i}a_{\ell,j} k_{\widetilde{X}_i,\widetilde{X}_j} \tag{4.57}$$

$$k_{\widetilde{Z}_\ell^3} = \mathbb{E}[(\sum_{i=1}^{N} a_{\ell,i}\widetilde{X}_i)^3] - 3\mathbb{E}(\sum_{i=1}^{N} a_{\ell,i}\widetilde{X}_i)\mathbb{E}[(\sum_{i=1}^{N} a_{\ell,i}\widetilde{X}_i)^2] + 2[\mathbb{E}(\sum_{i=1}^{N} a_{\ell,i}\widetilde{X}_i)]^3 \quad (4.58)$$

$$= \sum_{i=1}^{N} a_{\ell,i}^3 k_{\widetilde{X}_i^3} + 3\sum_{i=1,i\neq j}^{N} a_{\ell,i}^2 a_{\ell,j} k_{\widetilde{X}_i^2,\widetilde{X}_j} + 6\sum_{i=1,i<j<s}^{N} a_{\ell,i}a_{\ell,j}a_{\ell,l}k_{\widetilde{X}_i,\widetilde{X}_j,\widetilde{X}_s\cdots} \quad (4.59)$$

$$\vdots \quad (4.60)$$

$$(4.61)$$

Based on either (4.54) or (4.55), cumulants of output random variables can be calculated from cumulants of input random variables. Probability distributions of output random variables are then obtained by adopting the technique presented in Section 4.4.2.

When solving a cumulant-based POPF above, the operational limitations of random variables are not considered in their distributions. In fact, operational limitations must be enforced during the optimization process [59]. For example, suppose a random variable $\widetilde{Z}_i$ has lower limit of 0.9 p.u. and upper limit of 1.1 p.u. (such as random variable of a nodal voltage) as shown in Fig. 4.5. In this case, the PDF of $\widetilde{Z}_i$ should be truncated on both sides at its lower limit (0.9 p.u.) and upper limit (1.1 p.u.) since the distribution beyond the limits is not valid. The resulting truncated PDF is normalized to have total probability equal to 1 [60]. Analogously, if a random variable has only upper limit (e.g., random variable of a branch current), its PDF should be truncated on the right side at the upper limit (see Fig. 4.6 for an upper limit of 0.52 p.u.). Techniques for truncation of a PDF can be found in [60].

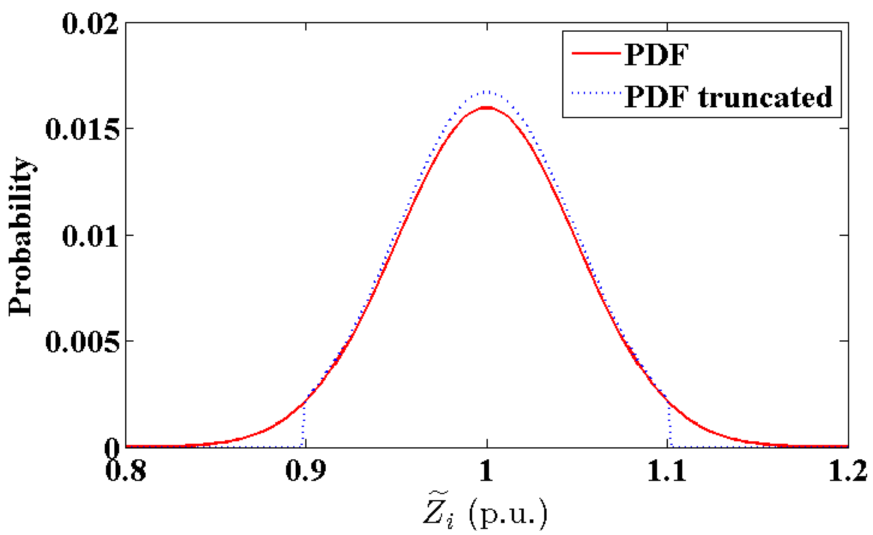

Figure 4.5: *Example of truncation on both sides of a PDF*

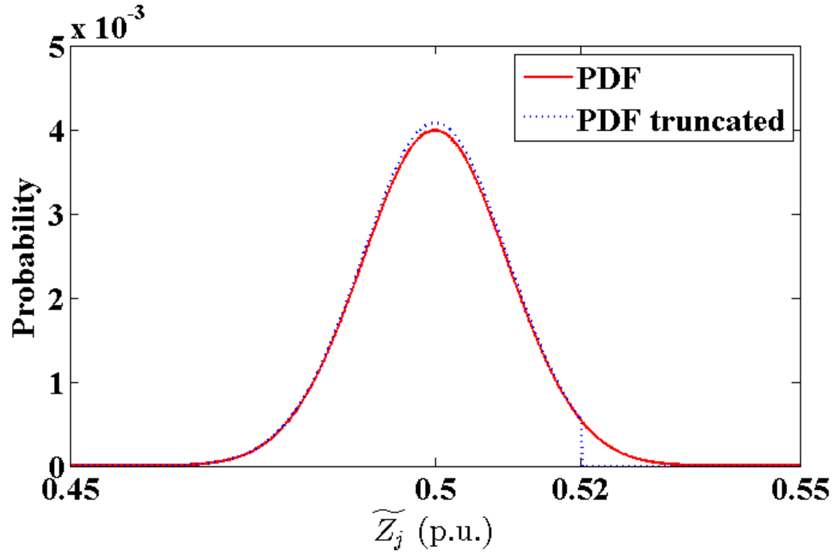

Figure 4.6: *Example of truncation on the right side of a PDF*

4.5 Recourse-based stochastic programming

4.5.1 Introduction

Handling uncertainty in an optimization problem requires some knowledge about the uncertainty. However, there is not always sufficient information about it; hence, many methods have been developed to model the uncertainty. Major approaches recognized to deal with uncertainty in optimization include fuzzy programming, stochastic programming, and robust optimization. In fuzzy programming, if no historical data are available, it is difficult to represent uncertainty with probabilistic distributions. Therefore, fuzzy numbers are adopted. In stochastic programming, uncertain parameters are represented as random variables with an assumption that their probability distributions can be known or estimated. This programming approach usually leads to specific procedures that take into account the probabilistic aspects. Robust optimization, which seeks to optimize system performance against the worst-case scenario, assumes uncertain data belong to some uncertainty set. Basic versions of robust optimization assume constraint violation cannot be allowed for any realization of the data in the uncertainty set [61, 62].

Stochastic Programming (SP) was first introduced by George Dantzig in the 1950s. Since then, major progress has been made in developing algorithms or techniques for solving them. As a result, SP has become an optimization approach for making decisions under uncertainty in large-scale models. In probabilistic approaches such as cumulant or point estimate method, a deterministic formulation is retained and uncertain system inputs (e.g., load and generation) are represented by probability distributions. Moreover, its optimal solution, i.e., the values of control variables, is not influenced by the randomness of uncertain system inputs, but only the probability distributions of control variables are determined by them. On the contrary, stochastic programming approaches not only treat uncertain system inputs as random distributions, but also establishes stochastic formulation for the problem. That is, either the objective function or constrains in the optimization model are described as probability equations or inequalities. The randomness of uncertain system inputs directly influences the optimization result during the solution of stochastic problems [63].

SP traces its root to [64], where recourse models were first introduced, and [65], where probabilistic constraint models were introduced. Recourse models involve some decisions or *recourse actions* taken after uncertainty is known. Uncertainty is usually described using probability distributions, densities or, more generally, probability measures. In recourse models, there are a number of decisions made without full information on the uncertain parameters. All these decisions are called *first-stage decisions* and the period when these decisions are taken is called the *first stage*. After full information is received on the realization of the random events, *recourse actions* or *corrective actions* are taken in later stages. In probabilistic or chance-constraint model, some of the constraints or the objective are expressed in terms of probabilistic statements about first-stage decisions. The idea is that infeasibilities in the second stage are allowed at a certain penalty. In this model, the focus is on system reliability which is expressed as a minimum requirement on the probability of satisfying constraints [66, 67].

A basic formulation of recourse model is the two-stage stochastic programming model. Under the standard two-stage model, the set of decisions is divided into two groups. The *first-stage* or *here-and-now* decision variables are those that have to be decided before the realization of random variables and once the uncertain parameters are known, further actions can be made by selecting, at a certain cost, the values of *second-stage* or *wait-and-see* variables. These second-stage decisions can be considered as corrective measures or recourse against any infeasibility arisen due to a particular realization of uncertain parameters. Due to uncertainty, the second-stage cost is a random variable. The goal of a two-stage model is to identify a first-stage decision that is well positioned against all possible observations of random parameters. An optimal solution tends to have the property that the first-stage decision leaves the second-stage decision in a way to exploit advantageous outcomes of random events without excessive vulnerability to disadvantageous outcomes. The worst-case version of this model corresponds to adjustable robust optimization model, in which the probability measure of random parameters belongs to an uncertainty set.

The two-stage formulation can be extended to a multi-stage setting when a sequence of decisions is made to react to outcomes that evolve over time. In other words, when the pattern "decide-observe-decide..." is repeated several times, a multi-stage problem is formed. In multi-stage formulation, uncertainty is modeled as a filtration process and under discrete distributions, which reduces to a scenario tree of parameter realizations [67]. Recourse models have been applied to linear, integer, and non-linear programming. In the planning problem in this research, a two-stage non-linear stochastic programming is applied.

4.5.2 Two-stage non-linear stochastic programming

The idea is to take first-stage decisions that are in average optimal, with the possibility to take some corrective decisions after uncertainty is revealed. This defines an objective function and constraints associated to the first-stage variables, whereas for the second-stage variables, another objective function and constraints, which depend on the realization of random parameters, are considered. The two stages are then combined by adding the expectation of the second-stage objective to the first-stage objective. The resulting program is called two-stage stochastic (nonlinear) program with (additive) recourse. Generally, a two-stage stochastic programming problem has the form [61, 68]:

$$\begin{aligned} \min_{\mathbf{x}} \quad & z(\mathbf{x}) = f(\mathbf{x}) + \mathcal{Q}(\mathbf{x}) \\ \text{s.t.} \quad & g_1(\mathbf{x}) \leq 0 \\ & g_2(\mathbf{x}) = 0 \end{aligned} \tag{4.62}$$

where, $f(\mathbf{x})$ is the first-stage objective function; $g_1(\mathbf{x})$ and $g_2(\mathbf{x})$ are first-stage inequality and equality constraints, respectively; $\mathcal{Q}(\mathbf{x})$ = $\mathbb{E}[\mathrm{Q}(\mathbf{x},\boldsymbol{\xi})]$ and $\mathrm{Q}(\mathbf{x},\boldsymbol{\xi})$ is the optimal value of the second-stage problem:

$$\begin{aligned} Q(\mathbf{x}, \boldsymbol{\xi}) = \min_{\mathbf{y}} \quad & F(\mathbf{y}, \boldsymbol{\xi}) \\ \text{s.t.} \quad & G_1(\mathbf{y}, \boldsymbol{\xi}) \leq 0 \\ & G_2(\mathbf{y}, \boldsymbol{\xi}) = 0 \end{aligned} \tag{4.63}$$

where, $\mathbf{x}$ is a vector of first-stage decision variables, $\mathbf{y}$ is a vector of second-stage decision variables, $\boldsymbol{\xi}$ is a vector of realizations of random variable $\widetilde{\Xi}_i$, and the expectation operator $\mathbb{E}$ at the first-stage problem (4.62) is taken with respect to probability distribution of the random parameters $\boldsymbol{\xi}$. The second-stage decision vector $\mathbf{y}$ is sometimes written $\mathbf{y}(\boldsymbol{\xi})$ or even $\mathbf{y}(\boldsymbol{\xi}, \mathbf{x})$, to stress that $\mathbf{y}$ differs according to the outcome of the random events and of the first-stage decisions. Thus, the sequence of events and decisions in the two-stage problem can be summarized as in (4.5.2). That is, the first-stage decisions $\mathbf{x}$ should be made *before* a realization of the random parameter $\boldsymbol{\xi}$ is obtained and hence, should be independent of the random parameter, while the second-stage decision variable $\mathbf{y}$ is made *after* observing the random parameter and are functions of the random parameter [61, 68].

$$\text{Decision} \quad \mathbf{x} \rightarrow \text{Observation} \quad \boldsymbol{\xi} \rightarrow \text{Decision} \quad \mathbf{y}(\boldsymbol{\xi})$$

This decision process can be better visualized by means of a graph called scenario tree (Figure 4.7). The root of this tree corresponds to the first-stage decision, which is usually planning decision, made before any realization of the random parameters. The nodes connected to the root are the second-stage nodes and represent the points where second-stage decisions, which are usually operational decisions, are made. Each realization ξ_i of the random variable $\widetilde{\Xi}_i$ in the second-stage, is associated with a node and each node is associated with a probability of occurrence. A branch emanating from a node represents a scenario, which is possible realizations of the uncertain parameters from that node.

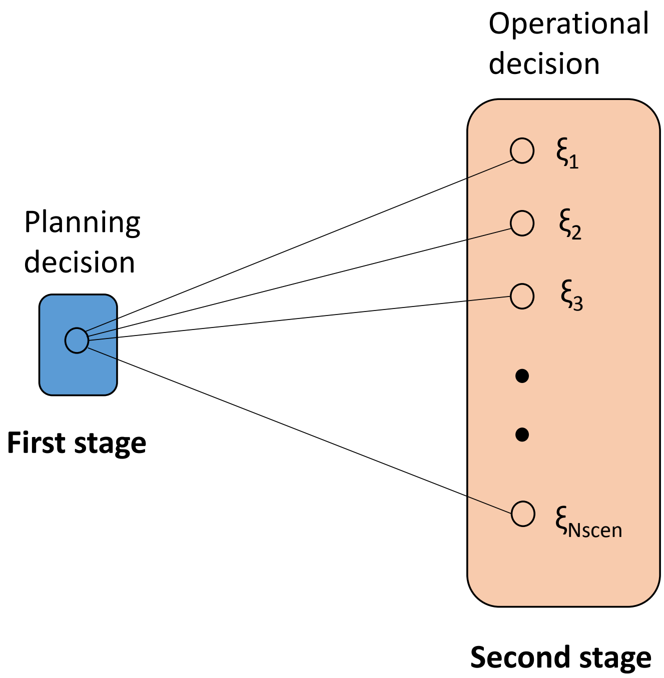

Figure 4.7: *Two-stage scenario tree*

4.5.3 Solution method

If $\widetilde{\Xi}_i$ is a continuous random variable, $\mathcal{Q}(\mathbf{x})$ is differentiable even if Q($\mathbf{x}$, $\boldsymbol{\xi}$) is not everywhere (but almost everywhere) differentiable with respect to x. However, if $\widetilde{\Xi}_i$ is discrete, $\mathcal{Q}(\mathbf{x})$ is no more everywhere differentiable. Since non-differentiable problems are difficult to manage, especially for non-linear non-convex functions, a formulation that restores the differentiability property is applied. Assume $\widetilde{\Xi}_i$ is a discrete random variable with N_{scen} possible realizations ξ_ω, $\omega = 1, \ldots, N_{scen}$. Let p_ω be the probability of each realization ω of the random variable $\widetilde{\Xi}_i$. Practical methods for two-stage problems are usually based on the extensive form, also called *dual decomposition* structure, of the stochastic program (4.62) - (4.63) [61]:

$$\begin{aligned}
\min_{\mathbf{x}} \quad & \{z(\mathbf{x}) = f(\mathbf{x}) + \sum_{\omega=1}^{N_{scen}} p_\omega F(y_\omega, \xi_\omega)\} \\
\text{s.t.} \quad & g_1(\mathbf{x}) \leq 0 \\
& g_2(\mathbf{x}) = 0 \\
& G_1(y_\omega, \xi_\omega) \leq 0 \\
& G_2(y_\omega, \xi_\omega) = 0
\end{aligned} \tag{4.64}$$

This formulation is obtained by defining second-stage vectors, one for each realization of $\widetilde{\Xi}_i$ while maintaining only one variable for the first-stage. The resulting problem is then differentiable, and has a formulation similar to classical mathematical programs.

The problem (4.64) already includes *nonanticipativity* constraints. Nonanticipativity constraints guarantee that the first-stage variables are identical across all scenarios and scenario-related programs are linked only by these constraints. The formulation (4.65) is the reformulation of problem (4.64), and it represents the requirement of nonanticipativity explicitly with nonanticipativity constraints. In this case, the first-stage variable x is introduced for each scenario and the last constraints represent nonanticipativity constraints.

$$\begin{aligned}
\min_{\mathbf{x}} \quad & \{z(\mathbf{x}) = \sum_{\omega=1}^{N_{scen}} p_\omega[f(x_\omega) + F(y_\omega, \xi_\omega)\} \\
\text{s.t.} \quad & g_1(x_\omega) \leq 0 \\
& g_2(x_\omega) = 0 \\
& G_1(y_\omega, \xi_\omega) \leq 0 \\
& G_2(y_\omega, \xi_\omega) = 0 \\
& x_1 = x_2 = ... = x_{N_{scen}}
\end{aligned} \tag{4.65}$$

Different algorithms have been proposed for solving stochastic programs of various types. At first, if $\mathcal{Q}(\mathbf{x})$ can be explicitly computed, an explicit mathematical program can be obtained. The resulting program is a nonlinear program and traditional algorithms can be employed to solve it. If dual block-angular structure is detected, then decomposition algorithms such as the L-shaped method and regularized decomposition can be adopted. If any suitable transformation can not be found and algorithms cannot be directly used, then a program approximation may help [69].

4.5.4 Scenario generation and reduction

The two-stage stochastic problem (4.64) has to be solved based on a discrete distribution with finite support of the random variable $\widetilde{\Xi}_i$, where each scenario or realization ξ_ω appears with probability p_i > 0, i = 1,...N_{scen}, and $\sum_{i=1}^{N_{scen}} p_i = 1$. Therefore, a necessary step in applying stochastic programming approach is generating a set of scenarios that realistically represents parameter uncertainties. Probability measure of random parameters can be empirically built from historical data or can be generated by applying time series models when historical data is not available. In this research, the probability measure of random parameters is assessed using historical data. In this way, a more accurate estimation of uncertainty is obtained. Other methods of estimating uncertainty sources based on assumptions or approximation will lead to a less accurate estimation of uncertainty.

In order to make a more accurate approximation of the probability measure of random variables, a large number of scenarios is required, but solving the problem (4.64) in a reasonable computational time prefers a smaller number of scenarios. This results in the need to approximate the original scenario set into a smaller subset, which still preserves essential features of the original one, by applying scenario reduction techniques. In this research, the scenario reduction is performed by a clustering approach, named Principal Component Analysis (PCA)-guided search for K-means clustering technique [70]. Clustering, also known as unsupervised classification, is a method of creating groups of objects, or clusters, in such a way that all objects within a single cluster are very similar while objects in different clusters are quite distinct. The aim of data clustering is to discover the natural grouping(s) of a set of patterns, points, or objects. One of the most popular, simple and efficient clustering algorithms is K-means. Although this clustering algorithm was proposed long time ago and thousands of clustering algorithms have been published since then, it is still widely used [71]. However, K-means clustering algorithm might converge quickly to a local solution from an initial set of cluster centroids. Experimentally, K-means algorithm can be easily trapped in a local minima near the initialization. This is because the formulation of K-means is non-convex and there are exponentially many local solutions in high dimensional data [70].

PCA is one of the most popular data mining statistical approaches. It uses an orthogonal transformation to convert a data set of possibly correlated variables into another set (with the same size) of linearly uncorrelated variables called Principal Components (PCs). PCA applies a mathematical technique called eigen analysis to solve for the eigenvalues and eigenvectors of a square symmetric matrix such as covariance matrix or correlation matrix, calculated from the data matrix. One of the attractive features of PCA is that it can approximate a large data set by reducing its dimension [72]. Variance of each PC is equal to the eigenvalue associated with that PC. The first PC, corresponding to the largest eigenvalue, is the most important component that contains most of the variance in the data set, followed by the second PC, and so on; hence, the first few PCs can account for most of the information in the data set and can be used as a replacement of the original one.

In K-means algorithm, the partition is found such that the squared error between the empirical mean of a cluster and the points in the cluster is minimized [71]. Let $X = \{x_i, i = 1, ..., n\}$ be the set of n d-dimensional points to be clustered into a set of K clusters $C = \{c_k, k = 1, ..., K\}$, μ_k be the mean of cluster c_k. The squared error between μ_k and the points in cluster c_k is defined as:

$$J(c_k) = \sum_{x_i \subset c_k} \parallel x_i - \mu_k \parallel^2 \tag{4.66}$$

K-means aims to minimize the sum of the squared error over all K clusters:

$$J(C) = \sum_{k=1}^{k} \sum_{x_i \subset c_k} \parallel x_i - \mu_k \parallel^2 \tag{4.67}$$

K-means algorithm starts with an initial partition with K clusters and assign patterns to clusters to reduce the squared error. The main steps of K-means algorithm is summarized in Algorithm 4.1 [71].

Algorithm 4.1 K-means clustering algorithm

1. Select an initial partition with K clusters.
2. Generate a new partition by assigning each pattern to its closest cluster center.
3. Compute new cluster centers.
4. Repeat steps 2 and 3 until cluster membership stabilizes.

In PCA-guided search for K-means clustering method, a search for initial set of cluster centroids is performed in PCA subspace. This algorithm takes advantage of the fact that the global solution to K-means clustering lies in the PCA subspace and K-means clustering is more efficient in low-dimensional space; thus, it produces much better results. The number of clusters is selected based on Silhouette criteria [73]. The Silhouette value is a measure of within-cluster (WC) and between-cluster (BC) dissimilarity of cluster members, in which WC dissimilarity is expected to be small while BC dissimilarity should be large. Given the initial cluster number is K. For a data point x_i, and its cluster membership c_i = $C(x_i)$, let $a_i(K)$ be the average distance between x_i and all other members in the cluster c_i (WC dissimilarity). Also, denoting l_i^o the index of the nearest cluster for x_i, that is:

$$l_i^o = argmin_{1 \leq k \neq c_i \leq K} \sum_{j=1}^{n_k} \parallel x_i - x_j^{(K)} \parallel_2^2 \tag{4.68}$$

where, n_k is the number of data points belonging to cluster c_i.

Let $b_i(K)$ be the average distance between x_i and cluster members in the nearest cluster l_i^o (BC dissimilarity), the Silhouette value is defined as:

$$s_i^o(K) = \frac{b_i(K) - a_i(K)}{max\{a_i(K), b_i(K)\}} \tag{4.69}$$

The optimal number of clusters $\hat{K}$ is then chosen such that $S^o(K) = \sum_{i=1}^{n} s_i^o(K)$ is maximized. If $S^o(K)$ is large, the average sample distance within the cluster is smaller than that to the samples in neighboring cluster, so x_i is well classified. If $S^o(K)$ is small, the average sample distance within the cluster is larger than that to the samples in neighboring clusters, which means x_i is misclassified. The value of Silhouette measure has a range of [-1, 1]. Silhouette values near +1 indicate that the sample is far from neighboring clusters. A value of 0 indicates the sample is on or very close to the boundary between two neighboring clusters while nega-

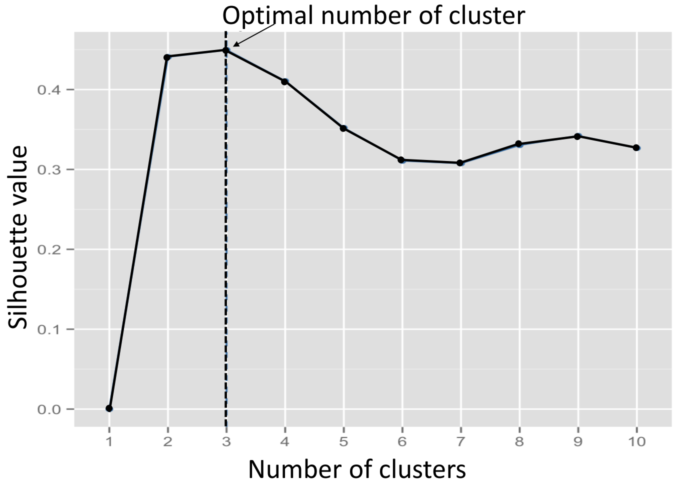

Figure 4.8: *Silhouette values for optimal cluster number [74]*

tive values indicate the sample might have been assigned to the wrong cluster. Fig. 4.8 is an example of Silhouette values, which suggests 3 clusters as an optimal number of clusters.

The algorithm of PCA-guided search for K-means clustering approach can be summarized as in Algorithm 4.2 [70]. After performing PCA-guided search for K-means clustering algorithm on the data set, clusters of similar data samples are obtained. A representative scenario of each cluster is then determined by averaging all the cluster members. Accordingly, the original data set is reduced to a significantly smaller one.

Algorithm 4.2 PCA-guided search for K-means clustering

1. Initialization: Choose the number of clusters using Silhouette criteria.
2. Perform PCA analysis on the data set to create another set of the same size of linearly independent variables called Principle Components (PCs). The first few components, which contain the highest amount of information (up to more than 90%) of the original data, are selected. The original data set is thus reduced to another data set with smaller dimensionality called PCA subspace.
3. Perform standard K-means clustering in the PCA subspace.
4. Use the cluster membership obtained in Step 3 to construct initial cluster centroids in the full space. Perform standard K-means clustering in the full space.

4.6 Summary

This chapter provides theory on two different approaches for incorporating uncertainty in an optimization problem, including cumulant-based probabilistic programming and two-stage stochastic programming. Generally, cumulant-based probabilistic approach relies on properties of cumulants of random variables when they are combined in a linearized fashion. In cumulant-based probabilistic optimal power flow, sources of uncertainty associated with the inputs are represented by probability distributions, then their cumulants are computed. Using input-output relationship, linearized around the solution of a deterministic optimal power flow, and based on the properties of cumulant, cumulants of output random variables can be calculated from cumulants of input random variables and distributions of output random variables are obtained by an approximation technique. Particularly, this technique allows the probabilistic optimal power flow model to take into account various types of probability distributions of inputs (including Gaussian/non-Gaussian, discrete/continuous distributions) which represent different sources of uncertainty in power systems.

In two-stage stochastic model, decisions are divided into two stages, i.e., the *first-stage* or *here-and-now* decisions have to be taken without a complete knowledge of random parameters, and the *second-stage* or *wait-and-see* decisions are taken after the uncertainty is revealed. These second-stage decisions are known as *corrective* or *recourse* actions against any infeasibility due to random variables. A scenario generation and reduction technique to create scenarios of random parameters as input of the problem has been explicitly described. Accordingly, probability measure of random parameters is assessed from historical data and then a clustering technique, namely PCA-guided search for K-means clustering algorithm, is adopted to reduce the original data set into a smaller one with representative scenarios.

CHAPTER 5

Energy Storage System Planning under Uncertainty

5.1 Introduction

In this chapter, the planning problem of ESSs under the uncertainty of wind power and load is investigated. Two approaches, based on techniques discussed in Chapter 4, are adopted, i.e., cumulant-based probabilistic and two-stage stochastic programming approach. Additionally, a sensitivity analysis, based on an economic criterion, is performed to identify candidate buses for ESS installation, thus reducing computational burden for ESS planning problems, especially large-size ones, with both approaches.

In the cumulant-based *probabilistic approach*, optimal placement is carried out by GA, based on the deterministic multi-period OPF model with ESS integration described in Chapter 3, using the expected value of random variables (load and wind generation). Cumulant-based probabilistic OPF is then applied to take into account the uncertainty and provide decision makers with necessary information on ESS capacities and used eventually to make final decision. This approach efficiently captures system uncertainties in the sizing of ESSs. Cumulant-based probabilistic OPF approach is less computationally intensive process compared to two-stage stochastic programming approach. Its accuracy depends on the quality of linearized relationship between input and output variables.

In the *stochastic programming approach*, a two-stage stochastic model is applied to determine ESS capacity taking into account the stochastic behavior of both wind power and load. Input random variables are represented by sets of scenarios. This approach is more computationally expensive than the cumulant-based proababilistic approach. The computing time exponentially grows with increasing number of scenarios of input random variables. Therefore, an important step of this approach is processing of input random variables, which can be dealt with by adopting scenario generation and reduction techniques.

Sensitivity analysis on ESS location is performed based on the deterministic OPF model with ESS integration in Section 3.4 and the economic criteria defined in Section 3.5. Candidate locations of ESSs for time-shifting and congestion relieving applications are identified while allowing an optimal operation for power systems regarding production cost, wind curtailment, and congestion relief, etc. These candidate locations are not necessary for the algorithms. They are necessary only to make both procedures tractable.

5.2 Outline of the chapter

The rest of the chapter is organized as follows:

The chapter starts with a literature review on ESS planning problems in Section 5.3. It follows by a description of the combined GA and cumulant-based POPF approach for optimal siting and sizing of ESSs in Section 5.4. Next, Section 5.5 describes the methodology of two-stage stochastic programming approach for optimal sizing of ESSs. In Section 5.6, a final procedure for ESS planning problems under uncertainty is introduced. In Section 5.7, all tests and results are presented and discussed, including tests to compare single-period and multi-period OPF models with ESSs, a sensitivity analysis to assess impacts of ESS locations on system operation based on an economic criteria, tests on both approaches for incorporating uncertainty in ESS planning problems, and tests for a comparison of both approaches. Section 5.8 summarizes the chapter.

5.3 Literature Review

In the recent years, there has been extensive study on the planning of ESSs in power systems for different applications with wind generation. Many papers found in the literature develop deterministic models for the planning problem. For example, in papers [75–77], different sizing methodologies, including power and energy sizing, for ESS have been presented. In [75], energy storage capacity is determined for dispatchability of wind farm to meet different confidence levels. Another size estimating method for ESS is provided in [76] to firm wind power output and allow for penetration into energy markets. Reference [77] introduces a methodology to minimize the capacity of ESS in a distributed configuration of wind power sources. An analytical technique is proposed in [78] to size ESSs for power systems with wind farms based on reliability cost and worth analysis. The authors in [79] present a methodology using discrete Fourier transform to determine maximum energy storage requirement for a balancing area or interconnections. This requirement is just the physical limit which could be theoretically accommodated by a power system. In [80], an OPF model is proposed to determine optimal ESS capacity and location. ESS capacity is determined to accommodate all amounts of spilled wind energy while its location ensures a minimized annual electricity cost. ARMA technique is adopted to generate annual hourly wind speed and load profile. A heuristic method is presented in [81] for sizing and placing energy storage in a transmission network. The authors couple operational simulations with planning, and use information from operational simulations such as flow patterns, congestion, and ramping restrictions for making planning decisions. In [82], a three-stage planning procedure is used to identify optimal locations and size of distributed storage units. In the first stage, optimal storage locations and parameters are determined for each day of the year individually. In the second stage, optimal energy and power ratings are determined and in the third stage, optimal operation of the storage units is simulated to quantify the benefits of mitigating congestion. An analytical approach and cost benefit analysis is provided in [83] to size ESSs for wind power firming. The effectiveness of the approach is validated by solving an ESS-sizing problem quantitatively. Paper [84] proposes a DC OPF framework for storage portfolio optimization in transmission-constrained network. The model investigates two problems, i.e., optimizing storage operation and location given a fixed technology portfolio and optimizing the storage portfolio, including storage size, technology, and network allocation).

Uncertainties have also been incorporated in existing research on ESS planning. Some papers develop analytical methods for optimal sizing of ESSs [85, 86]. ESS capacity can be estimated based on forecast errors, for reducing the uncertainty of short-term wind power forecasts up to 48 h [85]. This approach provides knowledge on the unserved energy, which represents the remaining forecast uncertainty. Thus, it permits the sizing of energy storage systems as a function of the desired remaining forecast uncertainty, reducing simultaneously power and energy capacity. A dynamic sizing approach is proposed in [86], where ESS is used as a means of risk hedging against penalties from the regulation market. Necessary storage capacity can be assessed for each delivery period, based on the degree of risk that the power producer accepts to be exposed to. This approach is shown to provide a significant reduction of the storage capacity used, without affecting the profit significantly. Other papers [87–93] develop numerical simulation techniques for optimal planning of ESSs. Paper [87] develops a model to size ESSs for wind farm applications, with the goal to keep the differences between the combined wind/ESS output and the predefined profile within a required limit. The model is formulated as a chance-constrained programming model. Genetic Algorithm combined with Monte-Carlo are applied to solve the problem. In [88], a probabilistic approach based on the probability distribution of ESS power profile is proposed to determine power capacity of hybrid ESS. The ESS capacity is specified to handle the wind power fluctuation with a magnitude less than a certain value corresponding to a preset confidence level. In [89], a two point estimate approach is employed for dealing with wind and load uncertainties in ESS optimal placement problem in a deregulated power system. Energy storage serves as a variable load to store the wind excess energy during the off-peak hours when the wind power exceeds the load. It then serves as a variable generator during the peak hours of the day to optimize wind revenues. A DC OPF model is developed to incorporate ESS into the system. Wind and load are stochastically modeled using historical data and curve fitting technique. A two-stage stochastic optimization approach is adopted in [90] to determine optimal capacity of ESS focusing on a 10 minute economic dispatch. Centroid linkage clustering technique is used to group similar scenarios into a reduced number of clusters. Paper [91] proposes a methodology based on stochastic optimization for storage sizing in isolated wind-diesel power systems. The problem is formulated as a two-stage stochastic optimization problem, with the objective of minimizing the cost of supplied energy, which results in a two-thirds reduction in ESS power rating and half the energy rating compared to the deterministic case (using the expected values). Peng Xiong et al [92] propose an approach for determining the optimal location and size of ESS in a power network with uncertain wind generation. The uncertainty of wind power output is represented by a scenario tree model. The model is formulated as a two-stage stochastic ESS planning model and Benders decomposition algorithm is utilized to make the problem tractability. A robust optimization approach is employed in [93] to minimize the investment in storage units while guaranteeing a feasible system operation, without load or renewable power curtailment, for all scenarios in the convex hull of a discrete uncertainty set.

As a conclusion, most models for ESS planning developed in the literature use a DC OPF or a relaxed formulation to incorporate ESS into power systems. Moreover, these models adopt single-period optimization approach, in which the optimal solution is independently solved at each period considered. However, with the incorporation of ESSs, single-period model does not take into account inter-temporal constraints relevant to the storage units. The approaches for placement of ESSs are demonstrated with small systems only. For larger systems, especially real-size ones, computational burden is still an issue.

5.4 Combined GA and POPF approach

5.4.1 Wind and load input

Based on a scale-up version of 3-year measured hourly wind power (from January 1, 2009 to December 31, 2011) of real wind farms in Sicily, Italy, long-term probability distribution for wind power is estimated using the methodology described in 4.4.2. Figure 5.1 shows long-term probability distribution of wind power output, for example, at bus 12 and hour 16, in which the discrete distribution is characterized by 20 impulses (corresponding to 20 clusters).

Total system load follows the typical daily load profiles of 4 seasons in [94]. Load uncertainty is modeled by assigning it among load buses according to different distributions: loads at buses 15, 38, 44, 50 and 56 are assumed to have Beta distributions with parameters computed by using expected values and standard deviations (assumed to be equal to 10, 12, 9, 8 and 11% of their expected values, respectively) [95]; loads at remaining buses are assumed normally dis-

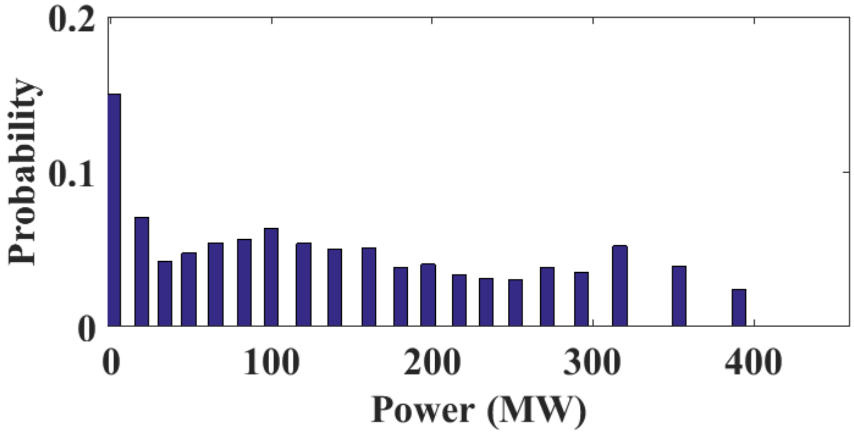

Figure 5.1: *Probability distribution of wind at bus 12 and hour 16*

tributed with standard deviations equal to 10% of the expected values. Expected values of wind power and total load for all seasons are depicted in Fig. 5.2.

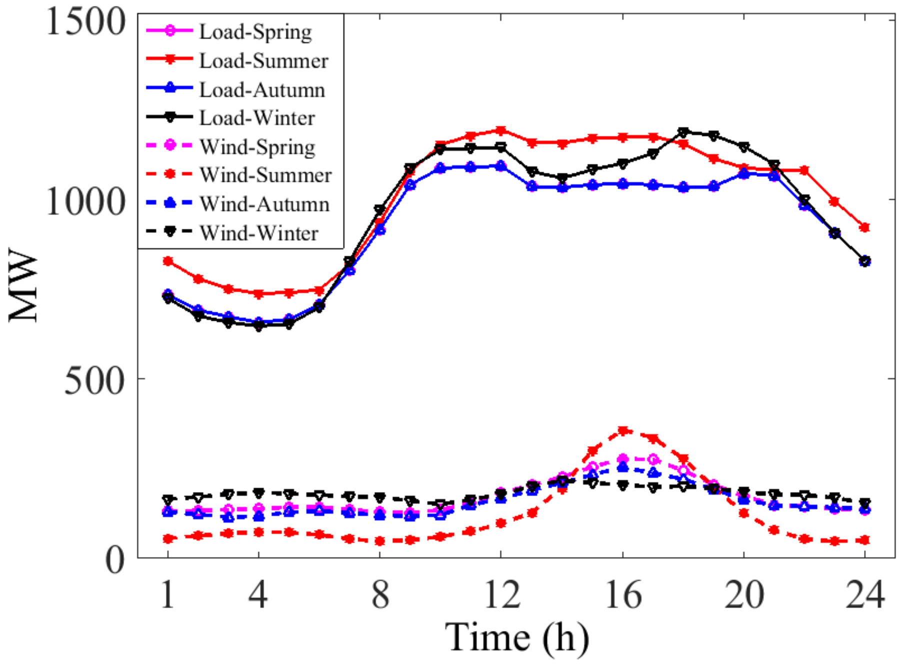

Figure 5.2: *Expected value of wind and load for all seasons*

5.4.2 Methodology

The optimal placement and sizing of ESSs is implemented based on a two-step algorithm: in the first step, optimal location of the ESSs and the expected value of the optimal size are determined by GA and the deterministic multi-period OPF described in Chapter 3. In this phase, the goal is to minimize ESS investment cost and total expected generation cost while maximizing the expected value of combined generation of wind and storage. In the second step, probabilistic assessment is carried out on the obtained ESS locations and capacities to be used for final decision making.

In this planning problem, not only the total generation cost but also ESS investment cost is minimized. ESS capital cost consists of energy-related cost and power-related cost, which is:

$$C_{inv_0} = \sum_{j=1}^{ns}(C_B B_j^{max} + C_R R_j^{max}) \tag{5.1}$$

where, *ns* is the total number of ESSs to be installed, B_j^{max} [MWh] and R_j^{max} [MW] are respectively energy capacity and power capacity of the ESS at bus *j*; C_B [€/MWh] and C_R [€/MW] are per-unit energy-related and power-related capital cost of the ESS.

With a life time of N years, the daily capital recovery factor is determined as in [96]:

$$I_{rec} = \frac{r(1+r)^N}{(1+r)^N - 1}\frac{1}{N_{day}} \tag{5.2}$$

where, *r* is annual interest rate, and N_{day} is number of days in a year.

ESS total capital cost C_{inv_0} is converted into ESS daily capital cost $C_{inv_{ESS}}(B_j^{max}, R_j^{max})$ by multiplying the energy-related cost and power-related cost by the above daily capital recovery factor:

$$C_{inv_{ESS}}(B_j^{max}, R_j^{max}) = I_{rec} C_{inv_0} \tag{5.3}$$

The objective function (3.24) of the deterministic OPF in Section 3.4 now becomes:

$$\text{Min} \quad \{C_{inv_{ESS}} + \sum_{t=1}^{T}[\sum_{i=1}^{ng}(c_{0_i} + c_{1_i}P_{G_i}^t + c_{2_i}P_{G_i}^{t^2}) + \sum_{j=1}^{ns}(c_{d_j}P_{d_j}^t - c_{ch_j}P_{ch_j}^t)]\} \tag{5.4}$$

The optimization is carried out on a daily basis, thus T = 24 hours. The inequality constraints on ESSs (3.14), (3.15), and (3.16) are also modified as follows:

$$R_j^{min} \leq P_{d_j}^t \leq R_j^{max} \tag{5.5}$$

$$R_j^{min} \leq P_{ch_j}^t \leq R_j^{max} \tag{5.6}$$

$$B_j^{min} \leq B_j^t \leq B_j^{max} \tag{5.7}$$

The maximum ESS capacity to be installed is limited by the following constraints, which also represents limitation on the budget for ESS installation:

$$\sum_{j=1}^{ns} R_j^{max} \leq R^{tot} \tag{5.8}$$

$$\sum_{j=1}^{ns} B_j^{max} \leq B^{tot} \tag{5.9}$$

where, R^{tot} and B^{tot} are respectively maximum allowable power and energy capacity of the ESSs to be installed.

The overall methodology is summarized in the flowchart in Fig. 5.3. Firstly, optimal

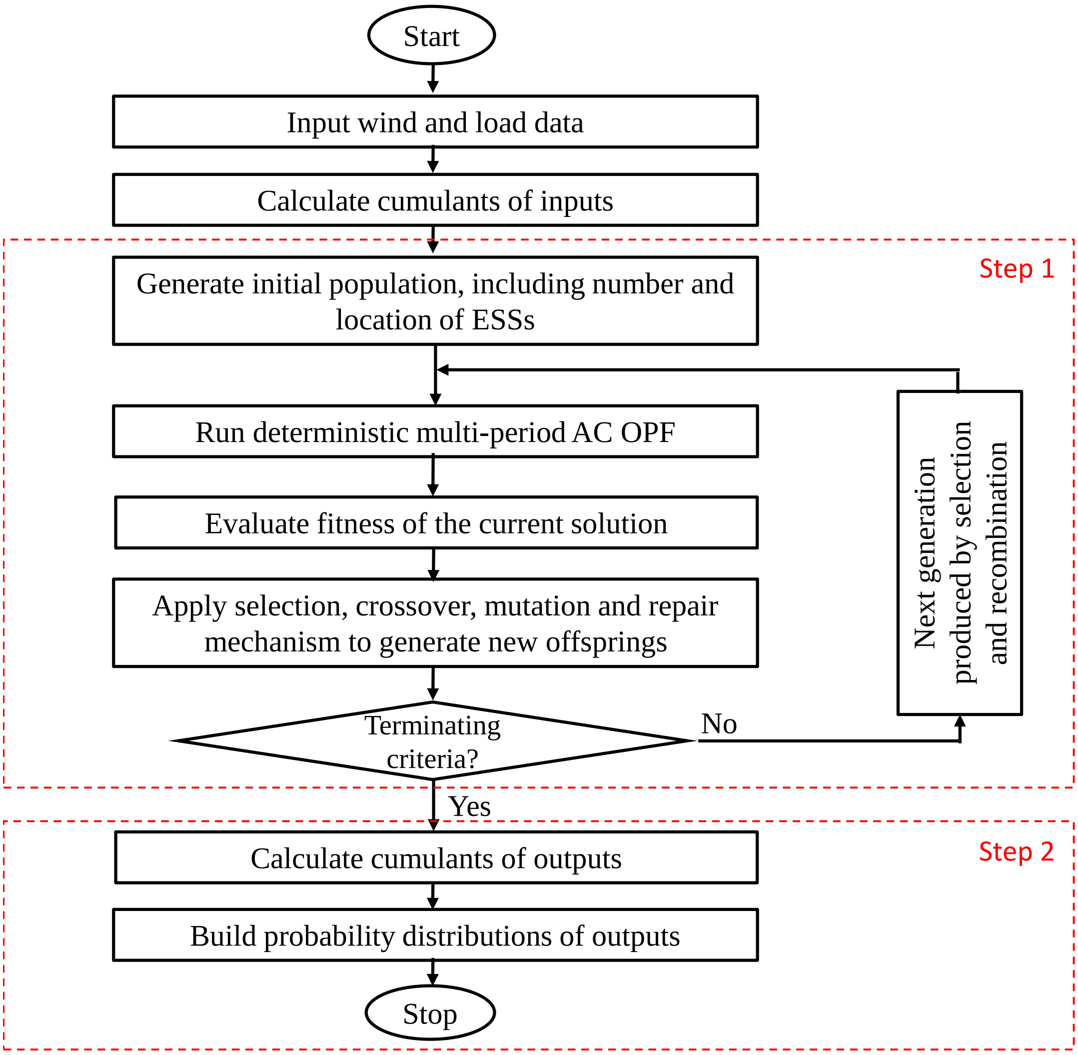

Figure 5.3: *Flowchart of the methodology*

locations and expected value of ESS capacities are determined based on the combined GA-deterministic OPF model (Step 1 in the flowchart). The location and number of ESSs to be installed are decided by GA while the capacities are determined by the OPF. GA is an attractive and powerful alternative to other optimization methods in many power system problems because of its robustness and efficiency [97–100]. It is appropriate to solve optimal placement problems since traditional derivative-based optimization approaches may handle with difficulty the non-convexity, non-linearity and discontinuity of the problem [101]. GA operates based on the mechanism of natural selection and genetics. It starts with a population of randomly generated candidates. Each candidate is called a chromosome and is made by a binary bit string structure that codes, in this approach, the candidate buses for ESSs. Each chromosome has its corresponding fitness which indicates its suitability as an optimal solution. The GA iteratively produces a new population from the old population by means of GA operators. When this cycle of genetic recombination process is iterated for many generations, the overall fitness of the population generally improves [102]. In this step, optimal placement of ESSs is determined by GA aimed at maximizing the combined generation of wind and the usage of ESSs. Accordingly, the fitness function of the GA is as follows:

$$\text{Fitness} = -\frac{\sum\limits_{t=1}^{T}[\sum\limits_{i=1}^{nb} P_{L_i}^t - (\sum\limits_{j=1}^{nw} P_{G_j}^t + \sum\limits_{k=1}^{ns} P_{d_k}^t)]}{\sum\limits_{t=1}^{T}\sum\limits_{j=1}^{nw} P_{W_j}^t} \tag{5.10}$$

where, $P_{L_i}^t$ is real power of load at bus *i* in period *t*, $P_{G_j}^t$ is wind generation at bus *j* in period *t*, $P_{d_k}^t$ is discharging power of the ESS at bus *k* in period *t*, $P_{W_j}^t$ is the available wind power at bus *j* in period *t*, *nb* is the number of system buses, *ns* is the number of ESSs to be installed, *nw* is the number of wind farms.

In this fitness function, the portion of power to supply load from wind and ESSs is determined relative to the available wind generation. Thus, higher value of the fitness function means higher amount of power from wind and ESSs is used to supply load and less amount of wind to be curtailed. With this fitness function, ESSs placed at the locations determined by GA can provide more effective operation by charging ESSs with more available wind generation and then discharging to supply load.

In order to find optimal locations of the ESSs, initially, the first population is randomly generated from the solution space to place the ESSs. The multi-period OPF is run with this placement of the ESSs to minimize the objective function (5.4) and its output is a time profile of the optimal operation of ESSs. GA, using results from the OPF, evaluates the fitness (5.10) of each individual in the population. The fitness of individuals is linearly ranked and stochastic universal sampling method [103] is applied to select individuals for breeding. Single point crossover method is applied on the selected individuals to produce new offspring which are then mutated to introduce new genes to the existing solutions in order to avoid local minima. Infeasible offspring possibly resulting from crossover and mutation operators are replaced by randomly feasible generated chromosomes which ensures the maximum number of ESSs to install is not violated. Finally, new offspring are evaluated and reintroduced into the current population to give new population. This routine is repeated until the GA convergence is reached. The best chromosome provides the optimal locations of ESSs, and the optimal solution from the OPF gives the optimal power capacity R^{max} and energy capacity B^{max} of the ESSs along with their corresponding optimal operational profiles. This means at the output of Step 1 in the flowchart, optimal ESS locations, expected value of ESS power and energy capacity, and optimal operational profiles, corresponding to the expected wind and load input, are obtained.

Next, the probabilistic part of the POPF is performed to assess the risk of not being able to store the available energy during operation of the ESSs due to wind and load random behavior (corresponding to Step 2 in the flowchart). In order to obtain probability distributions of output variables of the POPF (including ESS capacities), technique described in Section 4.4.2 is applied: first, cumulants of distributions of input variables (wind and load) are classified into two categories, i.e., discrete and continuous, then cumulants of each category of output random variables at each hour are separately calculated through input-output linearized relationship (obtained in Step 1). Using the technique presented in Section 4.4.2, probability distributions of ESS capacities are built at hours reaching the expected value capacities and the highest wind and load variability. Based on information from these probability distributions, decision makers will finally choose the size of ESSs to be installed.

5.4.3 Example

Consider a simple 3-bus system (Figure 5.4), which has 2 generators (a wind farm at bus 1 and a conventional generator at bus 2) and 2 loads at buses 2 and 3.

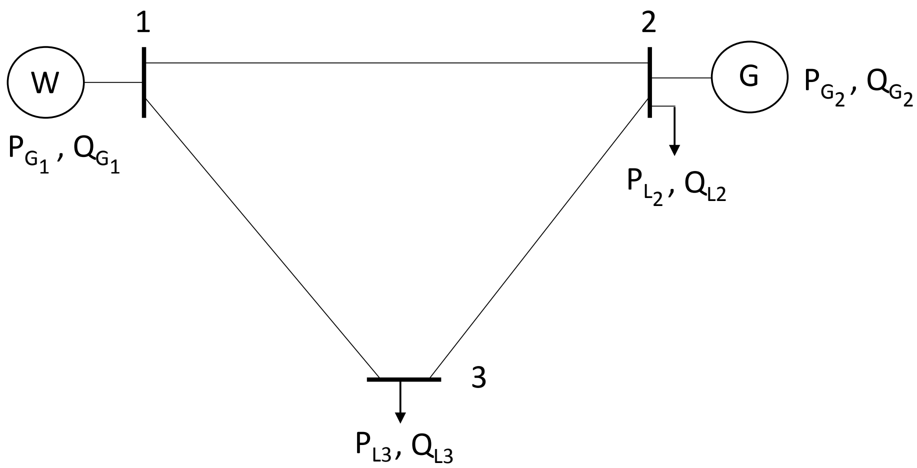

Figure 5.4: *3-bus system*

The deterministic OPF model for this system can be described as:

Objective function:

$$\text{Min} \quad \{C_{inv_{ESS}} + \sum_{t=1}^{T}[\sum_{i=1}^{2}(c_0 + c_1 P_{G_i}^t + c_2 P_{G_i}^{t2}) + \sum_{j=1}^{ns}(c_{d_j} P_{d_j}^t - c_{ch_j} P_{ch_j}^t)]\} \tag{5.11}$$

where, $P_{G_i}^t$ is real power generation at bus *i* in period *t*, which includes real power generation $P_{G_1}^t$ of the wind farm at bus 1 and $P_{G_2}^t$ of the conventional generator at bus 2; *ns* is the number of ESSs to be installed.

Power balance equations for the 3 buses:

$$P_1^t = P_{G_1}^t + P_{d_1}^t - P_{ch_1}^t = V_1^t \sum_{k=1}^{3} V_k^t [G_{1k}\cos(\theta_1^t - \theta_k^t) + B_{1k}\sin(\theta_1^t - \theta_k^t)] \tag{5.12}$$

$$Q_1^t = Q_{G_1}^t + Q_{d_1}^t - Q_{ch_1}^t = V_1^t \sum_{k=1}^{nb} V_k^t [G_{1k}\sin(\theta_1^t - \theta_k^t) - B_{1k}\cos(\theta_1^t - \theta_k^t)] \tag{5.13}$$

$$P_2^t = P_{G_2}^t - P_{L_2}^t + P_{d_2}^t - P_{ch_2}^t = V_2^t \sum_{k=1}^{3} V_k^t [G_{2k}\cos(\theta_2^t - \theta_k^t) + B_{2k}\sin(\theta_2^t - \theta_k^t)] \tag{5.14}$$

$$Q_2^t = Q_{G_2}^t - Q_{L_2}^t + Q_{d_2}^t - Q_{ch_2}^t = V_2^t \sum_{k=1}^{nb} V_k^t [G_{2k}\sin(\theta_2^t - \theta_k^t) - B_{2k}\cos(\theta_2^t - \theta_k^t)] \tag{5.15}$$

$$P_3^t = -P_{L_3}^t + P_{d_3}^t - P_{ch_3}^t = V_3^t \sum_{k=1}^{3} V_k^t [G_{3k}\cos(\theta_3^t - \theta_k^t) + B_{3k}\sin(\theta_3^t - \theta_k^t)] \tag{5.16}$$

$$Q_3^t = -Q_{L_3}^t + Q_{d_3}^t - Q_{ch_3}^t = V_3^t \sum_{k=1}^{nb} V_k^t [G_{3k}\sin(\theta_1^t - \theta_k^t) - B_{3k}\cos(\theta_3^t - \theta_k^t)] \tag{5.17}$$

Network inequality constraints include:

$$P_{G_1}^{min} \leq P_{G_1}^t \leq P_{G_1}^{max} \tag{5.18}$$

$$Q_{G_1}^{min} \leq Q_{G_1}^t \leq Q_{G_1}^{max} \tag{5.19}$$

$$P_{G_2}^{min} \leq P_{G_2}^t \leq P_{G_2}^{max} \tag{5.20}$$

$$Q_{G_2}^{min} \leq Q_{G_2}^t \leq Q_{G_2}^{max} \tag{5.21}$$

$$V_1^{min} \leq V_1^t \leq V_1^{max} \tag{5.22}$$

$$V_2^{min} \leq V_2^t \leq V_2^{max} \tag{5.23}$$

$$V_3^{min} \leq V_3^t \leq V_3^{max} \tag{5.24}$$

$$(I_{12}^t)^2 \leq (I_{12}^{max})^2 \tag{5.25}$$

$$(I_{13}^t)^2 \leq (I_{13}^{max})^2 \tag{5.26}$$

$$(I_{23}^t)^2 \leq (I_{23}^{max})^2 \tag{5.27}$$

$$(I_{21}^t)^2 \leq (I_{21}^{max})^2 \tag{5.28}$$

$$(I_{31}^t)^2 \leq (I_{31}^{max})^2 \tag{5.29}$$

$$(I_{32}^t)^2 \leq (I_{32}^{max})^2 \tag{5.30}$$

$$P_{G_1}^{t} - P_{G_1}^{t-1} \leq R_{U_1} \tag{5.31}$$

$$P_{G_1}^{t-1} - P_{G_1}^{t} \leq R_{D_1} \tag{5.32}$$

$$P_{G_2}^{t} - P_{G_2}^{t-1} \leq R_{U_2} \tag{5.33}$$

$$P_{G_2}^{t-1} - P_{G_2}^{t} \leq R_{D_2} \tag{5.34}$$

Constraints for ESSs include equations (5.35) - (5.45).

$$B_i^t = B_i^{t-1} + (\eta_{ch_i} P_{ch_i}^t - P_{d_i}^t / \eta_{d_i}) \Delta t \tag{5.35}$$

$$B_i^{t=T} = B_i^0 \tag{5.36}$$

$$P_{ch_i}^{min} \leq P_{ch_i}^t \leq P_{ch_i}^{max} \tag{5.37}$$

$$P_{d_i}^{min} \leq P_{d_i}^t \leq P_{d_i}^{max} \tag{5.38}$$

$$B_i^{min} \leq B_i^t \leq B_i^{max} \tag{5.39}$$

$$(P_{d_i}^t - P_{d_i}^{t-1}) - (P_{ch_i}^t - P_{ch_i}^{t-1}) \leq R_{Us_i} \tag{5.40}$$

$$(P_{d_i}^{t-1} - P_{d_i}^t) - (P_{ch_i}^{t-1} - P_{ch_i}^t) \leq R_{Ds_i} \tag{5.41}$$

$$Q_{ch_i}^{min} \leq Q_{ch_i}^t \leq Q_{ch_i}^{max} \tag{5.42}$$

$$Q_{d_i}^{min} \leq Q_{d_i}^t \leq Q_{d_i}^{max} \tag{5.43}$$

$$\sum_{j=1}^{ns} R_j^{max} \leq R^{tot} \tag{5.44}$$

$$\sum_{j=1}^{ns} B_j^{max} \leq B^{tot} \tag{5.45}$$

ESS location is determined by running combined GA and the above described deterministic OPF (Step 1 in the flowchart). The fitness function is calculated by equation (5.10). This fitness function calculates the amount of power supplying load from wind and ESSs relative to the available wind power. Hence, the higher the fitness function, the higher amount of power from wind to supply load, and the less wind to be curtailed.

The output of this step will be the optimal location (among the 3 buses) of the ESSs to be installed, ESS power and energy capacities R^{max} and B^{max}, and the operational profile corresponding to the average wind and load.

In the next step (Step 2 in the flowchart), probabilistic assessment is performed on the obtained ESS capacities, which provides the probability distributions of ESS capacities (and also probability distributions of any other variables).

5.5 Two-stage stochastic programming approach

5.5.1 Methodology

5.5.1.1 Stochastic input

In this research, a scenario, which consists of 24-hour data, is used to represent uncertainties in wind power and load; however, any other significant time interval could also be used. Processing of the input wind and load data is summarized as follows:

(i) **Scenario generation**
Wind power and load scenarios are generated from historical data. Historical 5-minute wind power and load data are collected in 7 years, from 2007 to 2013 [46]. These wind and load data are averaged to create hourly data and then scaled down to a suitable level for the test systems. For the tests in sections 5.7.5.1 and 5.7.5.2, the same wind and load data are used but scaled down to a different level suitable with the test system. See Figure 5.5 as an example of wind and load data input for the IEEE 39-bus test system in Section 5.7.5.1.

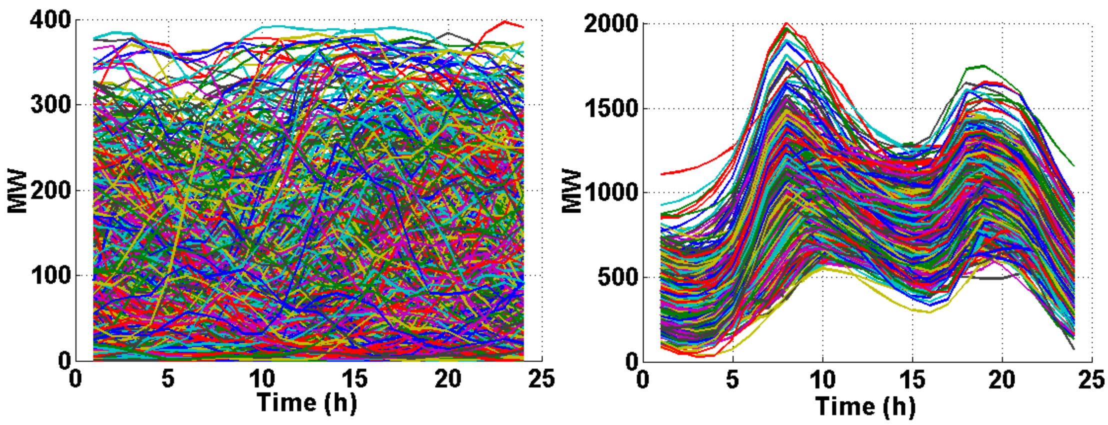

(a) *Wind data* **(b)** *Load data*

Figure 5.5: *Input data for IEEE 39-bus system*

(ii) **Scenario reduction**
A high number of scenarios can lead to intractability of the problem while a low number can originate a poor representation of the data. Therefore, a necessary step in preparing uncertain input for the stochastic model is to determine a number of representative scenarios which can closely approximate the original data set. The input data set described above is reduced to a tractable one using the clustering technique explained in Section 4.5.4. In particular, first, PCA analysis is performed on the above set of wind and load data to create another set of the same size of linearly independent variables called Principal Components (PCs). The first few components, which contain the highest amount of

information (up to more than 90%) of the original data, are selected. The original data set is thus reduced to another data set with smaller dimensionality called PCA subspace. The selected PCs of the above wind and load data are shown in Figure 5.6. Next, the number of clusters of each data set is selected based on Silhouette criteria as described in Section 4.5.4. K-means clustering is then performed in the PCA subspace with the selected number of clusters to obtain initial cluster centroids. Afterwards, the clustering is performed in the full space using the above initial cluster centroids and the original data sets are grouped into a number of distinct clusters. Finally, the representative scenario of each cluster is determined by averaging the members of the cluster and the probability of its occurrence is also calculated. The final wind scenarios and load scenarios of the above wind and load data are shown in Fig. 5.7, which consist of 6 scenarios of wind and 5 scenarios of load (as suggested by the Silhouette values).

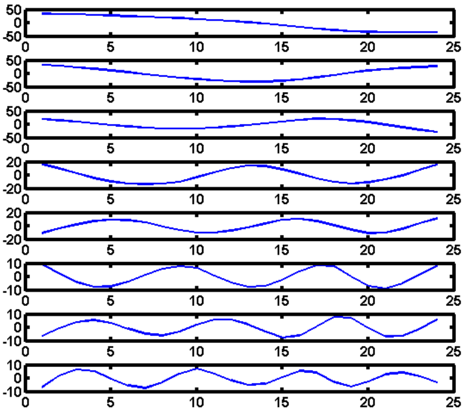

(a) *Wind PCs*

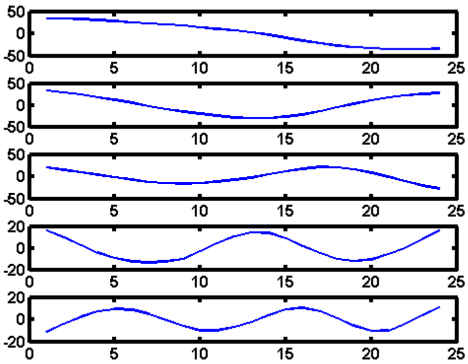

(b) *Load PCs*

Figure 5.6: *PCs of the input data*

These wind and load scenarios are used to create sets of wind-load scenario input for the problem. Each set of scenario consists of one scenario of wind and another scenario of load. These sets of scenarios are created by listing all possible combinations of wind scenarios and load scenarios. The probability of any combined wind-load scenarios is obtained by convolving the two probabilities of wind and load scenarios. For example, from the above wind and load data (Figure 5.5), 6 scenarios of wind and 5 scenarios of load are obtained, and each of which is associated with a probability of occurrence. Then, each scenario of wind is combined with 5 scenarios of load and a set of 30 wind-load scenarios is obtained as input for the test systems. The probability of each wind-load scenario in this set is determined by convolving probabilities of the corresponding wind and load scenarios.

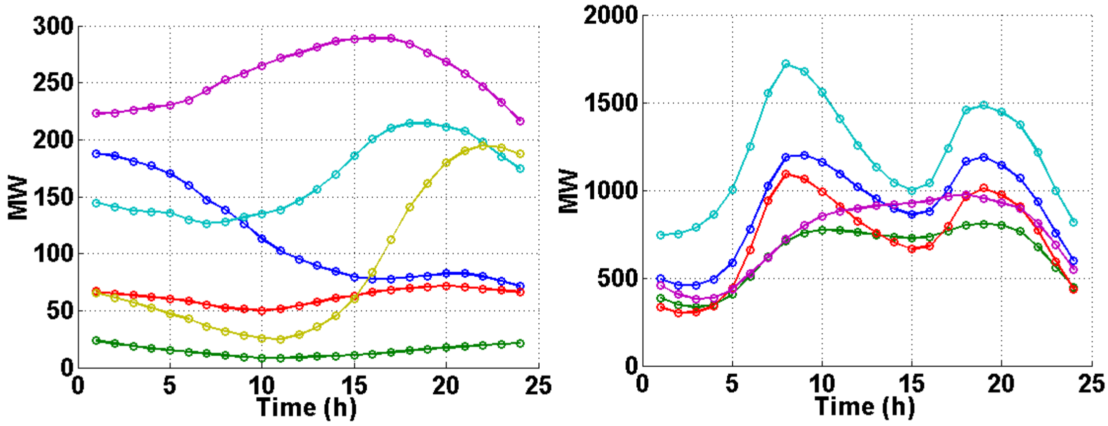

(a) *Wind scenarios* **(b)** *Load scenarios*

Figure 5.7: *Wind and load scenarios for the IEEE 39-bus system*

5.5.1.2 Mathematical formulation

The two-stage stochastic model has the goal of minimizing ESS installation cost in the first-stage and total expected generation cost in the second-stage. Thus, it is formulated as:

$$\begin{aligned} \min_{B_i^{max}, R_i^{max}} \quad & \{C_{inv_{ESS}}(B_i^{max}, R_i^{max}) + \mathcal{Q}(\mathbf{x})\} \\ \text{s.t.} \quad & \sum_{i=1}^{ns} B_i^{max} \leq B^{tot} \\ & \sum_{i=1}^{ns} R_i^{max} \leq R^{tot} \\ & B_i^{max} \geq 0, R_i^{max} \geq 0 \end{aligned} \tag{5.46}$$

where, B_i^{max} and R_i^{max} are respectively energy and power capacity of ESS installed at bus i; $C_{inv_{ESS}}$ is ESS investment cost as calculated in Section 5.4.2; B^{tot} and R^{tot} are respectively the maximum allowable energy and power capacity of ESSs to be installed, which represents the available budget for ESS installation; $\mathcal{Q}(\mathbf{x}) = \mathbb{E}[Q(\mathbf{x}, \boldsymbol{\xi})]$ and Q($\mathbf{x}$,$\boldsymbol{\xi}$) is the optimal value of the second-stage problem:

$$Q(\mathbf{x}, \boldsymbol{\xi}) = \min \quad \sum_{t=1}^{T} (PC^t) \tag{5.47}$$

where, PC^t is the production cost at each period t; T is the optimization period considered. The optimization is performed on a daily basis, thus T = 24 hours.

This objective function is subjected to the equality constraints 3.25 and inequality constraints (3.5) - (3.11) and (3.15) - (3.20).

Random variable $\widetilde{\Xi}_i$ of the problem, i.e., wind power and load, are represented by sets of scenarios. Each scenario represents 24-hour realization of the uncertain parameter and has a probability of occurrence associated with it. This also means in each period (hour), the random variables have a finite number of realizations, for example, $\xi_{i,\omega}$, ω = 1,...,N_{scen} with respective probabilities $p_{i,\omega}$. This can be illustrated by Fig. 5.8, in which each branch connected to the root represents each scenario of 24-hour realization of the random parameters in the second stage.

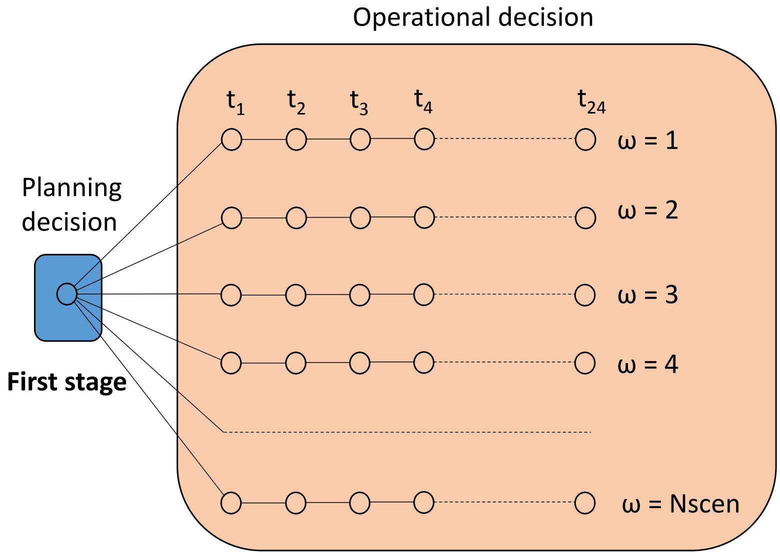

Figure 5.8: *Two-stage scenario tree with 24-hour realizations of random parameters*

With this discrete distribution of random variables, the two-stage problem is reformulated, according to 4.64, as follows:

The objective function is:

$$\begin{aligned}\min_{B_i^{max},R_i^{max},P^t_{G_{j,\omega}},P^t_{d_{i,\omega}},P^t_{ch_{i,\omega}}} \quad & \{C_{inv_{ESS}}(B_i^{max}, R_i^{max}) \\ & + \sum_{\omega=1}^{N_{scen}} p_\omega \sum_{t=1}^{T}[\sum_{j=1}^{ng}(c_{0_j} + c_{1_j} P^t_{G_{j,\omega}} + c_{2_j} P^{t^2}_{G_{j,\omega}}) \\ & + \sum_{i=1}^{ns}(c_{d_i} P^t_{d_{i,\omega}} - c_{ch_i} P^t_{ch_{i,\omega}})]\}\end{aligned} \tag{5.48}$$

In this equation, B_i^{max} and R_i^{max}, which are respectively energy rating and power rating of the ESSs at bus *i*, are control variables of the first-stage problem. $P^t_{G_{j,\omega}}$, $P^t_{ch_{i,\omega}}$ and $P^t_{d_{i,\omega}}$ are variables of the second-stage problem. They are respectively real generation power of generating unit at bus *i* in hour *t* and scenario ω, including power from both conventional and wind generators, and charging and discharging power of ESS at bus *i* in hour *t* and scenario ω. In this case, the problem is solved with a total of [(*ns* x 2) + (T x *ng* x N_{scen}) + (T x *ns* x N_{scen} x 2)] of control variables.

The equality constraints (3.25) and inequality constraints (3.5) - (3.11), and (3.15) - (3.20) have to be fulfilled for each realization of the random parameters. Specifically:

Power balance equations: Include equations for real and reactive power at each node *i* in each time period *t* for each scenario ω:

$$P^t_{G_{i,\omega}} - P^t_{L_{i,\omega}} + P^t_{d_{i,\omega}} - P^t_{ch_{i,\omega}} = \sum_{k=1}^{nb} V^t_{i,\omega} V^t_{k,\omega} [G_{ik} \cos(\theta^t_{i,\omega} - \theta^t_{k,\omega}) + B_{ik} \sin(\theta^t_{i,\omega} - \theta^t_{k,\omega})] \tag{5.49}$$

$$Q^t_{G_{i,\omega}} - Q^t_{L_{i,\omega}} + Q^t_{d_{i,\omega}} - Q^t_{ch_{i,\omega}} = \sum_{k=1}^{nb} V^t_{i,\omega} V^t_{k,\omega} [G_{ik} \sin(\theta^t_{i,\omega} - \theta^t_{k,\omega}) - B_{ik} \cos(\theta^t_{i,\omega} - \theta^t_{k,\omega})] \tag{5.50}$$

where, $P^t_{L_{i,\omega}}$ and $Q^t_{L_{i,\omega}}$ denote real and reactive power of load at bus *i* in hour *t* and scenario ω. $Q^t_{G_{i,\omega}}$ defines reactive power of generating unit at bus *i* in hour *t* and scenario ω. $Q^t_{L_{i,\omega}}$ is reactive power of load at bus *i* in hour *t* and scenario ω. $Q^t_{ch_{i,\omega}}$ and $Q^t_{d_{i,\omega}}$ are reactive charging and discharging power of ESS at bus *i* in hour *t* and scenario ω. $V^t_{i,\omega}$ and $V^t_{k,\omega}$ are voltage magnitudes of buses *i* and *k* in hour *t* and scenario ω. $\theta^t_{i,\omega}$ and $\theta^t_{k,\omega}$ are voltage angles of buses *i* and *k* in hour *t* and scenario ω.

Upper and lower limits for voltage magnitudes:

$$V_i^{min} \leq V^t_{i,\omega} \leq V_i^{max} \tag{5.51}$$

Bounds on real and reactive generation power:

$$P_{G_i}^{min} \leq P^t_{G_{i,\omega}} \leq P_{G_i}^{max} \tag{5.52}$$

$$Q_{G_i}^{min} \leq Q^t_{G_{i,\omega}} \leq Q_{G_i}^{max} \tag{5.53}$$

Branch current limits:

$$(I^t_{ij,\omega})^2 \leq (I_{ij}^{max})^2 \tag{5.54}$$

$$(I^t_{ji,\omega})^2 \leq (I_{ji}^{max})^2 \tag{5.55}$$

where, $I^t_{ij,\omega}$ and $I^t_{ji,\omega}$ are magnitudes of the current flowing from bus *i* to bus *j* and from bus *j* to bus *i* in hour *t* and scenario ω, respectively.

ESS budget constraints:

$$\sum_{i=1}^{ns} B_i^{max} \leq B^{tot} \tag{5.56}$$

$$\sum_{i=1}^{ns} R_i^{max} \leq R^{tot} \tag{5.57}$$

ESS energy balance equations:

$$B_{i,\omega}^{t} = B_{i,\omega}^{t-1} + (\eta_{ch_i} P_{ch_{i,\omega}}^{t} + P_{d_{i,\omega}}^{t}/\eta_{d_i})\Delta t \tag{5.58}$$

where, $B_{i,\omega}^{t}$ and $B_{i,\omega}^{t-1}$ are energy levels of ESS at bus *i* in hour *t* and *t-1* in scenario ω.

ESS energy continuity:

$$B_{i,\omega}^{t=24} = B_{0_{i,\omega}} \tag{5.59}$$

where, $B_{0_{i,\omega}}$ and $B_{i,\omega}^{t=24}$ are respectively energy level at the beginning and at the end of the day of the ESS at bus *i* in scenario ω.

ESS charging/discharging power bounds:

$$R_i^{min} \leq P_{d_{i,\omega}}^{t} \leq R_i^{max} \tag{5.60}$$

$$R_i^{min} \leq P_{ch_{i,\omega}}^{t} \leq R_i^{max} \tag{5.61}$$

$$Q_{s_i}^{min} \leq Q_{d_{i,\omega}}^{t} \leq Q_{s_i}^{max} \tag{5.62}$$

$$Q_{s_i}^{min} \leq Q_{ch_{i,\omega}}^{t} \leq Q_{s_i}^{max} \tag{5.63}$$

ESS energy limits:

$$B_i^{min} \leq B_{i,\omega}^{t} \leq B_i^{max} \tag{5.64}$$

where, $B_{i,\omega}^{t}$ is energy level of ESS at bus *i* in hour *t* and scenario ω.

5.5.2 Example

Take the 3-bus system in Figure 5.4 as an example and assume 30 wind-load scenarios (ω = 30) are obtained from historical wind and load input data by applying the technique described in 5.5.1.1. Assume 1 ESS, with capacity to be determined, is installed at the wind bus (bus 1). The two-stage stochastic model for this system can be formulated as:

The objective function is minimizing ESS installation cost and the total expected generation cost:

$$\begin{aligned} \min \quad & \{C_{inv_{ESS}}(B^{max}, R^{max}) + \sum_{\omega=1}^{30} p_\omega \sum_{t=1}^{T} [\sum_{j=1}^{2} (c_{0_j} + c_{1_j} P_{G_{j,\omega}}^{t} + c_{2_j} P_{G_{j,\omega}}^{t^2}) \\ & + (c_d P_{d_\omega}^{t} - c_{ch} P_{ch_\omega}^{t})]\} \end{aligned} \tag{5.65}$$

Assume the optimization is carried out on a daily basis, thus T = 24 hours. Control variables of the problems includes: B^{max}, R^{max}, $P_{G_{1,\omega}}^{t}$, $P_{G_{2,\omega}}^{t}$, $P_{d_\omega}^{t}$, $P_{ch_\omega}^{t}$; with ω = 1,2,...,30 and t = 1,2,...,24.

Network equality and inequality constraints in each period *t* and each scenario ω include:

Power balance equations for the 3 buses:

$$P_{G_{1,\omega}}^t + P_{d_\omega}^t - P_{ch_\omega}^t = \sum_{k=1}^{3} V_{1,\omega}^t V_{k,\omega}^t [G_{1k}\cos(\theta_{1,\omega}^t - \theta_{k,\omega}^t) + B_{1k}\sin(\theta_{1,\omega}^t - \theta_{k,\omega}^t)] \quad (5.66)$$

$$Q_{G_{1,\omega}}^t + Q_{d_\omega}^t - Q_{ch_\omega}^t = \sum_{k=1}^{3} V_{1,\omega}^t V_{k,\omega}^t [G_{1k}\sin(\theta_{1,\omega}^t - \theta_{k,\omega}^t) - B_{1k}\cos(\theta_{1,\omega}^t - \theta_{k,\omega}^t)] \quad (5.67)$$

$$P_{G_{2,\omega}}^t - P_{L_{2,\omega}}^t = \sum_{k=1}^{3} V_{2,\omega}^t V_{k,\omega}^t [G_{2k}\cos(\theta_{2,\omega}^t - \theta_{2,\omega}^t) + B_{2k}\sin(\theta_{2,\omega}^t - \theta_{k,\omega}^t)] \quad (5.68)$$

$$Q_{G_{2,\omega}}^t - Q_{L_{2,\omega}}^t = \sum_{k=1}^{3} V_{2,\omega}^t V_{k,\omega}^t [G_{2k}\sin(\theta_{2,\omega}^t - \theta_{k,\omega}^t) - B_{2k}\cos(\theta_{2,\omega}^t - \theta_{k,\omega}^t)] \quad (5.69)$$

$$-P_{L_{3,\omega}}^t = \sum_{k=1}^{3} V_{3,\omega}^t V_{k,\omega}^t [G_{3k}\cos(\theta_{3,\omega}^t - \theta_{3,\omega}^t) + B_{3k}\sin(\theta_{3,\omega}^t - \theta_{k,\omega}^t)] \quad (5.70)$$

$$-Q_{L_{3,\omega}}^t = \sum_{k=1}^{3} V_{3,\omega}^t V_{k,\omega}^t [G_{3k}\sin(\theta_{3,\omega}^t - \theta_{k,\omega}^t) - B_{3k}\cos(\theta_{3,\omega}^t - \theta_{k,\omega}^t)] \quad (5.71)$$

Network inequality constraints:

$$V_1^{min} \le V_{1,\omega}^t \le V_1^{max} \quad (5.72)$$
$$V_2^{min} \le V_{2,\omega}^t \le V_2^{max} \quad (5.73)$$
$$V_3^{min} \le V_{3,\omega}^t \le V_3^{max} \quad (5.74)$$
$$P_{G_1}^{min} \le P_{G_{1,\omega}}^t \le P_{G_1}^{max} \quad (5.75)$$
$$Q_{G_1}^{min} \le Q_{G_{1,\omega}}^t \le Q_{G_1}^{max} \quad (5.76)$$
$$P_{G_2}^{min} \le P_{G_{2,\omega}}^t \le P_{G_2}^{max} \quad (5.77)$$
$$Q_{G_2}^{min} \le Q_{G_{2,\omega}}^t \le Q_{G_2}^{max} \quad (5.78)$$
$$(I_{12,\omega}^t)^2 \le (I_{12}^{max})^2 \quad (5.79)$$
$$(I_{21,\omega}^t)^2 \le (I_{21}^{max})^2 \quad (5.80)$$
$$(I_{13,\omega}^t)^2 \le (I_{13}^{max})^2 \quad (5.81)$$
$$(I_{31,\omega}^t)^2 \le (I_{31}^{max})^2 \quad (5.82)$$
$$(I_{23,\omega}^t)^2 \le (I_{23}^{max})^2 \quad (5.83)$$
$$(I_{32,\omega}^t)^2 \le (I_{32}^{max})^2 \quad (5.84)$$

Constraints on the ESS include:

$$B^{max} \le B^{tot} \quad (5.85)$$
$$R^{max} \le R^{tot} \quad (5.86)$$
$$B_\omega^t = B_\omega^{t-1} + (\eta_{ch} P_{ch_\omega}^t + P_{d_\omega}^t/\eta_d)\Delta t \quad (5.87)$$

$$B_{\omega}^{t=24} = B_{0_{\omega}} \tag{5.88}$$

$$R^{min} \leq P_{d_{\omega}}^{t} \leq R^{max} \tag{5.89}$$

$$R^{min} \leq P_{ch_{\omega}}^{t} \leq R^{max} \tag{5.90}$$

$$Q_s^{min} \leq Q_{d_{\omega}}^{t} \leq Q_s^{max} \tag{5.91}$$

$$Q_s^{min} \leq Q_{ch_{\omega}}^{t} \leq Q_s^{max} \tag{5.92}$$

$$B^{min} \leq B_{\omega}^{t} \leq B^{max} \tag{5.93}$$

Solution of this problem will provide optimal power and energy capacity for the ESS to be installed.

5.6 Final Procedure

The procedure for ESS planning proposed by this research is summarized in the flowchart in Figure 5.9. For large systems, especially real-size ones, computational burden of a planning

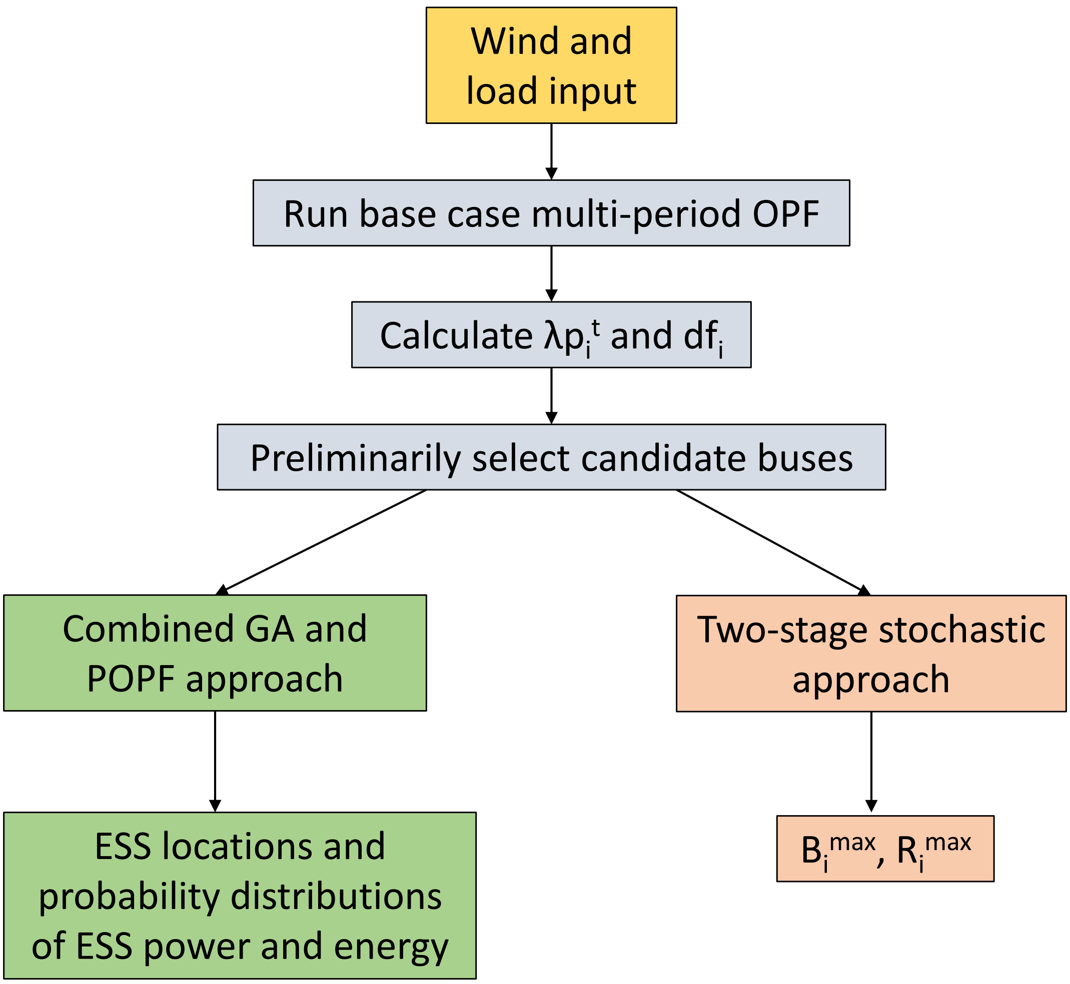

Figure 5.9: *Procedure of ESS planning*

problem is still an issue. Therefore, for the best planning of ESSs, it is necessary to preliminarily identify the most suitable area or the best candidate locations for installing these devices. This is carried out, in this research, by first running the base case multi-period OPF described in Section 3.2. The Lagrangian multiplier λp_i^t at each bus i in each period t is determined as a byproduct of the OPF. Then, the parameter $df_i = \sum_{t=1}^{T} \lambda p_i^t$ is calculated. Based on the values of df_i, the best candidate buses for ESS installation is preliminarily selected as described in Section 3.5. Next, to take into account wind and load uncertainties in ESS planning, one of the two approaches, i.e., either combined GA and POPF approach (Section 5.4) or two-stage stochastic programming approach (Section 5.5), can be applied. At the output of the combined GA and POPF approach, ESS locations and probability distributions of ESS power and energy capacity are provided while in two-stage stochastic programming approach, ESS power and energy capacity are determined.

5.7 Tests and Results

5.7.1 Test systems

In this section, different IEEE test systems used in the tests, including IEEE 14-bus system, 39-bus system, 57-bus system, and 118-bus system, will be described. For each system, the peak load and capacity of wind plants can be different in different tests carried out and will be specified in the following subsections case by case.

5.7.1.1 IEEE 14-bus system

The modified IEEE 14-bus system is shown in Fig. 5.10). In this system, load is supplied from both conventional and wind generation. There are 4 conventional generators at buses 1, 3, 6, and 8 with a total capacity of 732.4 MW. A wind plant is assumed to be at bus 2.

5.7.1.2 IEEE 39-bus system

In Fig. 5.11, the modified IEEE 39-bus system is shown. System load with peak value of 2007 MW is supplied from both conventional and wind generation. The system has 9 conventional generators with a total capacity of 2200 MW. There are 2 wind farms connected to buses 32 and 35.

5.7.1.3 IEEE 57-bus system

The modified IEEE 57-bus system is shown in Fig. 5.12). In this system, load is supplied from both conventional generators and wind. There are 6 conventional generators (at buses 1, 2, 3, 6, 8, and 9) with total capacity of 1565 MW. Wind farms are present in a windy area surrounding bus 12.

5.7.1.4 Modified IEEE 118-bus system

The modified IEEE 118-bus system can be found at [104]. For the test in Section 5.7.5.2, the system has 51 conventional generators of 6600 MW in total, system load with peak value

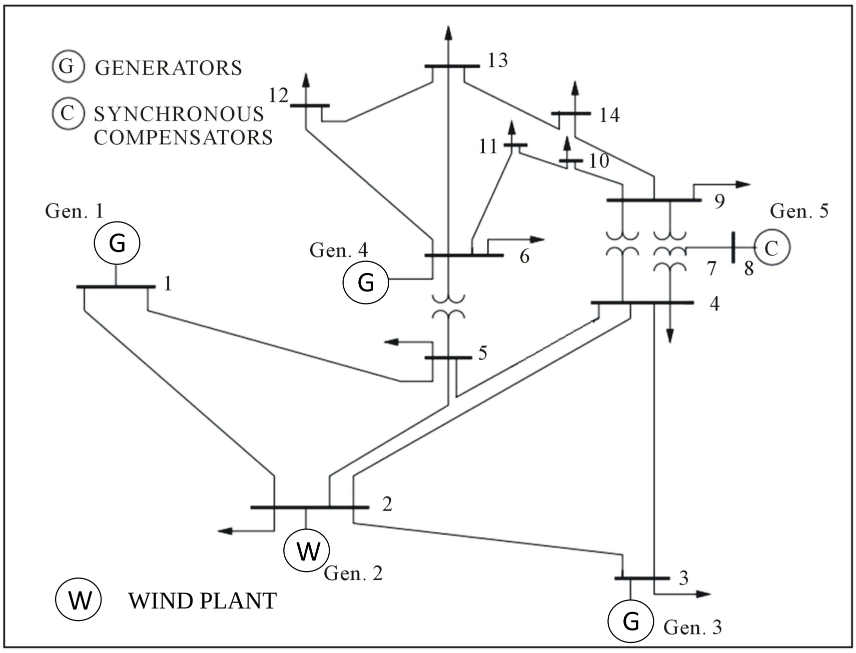

Figure 5.10: *IEEE 14-bus system [104]*

of 5038 MW is supplied from both conventional and wind generators. There are 3 large wind farms connected to buses 6, 62 and 112. Two ESSs, with capacity to be determined, are assumed to be installed at buses 6 and 62 (wind buses) to time-shift the wind energy.

For the test in Section 5.7.3.2, the system has 52 conventional generating units with a total capacity of 2500 MW, 2 large wind farms connected to buses 8 and 10 with a total installed capacity of 700 MW. Load with peak value of 2189 MW is supplied from both conventional and wind generators. Generation from the wind farms is likely to cause congestion on the way from wind to loads, which might result in wind curtailment.

5.7.2 Single-period vs. Multi-period model

In this section, the mathematical model described in Section 3.4 is tested on modified IEEE 14-bus system (described in 5.7.1.1) and modified IEEE 57-bus system (described in 5.7.1.3). The systems are modified in order to simulate a very high penetration of wind power. Wind data is taken from a 24-hour wind power profile of a wind farm in Sicily, Italy. Load is reproduced based on the load curve in [105].

5.7.2.1 IEEE 14-bus system

In this test, to study the combined operation of ESS and wind generation with each model, the wind plant at bus 2 is assumed to have an installed capacity of 400 MW and an ESS is added at bus 2 to time-shift the wind energy. Load with peak value of 438.7 MW is supplied from both conventional and wind generation. Parameters for the ESS system can be found in Table 5.1. Initial energy of the ESS is set to 0 MWh (parameter B_0 in Table 5.1). The optimization problem

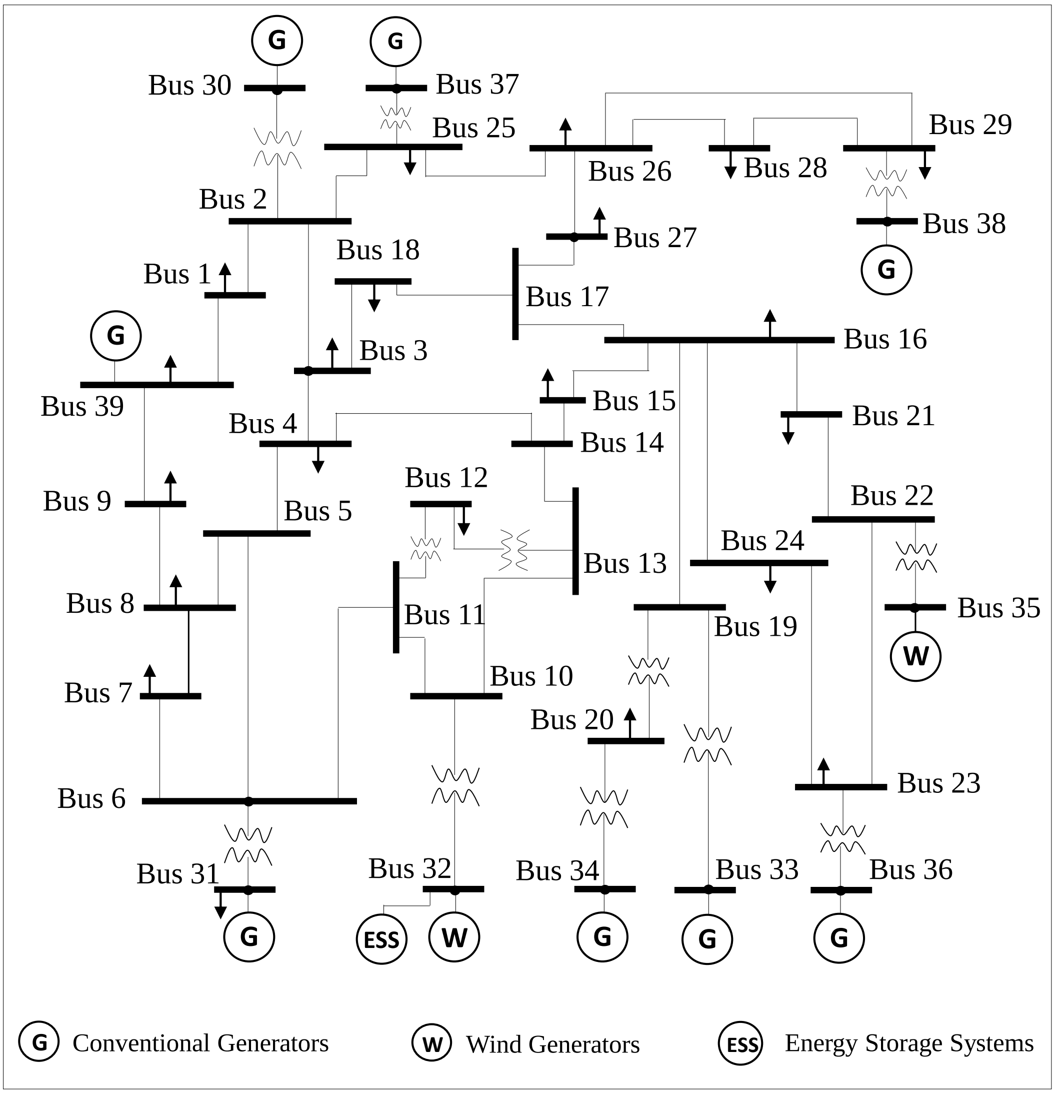

Figure 5.11: *IEEE 39-bus system [104]*

Table 5.1: *Parameters of the ESS*

P_{ch}^{max} [MW]	P_{d}^{max} [MW]	B_0 [MWh]	B^{max} [MWh]	η_{ch}	η_d
100	100	0	200	0.85	0.85

is run for a period of 24 hours, thus T = 24 hours. Operation of the ESS for both models are represented in figures 5.13 and 5.14.

As shown in the simulation results, the ESS is charged when wind power exceeds the load and then it is discharged when wind is insufficient to supply the load. At periods when there is extra wind power, after the storage has been charged up to its limits, either power or energy limit, the extra wind is necessarily curtailed. This situation can clearly be seen at hours 9, 10,

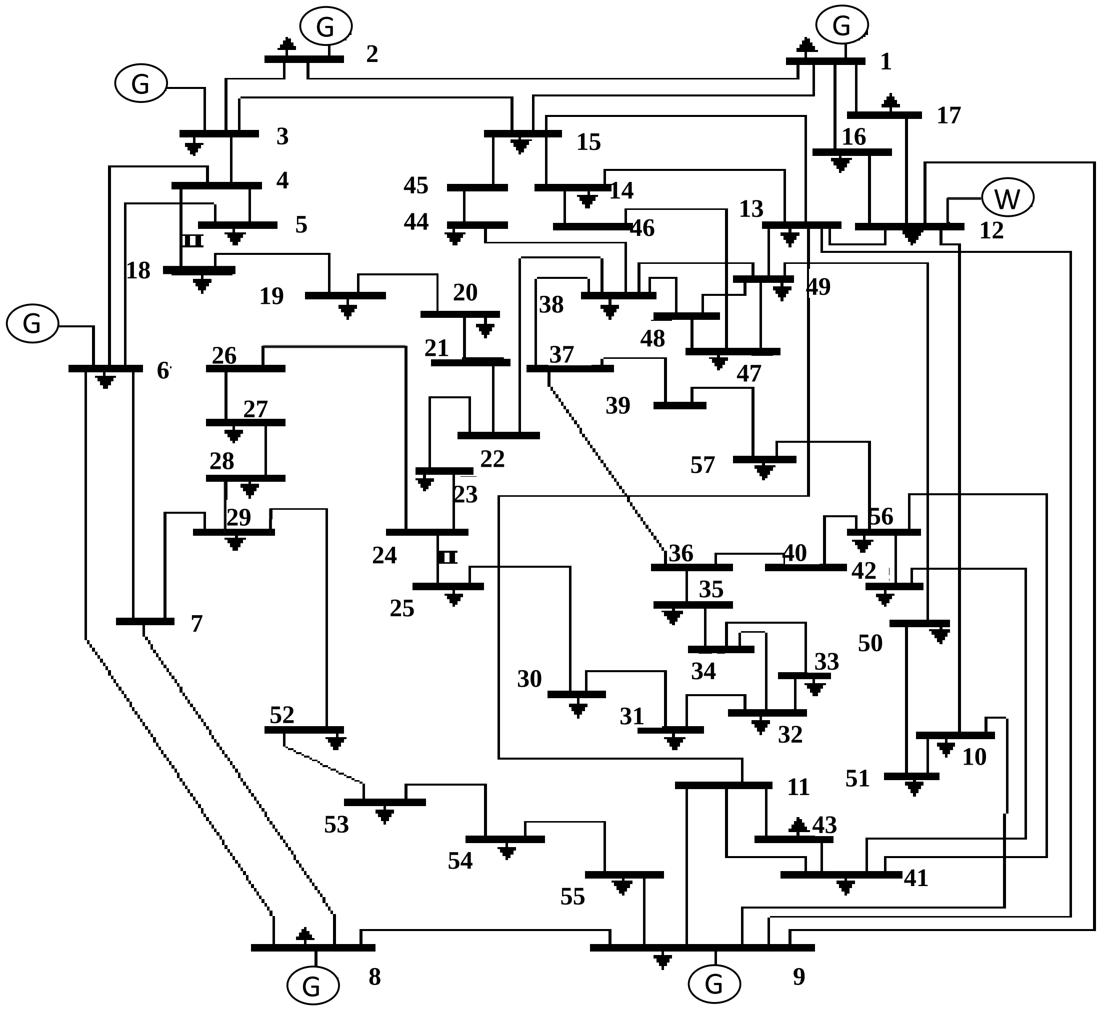

Figure 5.12: *IEEE 57-bus system [104]*

21 and 22 in Fig. 5.13 and hours 10, 21 and 22 in Fig. 5.14, in which the amounts of curtailed wind power are exactly the difference between forecasted wind power and used wind power. These amounts are 42.42 MW, 93.65 MW, 84.58 MW and 25.22 MW at hours 9, 10, 21 and 22 respectively in Fig. 5.13, and 44.41 MW, 103.99 MW and 32.29 MW at hours 10, 21 and 22 respectively in Fig. 5.14.

Daily operational schedules of the ESS for both models are presented in Table 5.2. P_{ch} and P_d are ESS charging and discharging power respectively, B is ESS energy level. In this table, P_{ch} is presented by a positive value while P_d has a negative value (the same sign convention has been used in figures 5.13 and 5.14).

From this table, it can be noted that the operational schedule for ESS at hours 1 to 11 and hours 20 to 24 in both models are basically similar, i.e. which periods the ESS should be charged and which ones it should be discharged. The only difference is in the amount of power/energy

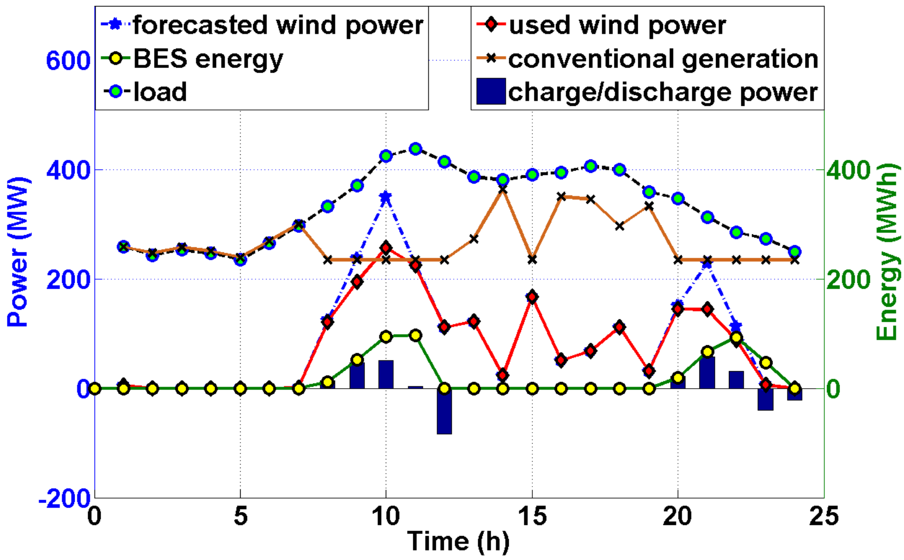

Figure 5.13: *ESS operation in single-period model*

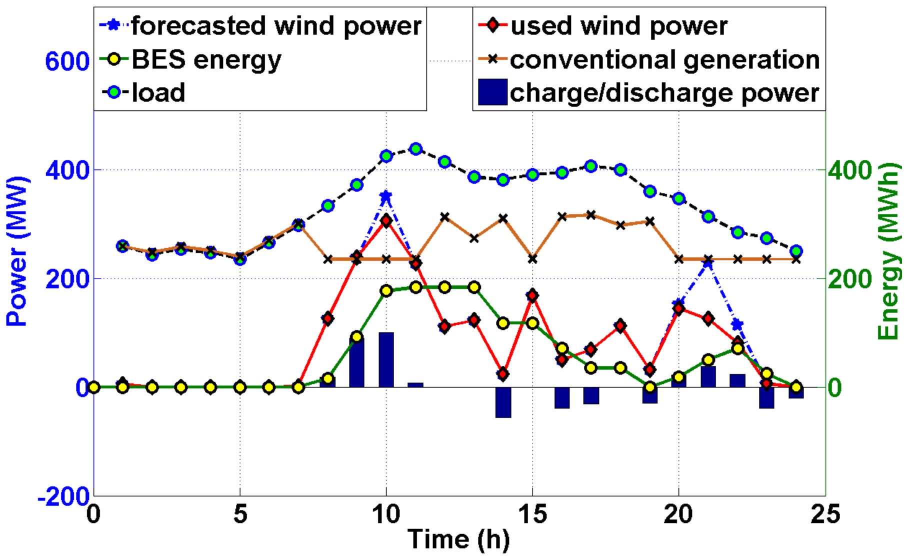

Figure 5.14: *ESS operation in multi-period model*

that ESS is decided to get charged or discharged. In the remaining hours, the differences are more clearly presented, in which ESS in single-period model is almost completely discharged in only hour 12 while in multi-period model, it is gradually discharged in hours 14, 16, 17 and 19, when wind reaches lowest values. This is because ESS in the multi-period model at all time tries to balance its charging/discharging power and energy for not only the current period but also look-ahead periods while ESS in the single-period model only cares about its charging/discharging at the current period.

Total amount of curtailed wind power is 259.40 MW in single-period model and 188.45

Table 5.2: *ESS operational schedule in single-period and multi-period models*

t [h]	P_{ch}/P_d [MW]	B [MWh]	t [h]	P_{ch}/P_d [MW]	B [MWh]
1	0.00	0.00	1	0.00	0.00
2	0.00	0.00	2	0.00	0.00
3	0.00	0.00	3	0.00	0.00
4	0.00	0.00	4	0.00	0.00
5	0.00	0.00	5	0.00	0.00
6	0.00	0.00	6	0.00	0.00
7	0.00	0.00	7	0.00	0.00
8	14.17	12.04	8	18.35	15.60
9	46.73	51.76	9	89.93	92.04
10	50.76	94.91	10	100	177.04
11	3.35	97.75	11	7.37	183.31
12	-82.91	0.21	12	0.00	183.31
13	-0.18	0.00	13	0.00	183.31
14	0.00	0.00	14	-55.87	117.58
15	0.00	0.00	15	0.00	117.58
16	0.00	0.00	16	-39.08	71.06
17	0.00	0.00	17	-30.90	35.25
18	0.00	0.00	18	0.00	35.25
19	0.00	0.00	19	-29.96	0.00
20	22.31	18.97	20	21.48	18.26
21	57.06	67.47	21	37.66	50.26
22	31.02	93.83	22	23.96	70.63
23	-39.45	47.42	23	-39.46	24.20
24	-21.88	0.00	24	-20.57	0.00

MW in multi-period model, which means multi-period model, with a 27% savings of wind power, can more efficiently use the variable wind power over the single-period one.

From the economic point of view, there is a small difference in the two models as noticed in the values of production cost (pc) (Table 5.3). The objective function consists of costs for

Table 5.3: *Production cost of both models for 14-bus system*

OPF model	pc [$]	Δ [%]
Single-period	479595.01	1.3
Multi-period	473427.04	

generating real power by both generating units and energy storages whereas production cost is the cost for generating real power by only the generating units (not including generating cost by the storages). The multi-period model results in roughly 1.3% lower in production cost than the single-period model. This indicates multi-period model could provide economically optimal solution compared to single-period model regarding the production cost and total amount of wind to be curtailed.

5.7.2.2 IEEE 57-bus system

In this section, to better understand the differences and similarities of both models, tests on modified IEEE 57-bus system (described in 5.7.1.3) are performed. In this system, load has a peak value of 1271.20 MW. Total installed capacity of wind farms is assumed to be 1000 MW. An ESS is also installed at bus 12. Parameters for this ESS can be found in Table 5.4. Initial energy B_0 of the ESS is set to 200 MWh.

Table 5.4: *Parameters of the ESS*

P_{ch}^{max} [MW]	P_d^{max} [MW]	B_0 [MWh]	B^{max} [MWh]	η_{ch}	η_d
200	200	200	400	0.85	0.85

Simulation results are represented in figures 5.15 and 5.16. Detailed operational schedule for the ESS in each model can be seen in Table 5.5.

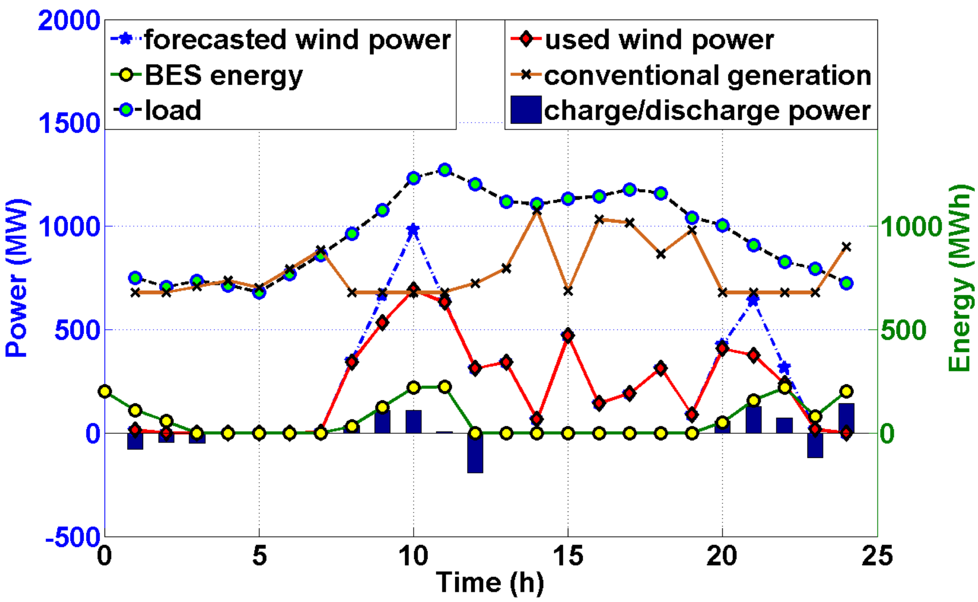

Figure 5.15: *ESS operation in single-period model*

As can be noticed from Fig. 5.15, 5.16 and Table 5.5, in this case study, multi-period model yields more remarkably different operational schedule from single-period model. For example, in single-period model (Fig. 5.15), the ESS immediately discharges all of its available energy (B_0) during low wind periods (hours 1, 2 and 3). ESS in multi-period model, on the contrary, only discharges with very small amounts at the first hours and waits until hour 6 and 7 to get discharged with higher amounts. When wind power is gradually increased (hours 8, 9 and 10), ESS in multi-period model is charged up to its limit whereas in single-period model it is

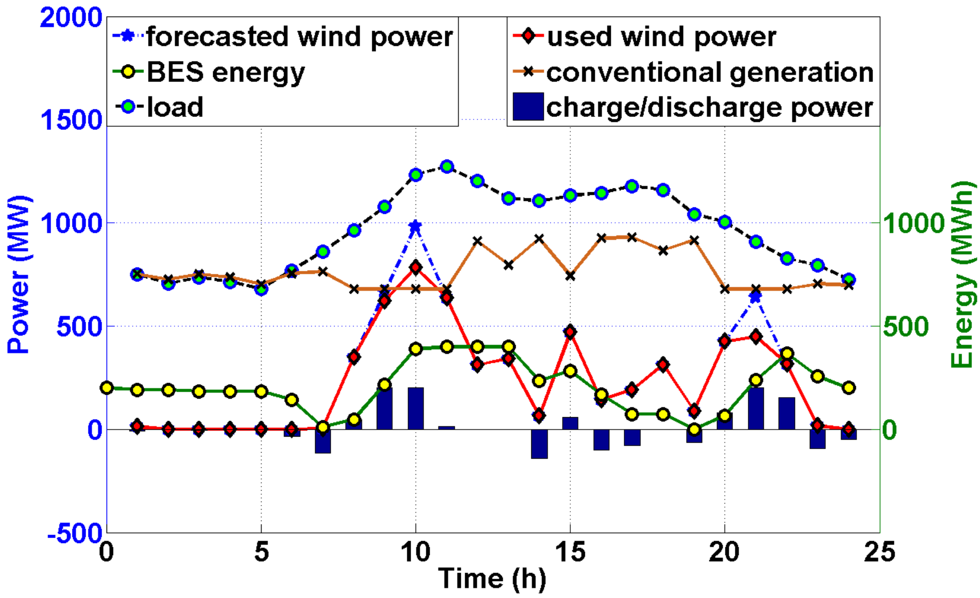

Figure 5.16: *ESS operation in multi-period model*

charged much less. In the next periods (hours 11 to 14), wind power starts to decrease and ESS in single-period model is discharged right at hour 12. ESS in multi-period model is discharged at hour 14 when wind reaches an extremely low value.

Values of production cost (pc) for this case study are shown in Table 5.6. From this table, multi-period model achieves approximately 1.75% production cost savings over single-period model.

Total amount of curtailed wind power is approximately 435.97 MW for multi-period model and 798.85 MW for single-period model. Again, in multi-period model, wind curtailment is minimized with a 45% savings of wind power over single-period model.

Furthermore, with the effective exploitation of ESS in multi-period model, dispatching profiles of conventional generating units in multi-period models (Fig. 5.14 and 5.16) are considerably flatter than those in single-period models (Fig. 5.13 and 5.15), which presumably results in better efficiencies (not accounted for here) and emission reduction.

To have an insight into the operation of ESS in both models, we further examine hourly LMP variations of the 57-bus system above. Fig. 5.17 shows hourly LMPs of all buses before adding ESS. Fig. 5.18 is the plot of hourly LMPs in multi-period model (with ESS installed) and Fig. 5.19 shows hourly LMP variations in single-period model (with ESS installed).

From figures 5.16 and 5.17, there is an interesting observation that operation of ESS in multi-period model completely follows the hourly LMP variations. In other words, multi-period model takes a picture of hourly LMP variations of the system. Then, to optimize the combined operation of the generating units and ESS, it tries to have the ESS charged at periods of low LMPs and discharged at periods of high LMPs. Accordingly, the ESS can help improve the

Table 5.5: *ESS operational schedule in single-period and multi-period models*

t [h]	P_{ch}/P_d [MW]	B [MWh]	t [h]	P_{ch}/P_d [MW]	B [MWh]
1	-77.92	108.33	1	-7.18	191.55
2	-44.29	56.23	2	0.00	191.55
3	-47.79	0.00	3	-6.13	184.33
4	0.00	0.00	4	0.00	184.33
5	0.00	0.00	5	0.00	184.33
6	0.00	0.00	6	-35.30	142.80
7	0.00	0.00	7	-113.87	8.84
8	36.89	31.36	8	45.60	47.60
9	110.75	125.50	9	200.00	217.60
10	108.79	217.97	10	200.00	387.60
11	7.63	224.46	11	14.59	400.00
12	-190.79	0.00	12	0.00	400.00
13	0.00	0.00	13	0.00	400.00
14	0.00	0.00	14	-141.65	233.36
15	0.00	0.00	15	59.21	283.68
16	0.00	0.00	16	-99.07	167.13
17	0.00	0.00	17	-80.08	72.92
18	0.00	0.00	18	0.00	72.92
19	0.00	0.00	19	-61.98	0.00
20	59.26	50.37	20	78.36	66.60
21	126.06	157.52	21	200.00	236.60
22	71.67	218.44	22	152.07	365.86
23	-117.67	80.01	23	-93.32	256.08
24	141.17	200.00	24	-47.67	200.00

Table 5.6: *Production cost in both models*

OPF model	pc [$]	Δ [%]
Single-period	878070.82	1.75
Multi-period	862944.14	

hourly LMPs by raising low prices and decreasing high prices as can be seen in Fig. 5.18.

Take hour 7 for example, ESS in multi-period model is discharged with highest amount at this hour (Fig. 5.16) even wind at previous hours are also very low because the model can see that the price at this hour gets highest value compared to prices at previous hours (Fig. 5.17). Contrarily, since single-period model does not have the ability to foresee hourly LMP variations of the system, it has the ESS discharged as soon as wind power is low (hour 1, 2 and 3). The hourly LMPs in single-period model can possibly be affected at periods when the ESS is charged or discharged and remain the same at other periods (see Fig. 5.19).

From the above analysis, it can be concluded that in single-period model, ESS is only oper-

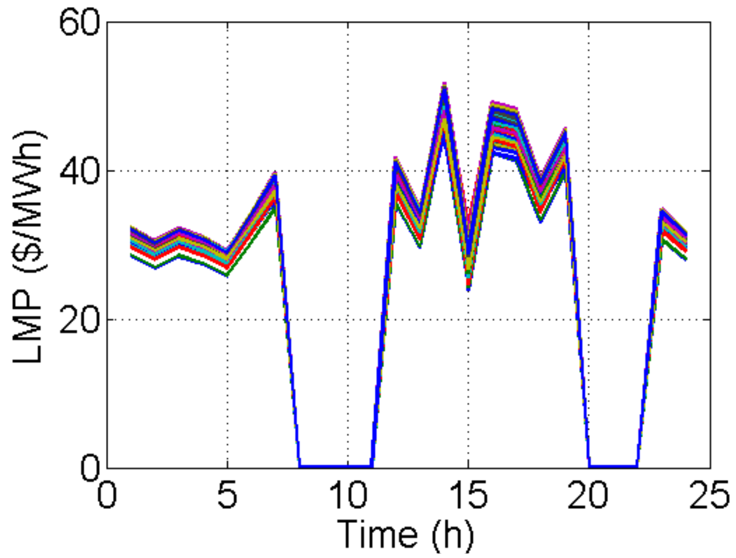

Figure 5.17: *Hourly LMPs of the system without ESS*

ated based on variations of wind power while in multi-period model, it is operated based on both wind and LMP variations. Also, since ESS is a time inter-dependent device, i.e., its operation at a period depends on that in the previous period, multi-period model is a more mathematically correct approach for studying this problem.

5.7.3 Sensitivity analysis on ESS location

In this section, tests are carried out with the methodology to define candidate ESS locations described in Section 3.5. In particular, first, the base case multi-period OPF (without ESSs installed) is run, which provides values of the Lagrangian multiplier λp_i^t. Next, the parameter df_i is computed and sorted. Buses with the highest values are selected as the best candidate buses for ESS installation while buses with the lowest values are the worst candidate buses. Then, tests are performed by installing different numbers of ESSs among the best and the worst candidate buses to assess impacts of ESS location on system operational parameters including production cost, amount of wind to be curtailed and marginal prices.

- Production cost: Cost for generating real power by the generating units only (not including generating cost by the storages).
- Amount of wind curtailment: Wind is curtailed once there is surplus wind but the ESSs have already reached their capacity limits, either power or energy limit. This curtailment of wind can be viewed as an undesirable loss of such a "cost-free" and clean energy.
- Marginal prices or LMP: LMP is an important price indicator of unit MWh injection at each node and congestion in the transmission network [106]. It consists of marginal unit cost, congestion cost, and cost due to losses. Reference [22] demonstrates that LMPs play a significant role in driving storage operation at low levels of ESS integration.

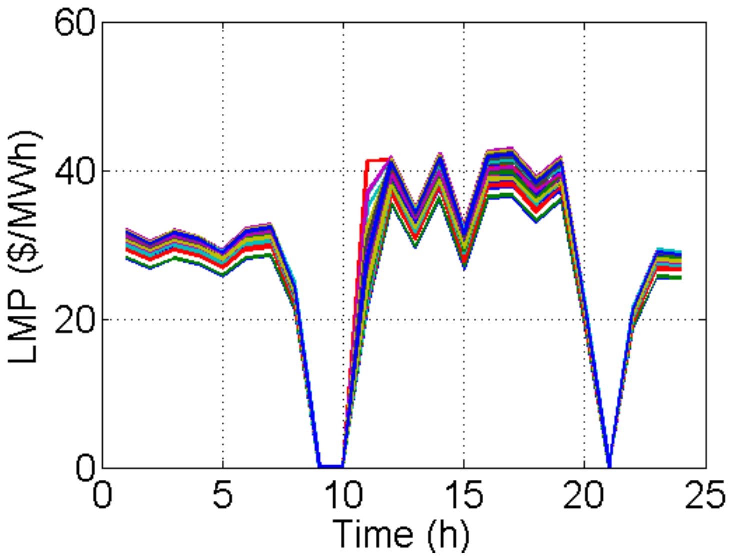

Figure 5.18: *Hourly LMPs of the system with ESS in multi-period model*

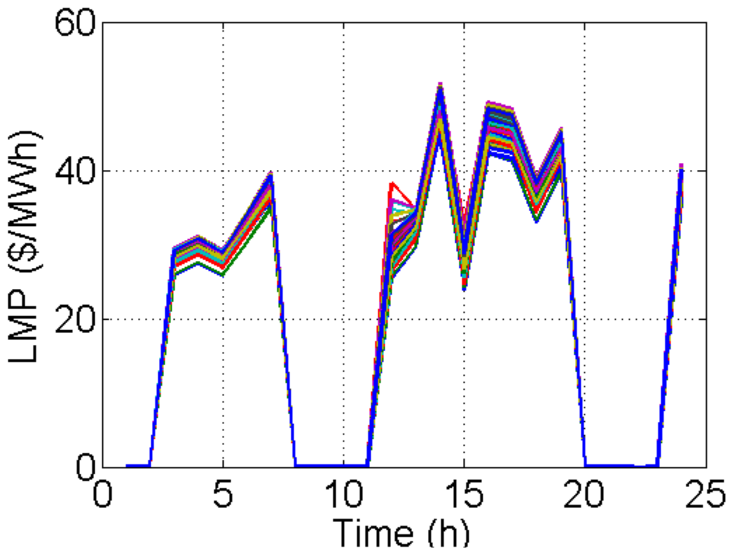

Figure 5.19: *Hourly LMPs of the system with ESS in single-period model*

In this test, wind data are taken from real wind records measured at wind farms in Sicily, Italy. Load data are also relevant to the typical load of a winter day in Italy. Both wind and load data are suitably scaled down to fit the case studies. Tests are carried out on IEEE 14-bus system without any congestion and on IEEE 118-bus systems with congestion.

5.7.3.1 IEEE 14-bus system

In this section, tests are performed on modified IEEE 14-bus system (described in Section 5.7.1.1). The wind plant at bus 2 has an installed capacity of 250 MW. ESSs are added to support wind generation due to its intermittent behavior, and hence help to reduce wind curtailment and improve the overall economics.

Parameters for the ESSs, small and big ones, are provided in tables 5.7 and 5.8. The big ESS in Table 5.8 are equivalent to two ESSs in Table 5.7 connected to the same bus.

Table 5.7: *Parameters for small ESS*

P_{ch}^{max} [MW]	P_{d}^{max} [MW]	B^{max} [MWh]	η_{ch}	η_{d}
30	30	120	0.90	0.90

Table 5.8: *Parameters for big ESS*

P_{ch}^{max} [MW]	P_{d}^{max} [MW]	B^{max} [MWh]	η_{ch}	η_{d}
60	60	240	0.90	0.90

In this system, loads with peak value of 732 MW are supplied from both conventional and wind generation. When wind is sufficient, it will be the priority source to supply loads and if there is still surplus wind power, ESSs will be charged. When wind power is not sufficient, ESSs will be discharged to supply loads while respecting all technical constraints. If both wind and ESS stored energy are not enough for the loads, conventional generators will be dispatched consequently.

After running the base case OPF model (without ESSs installed), the Lagrangian multipliers of real power at each bus in each hour are determined. The parameter df_i is then calculated for each bus i, including wind bus and load buses (Table 5.9).

Table 5.9: *Values of the parameter df_i at each bus*

Best candidate bus no.	df_i [$/MWh]	Worst candidate bus no.	df_i [$/MWh]
14	1739.16	11	1615.55
10	1662.22	4	1610.09
9	1657.42	12	1605.50
13	1633.53	5	1569.58
7	1622.41	2	1485.79

From this table, the first 5 buses (14, 10, 9, 13 and 7) with highest values of Lagrange multipliers are selected as the best candidate buses to install the ESSs.

Next, different cases where different numbers of ESS are placed in the system are considered to assess the quality of the sensitivities computed. The tests are categorized as in Table 5.10. Parameters of the big ESS in cases 7 and 8 are provided in Table 5.8.

The optimization problem is run for a period of 24 hours. Operation of the ESS for Case 2, with 1 ESS connected to bus 14 (the best candidate bus), are represented in Fig. 5.20. As shown

Table 5.10: *Tests for modified IEEE 14-bus system*

Case 0	No ESS connected to the network
Case 1	1 ESS connected to bus 2 (the worst candidate bus)
Case 2	1 ESS connected to bus 14 (the best candidate bus)
Case 3	2 ESSs, 1 at bus 2, the other at bus 14
Case 4	2 ESSs connected to buses 9 and 14 (best candidate buses)
Case 5	3 ESSs, 1 at bus 2, the others at buses 9 and 14
Case 6	3 ESSs connected to buses 9, 10 and 14 (best candidate buses)
Case 7	1 large ESS connected to bus 2
Case 8	1 large ESS connected to bus 14

in the figure, the ESS is charged when wind power exceeds the load and then it is discharged when wind power is insufficient to supply the load. At periods when wind is much higher than the load, after the storage has been charged up to its limits, either power or energy limit, the extra wind is necessarily curtailed.

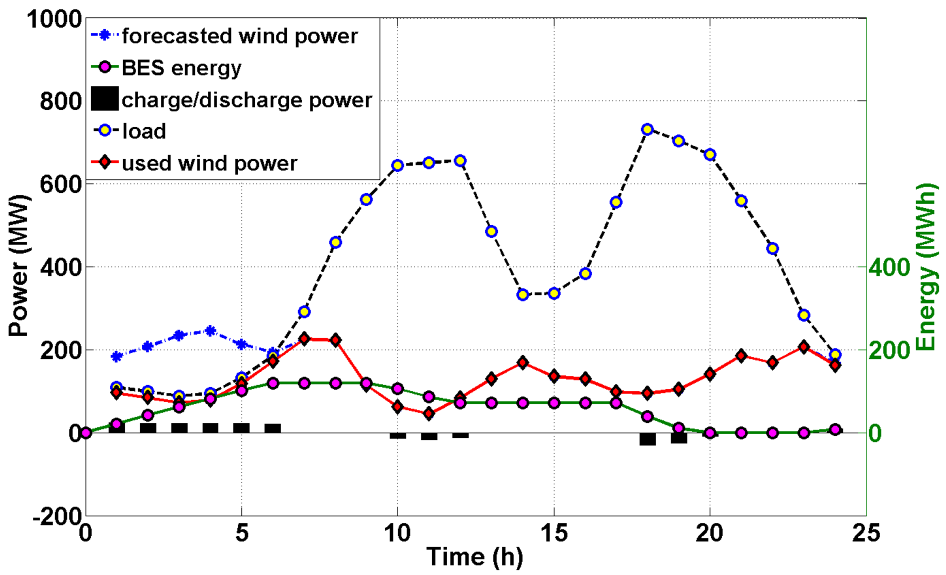

Figure 5.20: *Operational schedule of the ESS in Case 2*

To understand the operation of the ESSs in each case, the resulting production costs, amounts of curtailed wind power, and LMPs of the above mentioned cases will be compared.

(i) **Production costs**

Generation costs of all 8 cases are shown in Fig. 5.21. It can be clearly seen from this figure that the case without ESSs yields highest generation cost over the other cases. Cases with only 1 ESS connected to the network result in a noticeable reduction of generation cost and this reduction is higher in the case when the ESS is connected to the best candidate bus (Case 1 achieves about 1.9% cost savings while Case 2 obtains approximately 2.19% cost savings compared to Case 0). In cases 3 and 4, with 2 ESSs, and cases 5-6, with 3 ESSs connected to the system, the production cost is further reduced. In general, the selection of the best candidate buses improves system operation, although the effect due to the total ESS capacity looks more significant in this case. Quality of sensitivities computed can be evaluated by comparing cases 1-2 and 7-8: the comparison shows that the candidate buses for ESS installation are actually correctly identified. Also, from the above analysis, it can be observed that higher capacity of ESS added to the network can significantly improve the overall economics of the system.

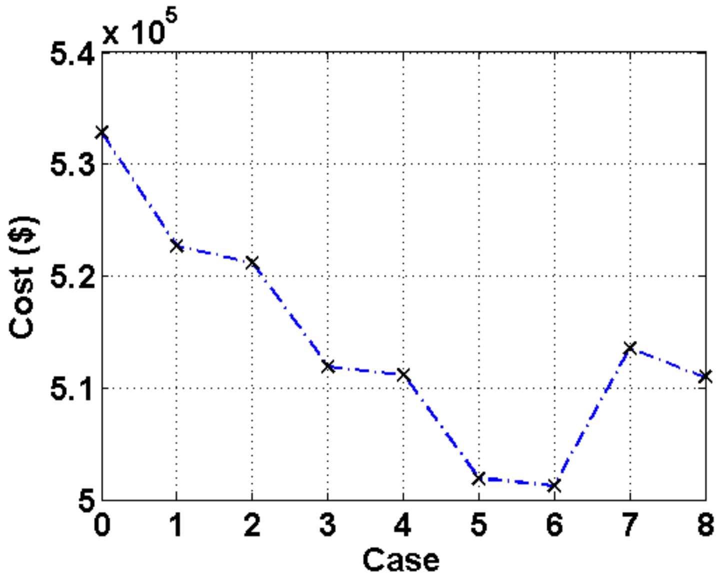

Figure 5.21: *Production costs of all cases*

(ii) **Curtailed wind energy**

As can be seen from Fig. 5.20, wind is possibly curtailed from hours 1 to 5, in which wind is higher than load. Amounts of wind curtailment in all 8 cases are shown in Fig. 5.22. Amounts of curtailed wind energy in all 8 cases vary similarly as the generation costs. It is worth noticing that Case 2 uses more wind power than Case 1 even the ESS in Case 2 is located far from the wind bus. The same occurs when comparing cases 7 and 8. Hence, it is important to observe that the computed sensitivities take correctly into account also wind curtailment.

(iii) **Locational Marginal Prices**

The addition of ESSs at different locations results in changes in LMPs at all buses. The hourly LMP variation of all 14 buses in Case 0 are presented in Fig. 5.23. During peak load periods, LMPs also reach peak values while during off-peak hours their values become much lower. This is understandable, since at peak load hours, cheap wind power

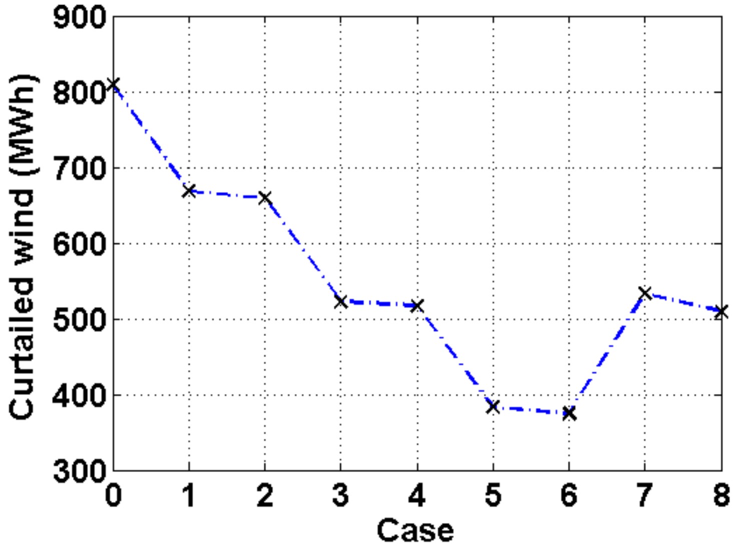

Figure 5.22: *Amount of curtailed wind of all cases*

is not sufficient to supply the load and more expensive conventional generators are dispatched instead, which causes an increase in LMPs.

Fig. 5.24 shows LMPs of Case 1, in which a BES is connected to bus 2 (the worst candidate bus). In this case, peak prices are noticeably reduced for the higher peak (hours 18 to 20), from peak value of about 140 $/MWh to around 115 $/MWh. The lower peak (during hours 10 to 12) is also slightly reduced (from peak value of about 105 $/MWh to 100 $/MWh). This indicates that the addition of the BES can provide additional cheap power to loads during peak periods. The reduction in LMP values in this case will affect the cost of supplying load at each bus.

In Case 2 (Fig. 5.25), both peaks are further reduced. The second peak (hours 18 to 20) is considerably reduced and becomes almost equal to the first peak (hours 10 to 12), i.e., about 90 $/MWh. This indicates the addition of BESs at a bus in the best candidate buses has more significant influence on marginal prices than the addition of BESs at a bus in the worst candidate buses, which means the computation of sensitivities is correct. For the remaining cases, similar conclusions can be drawn.

5.7.3.2 IEEE 118-bus system

To further investigate the sensitivity of ESS location and size in congestion relief application in a large network, tests are also carried out on modified IEEE 118-bus system (described in Section 5.7.1.4). In this case, ESSs are installed to charge this otherwise curtailed wind amount for later releasing and allow an efficient utilization of transmission lines. A congestion is observed during peak periods on lines 8-5 and 8-30, from wind farms to loads. Parameters for the ESSs are the same as those in the IEEE 14-bus system, i.e., shown in tables 5.7 and 5.8.

In this test, the calculated parameter df_i, the best candidate and worst candidate buses for

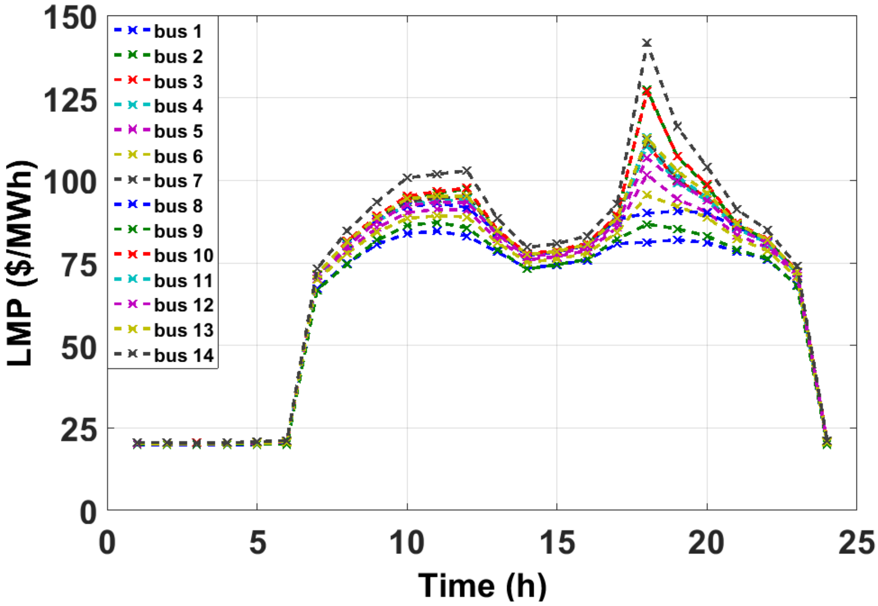

Figure 5.23: *Hourly LMP variation in Case 0*

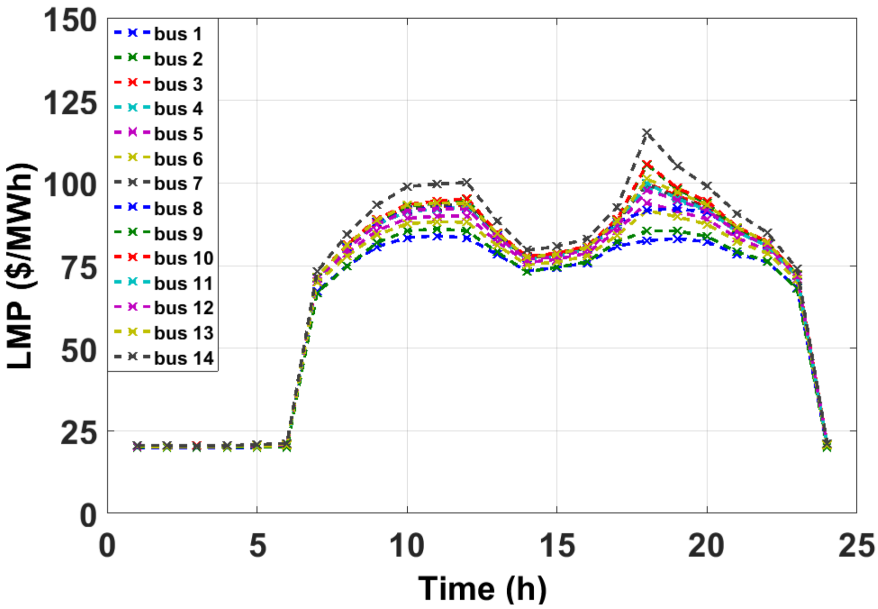

Figure 5.24: *Hourly LMP variation in Case 1*

installing ESSs are selected as shown in Table 5.11.

From this table, the best candidate buses include buses 5, 3, 7, 2, 11, 117, 13, 14, 109 and 16 while the worst candidate buses include buses 37, 114, 115, 23, 38, 17, 30, 8, 9 and 10. It is worth noticing that wind buses (8 and 10) are not in the best candidate set: this is however not odd, as the optimization is carried out from a system point of view. The tests carried out are described in Table 5.12.

Now, a plot is provided (Fig. 5.26) showing the operation of the ESS connected to bus 5 (the

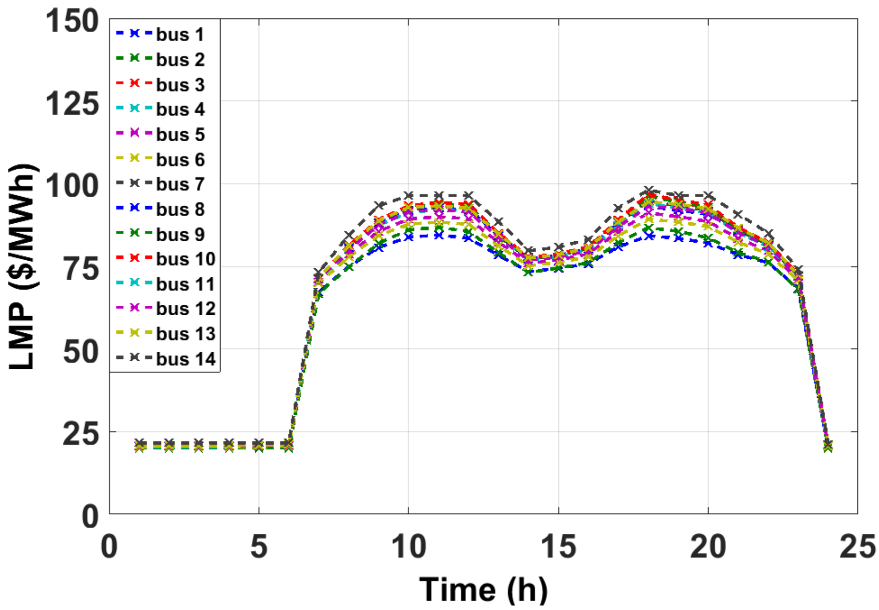

Figure 5.25: *Hourly LMP variation in Case 2*

Table 5.11: *The selected best and worst candidate buses*

Best candidate bus no.	df_i [$/MWh]	Worst candidate bus no.	df_i [$/MWh]
5	658.28	37	581.38
3	654.75	114	581.21
7	650.06	115	581.18
2	649.77	23	576.83
11	648.80	38	575.17
117	647.73	17	574.39
13	637.95	30	552.03
14	631.46	8	491.40
109	624.09	9	486.10
16	623.80	10	480.64

best candidate bus) to exclusively examine how it shifts wind to avoid transmission constraint.

From this figure, the ESS is charged during off-peak periods (hours 1 to 5 and hours 14 to 16), which are also periods without transmission congestion, and then discharged during peak periods (hours 10 to 12 and hours 17 to 20) when congestion occurs. Clearly, the ESS has thoroughly shifted wind power from wind side to load side to supply loads when wind power can not be transferred from wind farms to loads due to limited transmission capacity.

Also, Fig. 5.27 shows a plot of power flows on line 8-5, connecting wind farms and loads.

Table 5.12: *Tests for IEEE 118-bus system*

Case 0	No ESS connected to the network
Case 1	1 ESS connected to bus 8 (one of the worst candidate buses)
Case 2	1 ESS connected to bus 5 (best candidate bus)
Case 3	2 ESSs, 1 at bus 8 and the other at bus 5
Case 4	2 ESSs connected to buses 5 and 117 (best candidate buses)
Case 5	3 ESSs, 1 at bus 8, the others at buses 5 and 117
Case 6	3 ESSs, 2 at buses 8 and 10, the other at bus 5
Case 7	3 ESSs connected to buses 2, 5 and 117
Case 8	1 large ESS system connected to bus 8
Case 9	1 large ESS system connected to bus 5

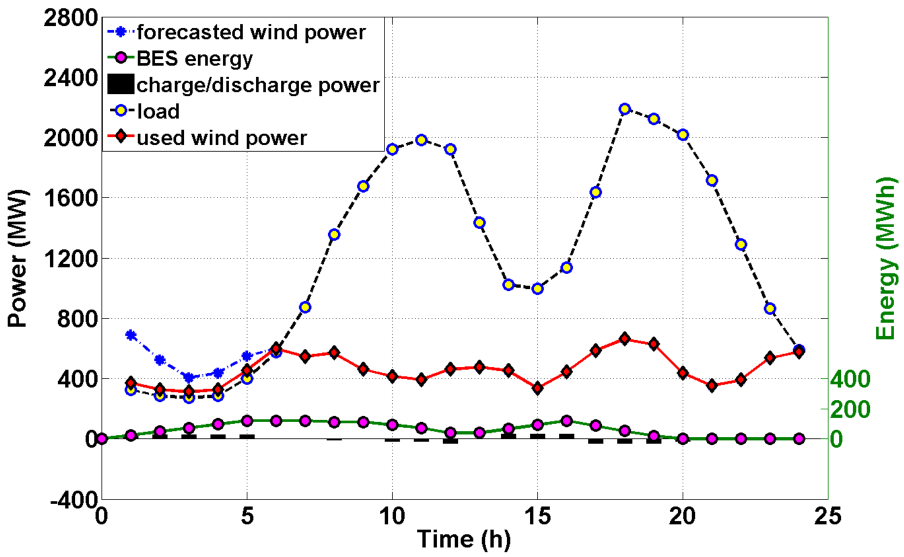

Figure 5.26: *Operation of the ESS in Case 2*

The dotted line with crosses in the plot corresponds to the unconstrained case without ESS: the power flow limit (the dotted red line with filled circle) is not enforced by the optimization procedure and this would cause the real-time curtailment of excess wind power. This figure clearly illustrates the alternative path that the ESS provides for wind power to alleviate the congestion, i.e., the full blue line with circles. In this way, power flow on line 8-5 during low load hours (hours 1 to 5 and 14 to 16) are increased but still lower than the flow limit. Such flow increase is due to the wind power flow used to charge the ESS at load bus. This stored energy is released to supply loads during peak periods, when congestion occurs. Consequently, wind power can still be supplied to loads while ensuring the flow limit.

The resulting production costs, amounts of curtailed wind power, and LMPs of the above mentioned cases are also compared.

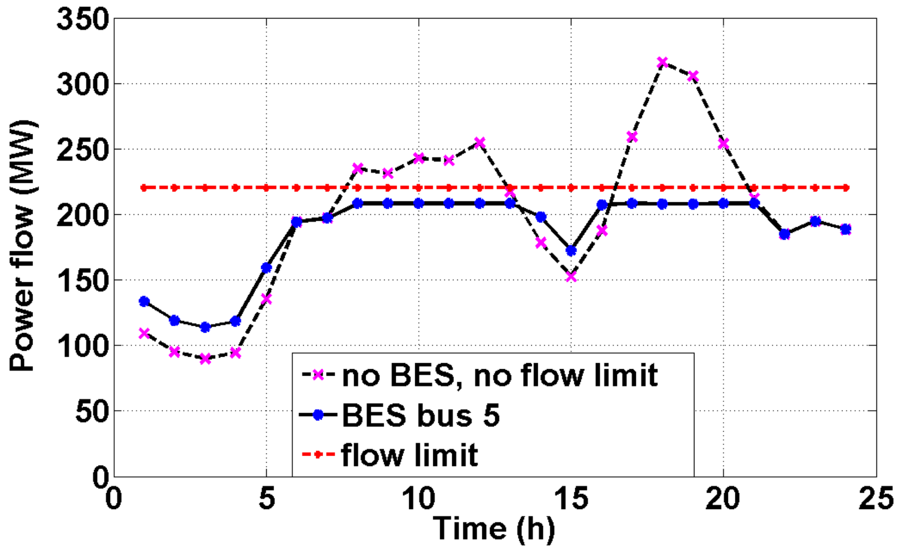

Figure 5.27: *Power flow on line 8-5 in Case 2*

(i) **Production costs**

In Fig. 5.28, a plot of production costs of the system in all cases is provided. Case 0 yields the highest cost compared to the others. From cases 1 to 5, the cost is gradually reduced. This demonstrates that higher numbers of ESS installed return more economical operation of the system. The effectiveness of a good selection of candidate buses by the sensitivity computation is clear by looking at cases 1 and 2: Case 2 results in higher saving as compared to Case 1. Similarly, cases 4 and 7 where there are more ESSs installed at the best candidate buses also result in lower production costs compared to Case 3, and cases 5 and 6, respectively. Cost savings in Case 8 is lower than that in Case 3 and Case 9. From this analysis, it can be deduced that in such a congested system, storage devices placed at the best candidate buses can provide far more economical operation than those placed at the worst candidate buses. Thus, it is important to figure out the best candidate locations for the planning of storage devices. Moreover, in this case, a large ESS connected to a bus in the best candidate buses can operate as efficiently as several ESSs distributed among the best candidate buses.

(ii) **Curtailed wind energy**

Amounts of curtailed wind energy in all cases are represented in Fig. 5.29. Considering Case 1 and Case 2, for instance, the conclusion is that the difference in total cost (Fig. 5.28) is not due to wind curtailment, like for the 14-bus test system above, but due to congestions: the optimal placing of ESS allows, in this case, to best relieve the congestions due to wind power. In this case, the amount of wind energy to be curtailed is not affected by centralized or decentralized placement of the storage devices.

(iii) **Locational Marginal Prices**

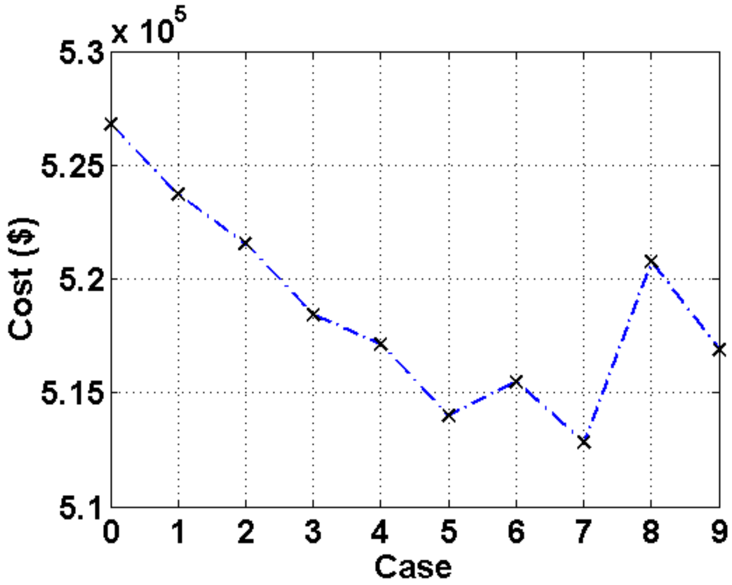

Figure 5.28: *Production costs of cases 0 to 9*

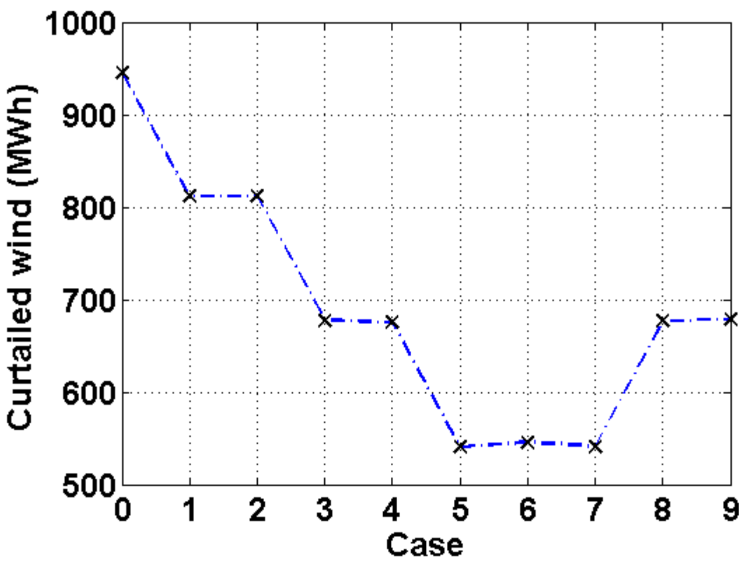

Figure 5.29: *Amounts of curtailed wind of cases 0 to 9*

Hourly LMP variation of all buses for each case is also shown to discuss the impacts of ESS location and size on LMPs. Hourly LMP variation of Case 0 is shown in Fig. 5.30. In this figure, curves with the highest peaks belong to load buses on the receiving side of congested lines and curves with the lowest prices belong to wind buses. During off-peak periods, LMPs are about the same for all buses since there is no congestion.

Hourly LMP variation in Case 1, when there is 1 ESS connected to bus 8 (one of the worst candidate buses), is basically the same as in Case 0. In Case 2, with 1 ESS added at bus 5 (the best candidate bus), the higher peak prices during the first peak hours are noticeably

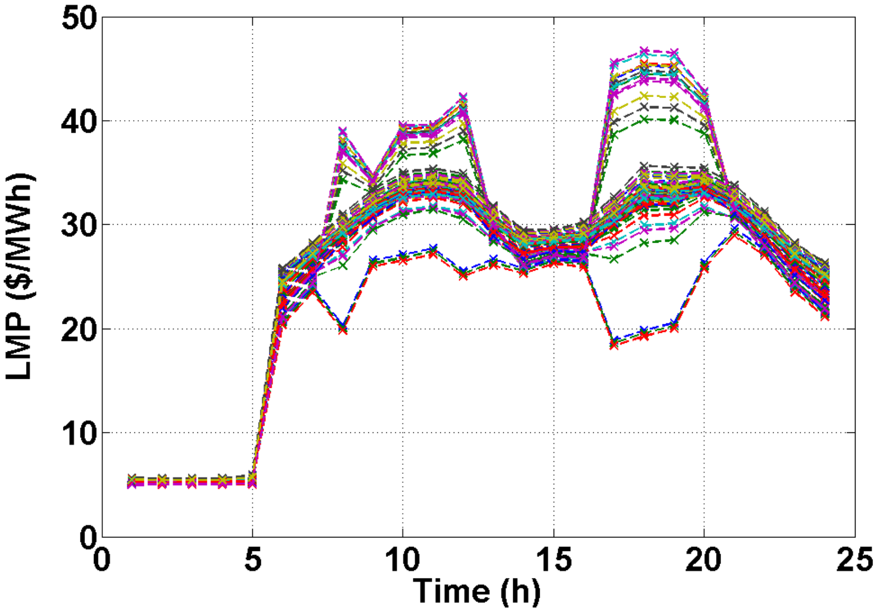

Figure 5.30: *Hourly LMP variation of Case 0*

lowered and those during the second peak hours are also considerably lowered at some periods (hours 17 and 20) as shown in Fig. 5.31. Peak prices are not reduced at hours 18

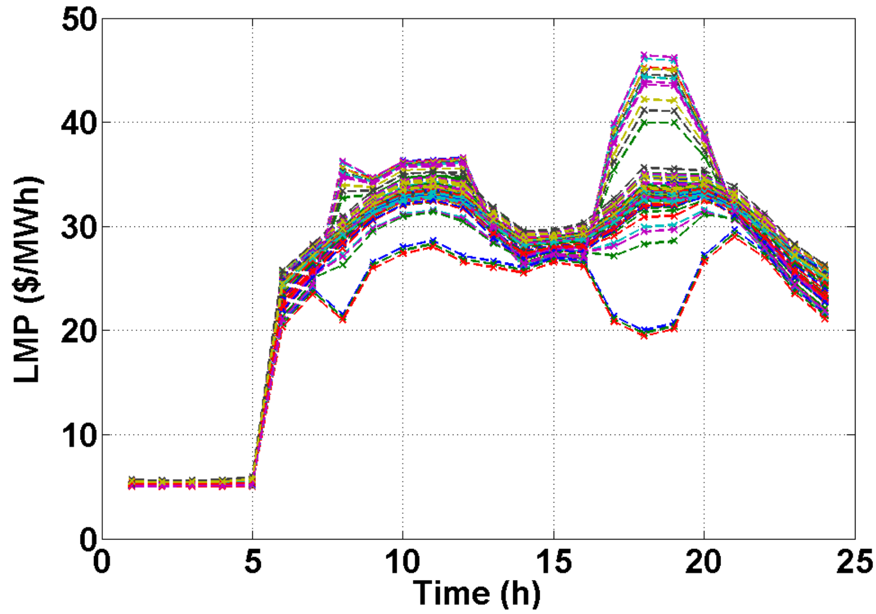

Figure 5.31: *Hourly LMP variation of Case 2*

and 19 of the second peak period because the limited capacity of the ESS is not enough to supply the high load during these hours. For these peak prices to get reduced, higher capacity of the ESS is required. In this case, to avoid transmission congestion, the ESS is charged by wind power during low load periods, when there are no congestions, and then discharged to supply the cheap energy to loads during congestion hours, hence it can help to reduce the marginal cost during peak hours of these load buses. This operation of the ESS has effectively supported wind generation and efficiently makes use of the available transmission capacity.

In Case 4 (2 ESSs connected to the best candidate buses), LMP values of the higher peak curves are further reduced during the first peak periods and during hours 17 and 20 of the second peak (Fig. 5.32).

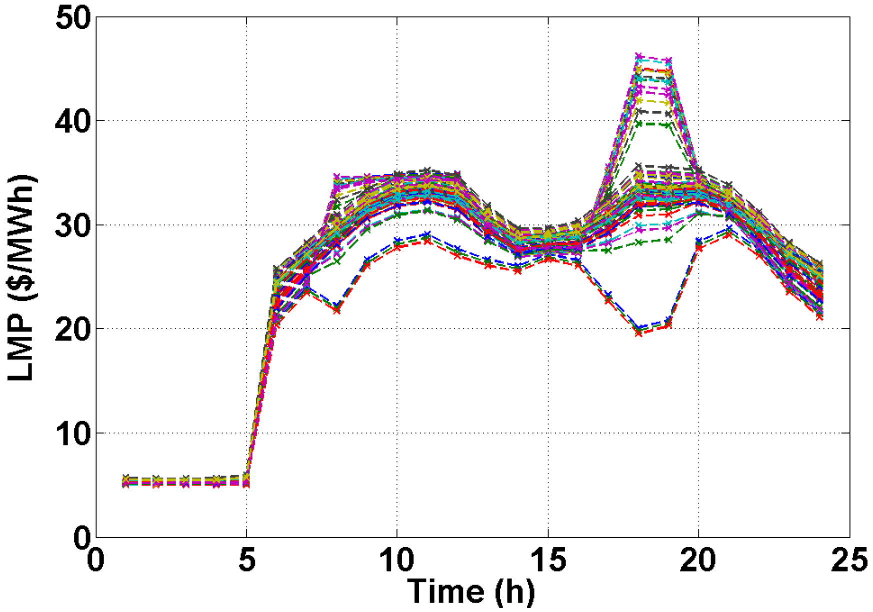

Figure 5.32: *Hourly LMP variation of Case 4*

In this test, sets of the best and the worst candidate buses for installing ESSs have been identified based on an economic criteria, i.e., the Lagrangian multipliers. Operation of ESSs is assessed in two different applications, i.e., time-shifting wind to meet demand and mitigating transmission congestion to avoid wind curtailment and allow an efficient utilization of transmission capacity. Installation of ESSs at the best candidate buses, in both applications, is shown to provide much better operation than at the worst candidate ones.

5.7.4 Tests on the combined GA and POPF approach

Test on this approach is carried out on modified IEEE 57-bus system as described in 5.7.1.3. In this system, total load has a peak of 1620 MW. A wind farm of 450 MW installed capacity is connected to bus 12 and other smaller wind farms are connected to busses close to bus 12 for a total wind capacity of 750 MW, accounting for 46.3% of wind power penetration. ESSs are to be placed to time-shift wind energy from off-peak load periods (low electricity price) to peak periods (high electricity price) to add economic value to wind energy and avoid wind generation curtailment. Capacities of these ESSs are to be defined by the solution of the OPF. Accordingly, total generation cost of the system is minimized while wind generation is maximized. The ESSs are assumed of Compressed Air Energy Storage (CAES) technology. These CAES systems have equal charging and discharging efficiency, equal to η. Parameters of the CAES are shown in Table 5.16 [15]. Without loss of generality, the ESSs is assumed to start with an initial energy level of 0 MWh.

Table 5.13: *Parameters of the CAES*

C_B ($/kWh)	C_R ($/kW)	N (years)	η	r (%)
5	700	30	0.85	10

In this test, the combined GA-Probabilistic OPF (POPF) model (presented in Section 5.4) is applied to optimally place and size ESSs in power systems while minimizing ESS investment cost and the total generation cost. Wind and load input data are as described in 5.4.1.

The approach is first carried out with the whole-year data of wind and load. Results of the combined GA and deterministic OPF in this case are summarized in Table 5.14.

Table 5.14: *Simulation results for whole-year*

Optimal location (Bus number)	B^{max} (MWh)	R^{max} (MW)
12	495.2	95.6
29	172.2	31.0

Next, in order to capture seasonal variations of wind and load, the optimization is carried out separately on different seasons. This is done just for sensitivity purpose only, optimal locations and capacities of ESSs are still determined based on the whole-year data above. The corresponding simulation results are shown in Table 5.15, in which optimal locations of ESSs along with their optimal power and energy capacities in each season are presented.

Table 5.15: *Simulation results for all seasons*

Season	Optimal location (Bus number)	B^{max} (MWh)	R^{max} (MW)
Spring	12	483.1	105.4
	29	155.9	32.5
Summer	12	296.4	67.9
	38	49.5	12.0
Autumn	12	468.9	98.2
	29	157.2	31.1
Winter	12	758.2	144.2
	29	211.9	39.1

As can be seen from Table 5.14 that there are 2 ESSs chosen to install, a bigger one at wind bus (bus 12) and a smaller one at load bus (bus 29). Similar results can be observed in Table 5.15. Basically, the location in Table 5.14 is the optimal one for three seasons out of four, taken separately, with one ESS in the windy area and the other in the load center, to support wind generation. In particular, the model would install the biggest ESS at bus 12 (windy area) in all seasons and a smallest ESS at bus 38 (load bus) in summer and at bus 29 (load bus) in the remaining seasons. Both buses 38 and 29 are load centers. The difference in ESS optimal location between summer and the other seasons may result from the relatively high difference in load and wind profiles in summer compared to the other seasons as seen in Fig. 5.2. Power and energy capacities of both ESSs reach highest values in winter when wind power during off-peak periods is the highest. Contrarily, in summer, wind power at off-peak periods is notably lower compared to other seasons and the ESSs are charged and discharged with lower values of power and energy.

As an example, in Fig. 5.33, the expected value of operational schedule for wind and ESS at bus 12 in the spring period (corresponding to the Spring row of Table 5.15) is shown. The storage is effectively used to time-shift wind energy by charging wind power at low load periods (hour 1 to 7) and then releasing it during the first peak periods of hour 9 to 12 and the second peak periods of hour 20 to 22. In this case, there is no wind curtailment and wind power output is fully dispatched. As such, the conventional generation is remarkably reduced during these hours. This operation of the ESS closely follows hourly LMP variations of the system as shown in Fig. 5.34. Clearly, the storage is charged during low price periods and then discharged during high price periods. Note also that during high price periods, the storage is decided to discharge more at hours with higher price and vice versa. For example, during the first peak period, the storage is discharged more at hour 10 when the price is higher than at hour 12 when the price gets lower. Similarly, during the second peak period, it is more discharged at hour 21 than at hour 20 when the price is lower.

Since input variables (i.e., wind and load) of the above-mentioned OPF problem are actually stochastic, power and energy capacities of the ESS (i.e., output of the combined GA-OPF problem) can be considered as expected value of the corresponding random variables. In order to carry out Step 2 of the procedure described in Section 5.4.2, the probabilistic assessment is performed on ESS capacities shown in Table 5.14 at the corresponding buses.

Figure 5.35, analogously as in Fig. 5.33, depicts expected values of hourly power and energy of the ESS at bus 12 in Table 5.14. According to this figure, the ESS reaches its power capacity (R^{max}) at hours 4 and 5, and reaches its energy capacity (B^{max}) at hour 7, after 6 consecutive charging periods. Since wind and load variation is highest at hour 4, we choose to perform probabilistic assessment for ESS power capacity based on its operation at hour 4.

In Fig. 5.36, results of the POPF are shown: CDF of ESS power capacity. In this case, installation of the capacity according to Table 5.14 would be not enough in some operating

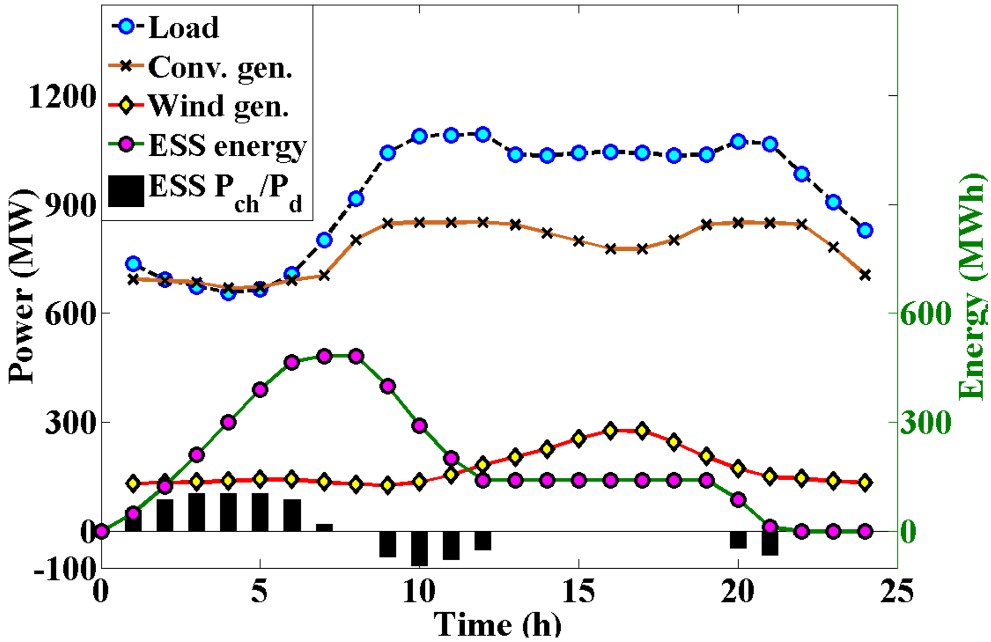

Figure 5.33: *Operation of wind and ESS at bus 12 in spring*

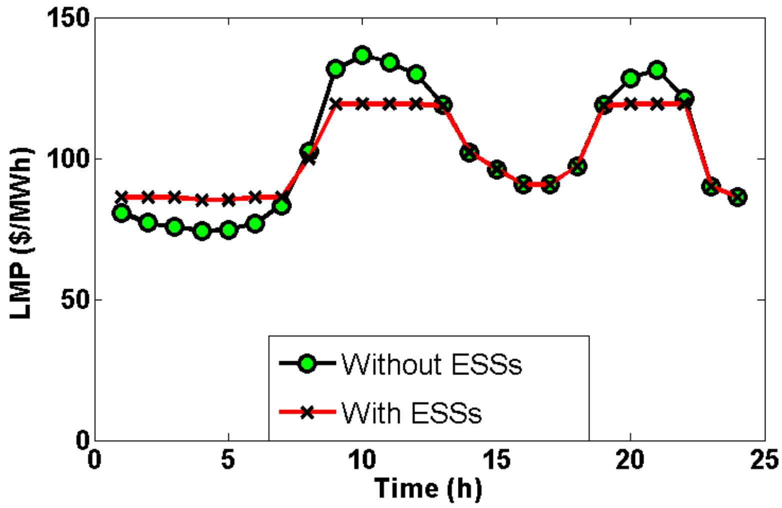

Figure 5.34: *Hourly LMPs at bus 12*

conditions. If the decision maker decided to install ESS for a capacity of 143 MW, almost the whole range of the probability distribution would be covered. If a lower value of capacity is decided, it will lead to a risk of not having enough power capacity for handling uncertainty in the system. For example, using 122, 116, 104 and 102 MW will cover 99, 95, 85 and 75% of the whole range of the probability distribution, respectively. This means that if 5% of risk is accepted, for instance, power capacity of the ESS is approximately 18.9% reduced. Similarly, with 15% and 25% of risk allowed, power capacity of the ESS is roughly 27.3% and 28.7% reduced, respectively.

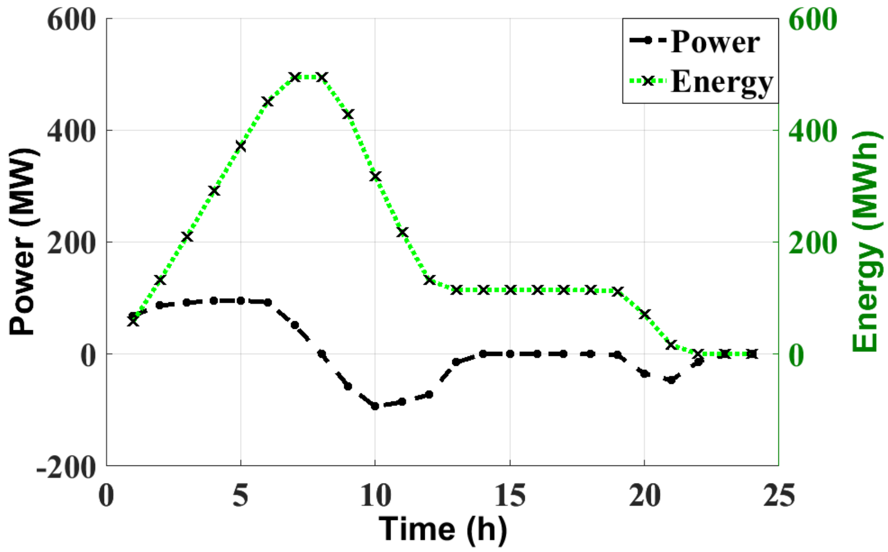

Figure 5.35: *Power and energy of ESS at bus 12*

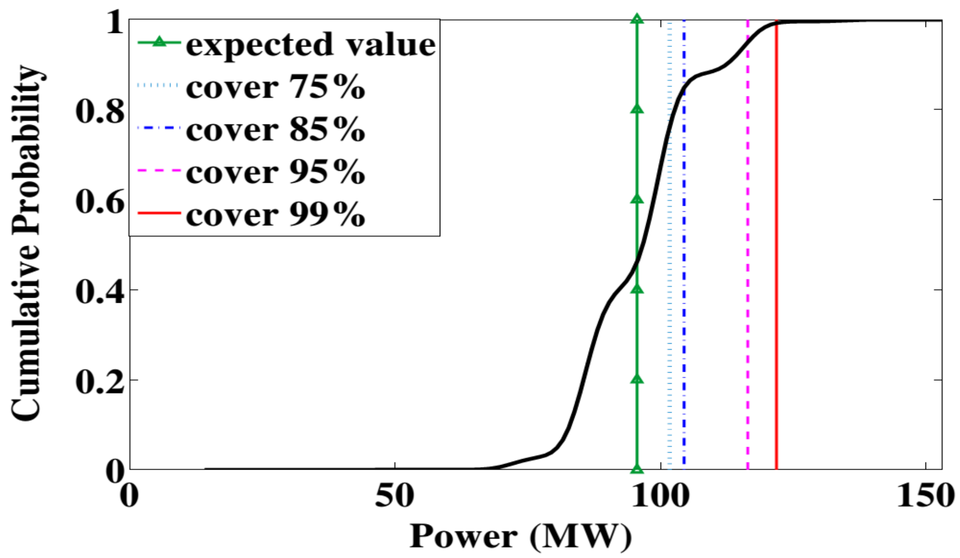

Figure 5.36: *CDF of power capacity of ESS at bus 12, hour 4*

From the probabilistic assessment of power from hour 1 to hour 7, we obtain probabilistic energy sizing of the ESS, based on the relationship between its power and energy in equation (3.12). In other words, ESS energy level at hour 7 is the cumulative sum of charging power along with its efficiency from hour 1 to hour 7. In Fig. 5.37, energy capacity of the ESS is probabilistically assessed. As can be noticed from this figure, the use of 708, 627, 592 and 572 MWh will cover 99, 95, 85 and 75% of the whole range of the probability distribution, respectively. This also means that a 5%, 15%, and 25% of risk accepted will result in a reduction of 20.4%, 24.9%, and 27.4% of the energy capacity, respectively. In this case, if the decision maker needs to cover 85% of wind and load variations, for instance, power and energy capacity

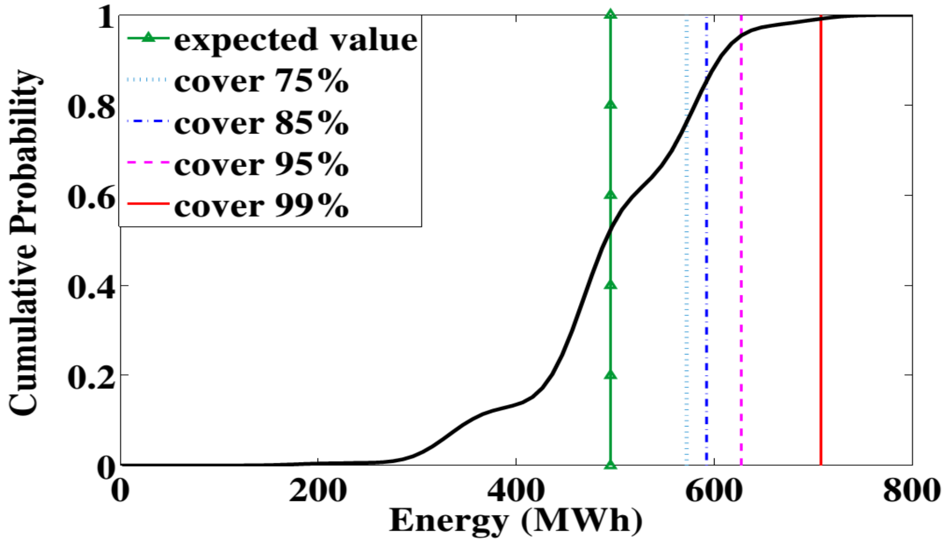

Figure 5.37: *CDF of energy capacity of ESS at bus 12, hour 4*

of the ESS at bus 12 has to be 104 MW and 592 MWh, respectively.

The results show that to completely cover the whole range of uncertainties, ESS power and energy capacities are necessarily much higher than the expected value capacities. However, if a certain level of risk is acceptable, both power and energy capacities will become considerably smaller and the model allows this risk estimate.

5.7.5 Tests on two-stage stochastic approach

5.7.5.1 IEEE 39-bus system

In this section, test on the two-stage stochastic approach (Section 5.5) is performed with modified IEEE 39-bus system (described in 5.7.1.2) to determine optimal capacities of ESSs in its combined operation with wind generation while taking into account the stochastic behavior of wind and load. In order to test the model with different wind penetration levels, which is defined as the ratio between wind farm installed capacity and the peak load, the total installed capacity of both wind farms are assumed 400 MW, 600 MW, and 800 MW, accounting for 20%, 30%, and 40% of wind penetration, respectively. Three different ESS technologies are considered, i.e., Battery Energy Storage (BES), Compressed Air Energy Storage (CAES) and Pumped Hydro Storage (PHS). Parameters of these storage technologies are shown in Table 5.16 [15, 107, 108], assuming $\eta_{ch} = \eta_d = \eta$ for each technology.

Wind and load scenarios are generated using the technique described in Section 5.5.1.1. For this test, there are 6 scenarios of wind and 5 scenarios of load as shown in Figure 5.7. Each scenario of wind is then combined with each scenario of load, which results in a set of 30 wind-load scenarios as the input of the model, each is associated with a probability.

The test is performed first with BES system, and then repeated for the remaining ESS tech-

Table 5.16: *Parameters of three ESS technologies*

	C_B (€/kWh)	C_R (€/kW)	N (years)	η	r (%)
BES	330	400	10	0.85	5
CAES	5	700	30	0.79	
PHS	14	1000	30	0.87	

nologies considered, i.e., CAES and PHS. It turns out that due to the high investment cost of BES, the model does not select this technology for any wind penetration levels. In other words, installing BES in this case does not yield any benefit for the system since its capital cost overweigh the profit from the combined operation of wind and BES. The model, instead, chooses to install CAES and PHS systems. Optimal capacities of the CAES and PHS are shown in Table 5.17. ESS of both technologies is installed at wind penetration level 30% and 40%. At 20% wind penetration level, which is 400 MW total wind installed capacity, since the amount of excess wind power to be time-shifted is also not enough to cover the investment cost of both CAES and PHS, the model does not install the storage device. At higher wind penetration levels (30% and 40%), the model decides to install either CAES or PHS systems and capacity of the storage device is gradually increased with the penetration of wind. Capacities of CAES system is larger than those of PHS; in particular this capacity difference is higher at higher wind penetration levels. As noted from Table 5.16, even though PHS technology has higher efficiency than CAES, its higher daily capital cost still results in smaller capacities of the storage device.

Table 5.17: *Optimal capacities of ESS in IEEE 39-bus system*

Wind	20%		30%		40%	
	PHS	CAES	PHS	CAES	PHS	CAES
B^{max}(MWh)	0.0	0.0	74.4	83.1	109.3	162.8
R^{max}(MW)	0.0	0.0	12.2	15.0	18.3	29.5

Test is also performed for the case when there is no ESS installed to compare the yearly operational cost of the system in both cases, with and without the storage device (Table 5.18).

Table 5.18: *Operational cost of 39-bus system with and without ESS [M€/year]*

Wind	30%	40%
No ESS	463.55	445.88
CAES	457.75	437.72
PHS	458.02	439.10

As can be seen from this table, the total yearly cost of the system is considerably lower when there is ESS installed. Moreover, the case of PHS results in a slightly higher yearly cost compared to that of CAES. The cost difference between three cases is higher at higher wind penetration levels, when higher ESS capacities are installed. That is, the CAES gains a cost reduction of 1.25% at 30% wind penetration and 1.83% at 40% wind penetration while the PHS yields 1.18% cost reduction at 30% wind penetration and 1.52% at 40% wind penetration, with respect to the operational cost in the case without ESSs.

Daily operation of the CAES in all scenarios at 30% wind penetration level, for example, can be seen in Figure 5.38. Basically, in many scenarios (corresponding to load scenarios with higher peaks in Figure 5.7b), the CAES is charged at off-peak periods (hours 1 to 5 and hours 13 to 16) and then discharged at peak periods (hours 7 to 12 and hours 18 to 20). In other scenarios (corresponding to load scenarios with lower peaks in Figure 5.7b), it is charged at off-peak periods (hour 1 up to 7) and gradually discharged at high load periods (hours 9 to 11, 12 to 16, and 17 to 21). In other words, the storage has been fully employed to time-shift wind energy for matching the demand in all scenarios of wind and load.

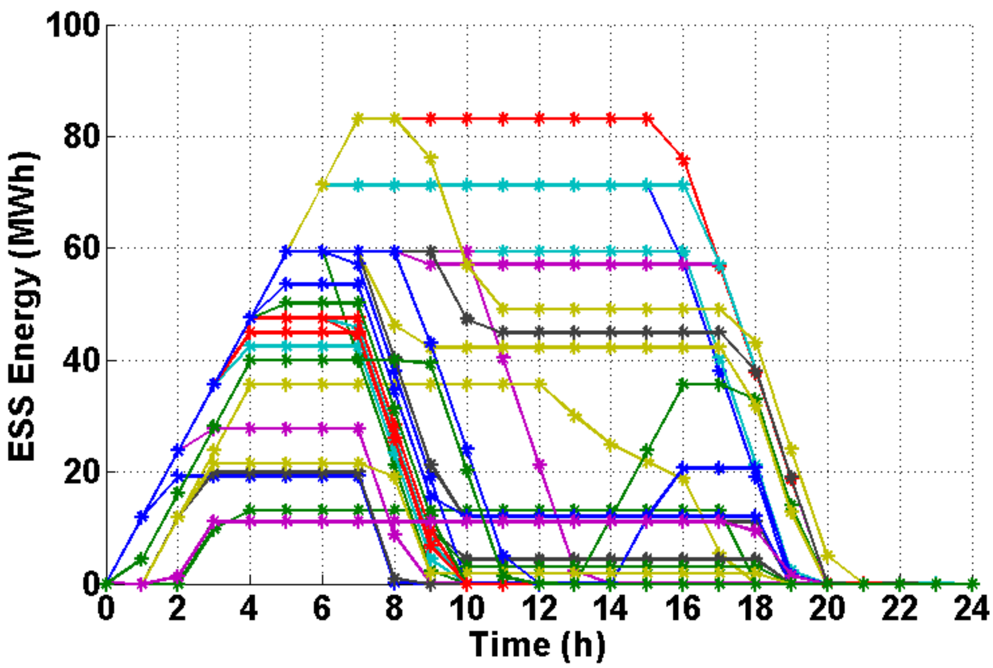

Figure 5.38: *Energy level of the CAES in daily operation*

5.7.5.2 IEEE 118-bus system

To further examine the performance of the model, tests on modified IEEE 118-bus system (described in Section 5.7.1.4) are also carried out. The 3 wind farms connected to buses 6, 62 and 112 are assumed to have a total installed capacity of 1000 MW, 1500 MW, and 2000 MW, accounting for 20%, 30%, and 40% of wind penetration respectively. Wind data are assumed to be the same for the 3 wind farms.

Wind and load scenarios are also generated as in Section 5.5.1.1. In this case, there are also 6 scenarios of wind and 5 scenarios of load obtained. A set of 30 wind-load scenarios as input for the model is created by combining each wind scenario with each load scenario; each wind-load scenario has a probability of occurrence.

In this test, the model is also run with the set of 30 wind-load scenarios for each of the above three ESS technologies at wind penetration levels of 20%, 30%, and 40%. The model again does not choose to install BES due to its high daily investment cost but it installs CAES at both buses, i.e., buses 6 and 62, for all wind penetration levels, from 20% to 40%. For PHS technology, the model only install 1 ESS at bus 62 at 30% and 40% of wind penetration levels. Optimal capacities of the CAES and PHS systems can be seen in Table 5.19 and 5.20.

Table 5.19: *Optimal capacities of CAES at buses 6 and 62 in 118-bus system*

Wind	20%		30%		40%	
Bus	6	62	6	62	6	62
B^{max}(MWh)	0.0	15.5	82.2	154	225.4	295.4
R^{max}(MW)	0.0	3.3	14.9	27.8	31.7	39.0

Table 5.20: *Optimal capacities of PHS at buses 6 and 62 in 118-bus system*

Wind	20%		30%		40%	
Bus	6	62	6	62	6	62
B^{max}(MWh)	0.0	0.0	0.0	43.6	0.0	217.6
R^{max}(MW)	0.0	0.0	0.0	8.4	0.0	35.7

At 20% wind penetration, only 1 CAES with quite small capacity is installed at bus 62. From 30%, 2 CAES are installed, a smaller one at bus 6 and a larger one at bus 62. Since installed capacities of wind farms are the same at both buses, higher load at bus 62 can possibly result in higher capacity of the CAES at this bus. There is only 1 ESS of PHS technology installed at bus 62, with smaller capacities than those of CAES. Similar to simulation results in the 39-bus system above, when wind penetration level is increased, the model also installs higher capacities of the storage devices for both buses. This indicates that a higher penetration of wind results in more surplus wind power, making it more beneficial to deploy a larger storage device.

Yearly operational cost of the system is also provided in Table 5.21. The CAES gains a cost reduction of 0.07% at 20% wind penetration, 1.34% at 30% wind penetration and 1.62% at 40% wind penetration while the PHS yields 0.09% cost reduction at 30% wind penetration and 1.22% at 40% wind penetration, with respect to the operational cost in the case without ESSs installation.

Table 5.21: *Operational cost of 118-bus system with and without ESS [M€/year]*

Wind	20%	30%	40%
No ESS	995.24	955.43	920.89
CAES	994.54	942.63	905.97
PHS	995.24	954.57	909.66

The tests are implemented in GAMS on a PC with Intel Core i7 - 3.4 GHz CPU and 8.0 GB of memory, using IPOPT solver with an optimality gap of 0.5%. The direct method, which is the deterministic equivalence of stochastic programming model, is adopted to solve the problem. Computation time for the 39-bus system, which has a total of 137522 variables, 123150 equality constraints and 36720 inequality constraints, is 19 minutes. The 118-bus system, consisting of 516244 variables, 437820 equality constraints and 139680 inequality constraints, requires 28 minutes. Tests are also performed on a reduced model by removing the constraints on branch current limit, i.e. constraints (5.54) - (5.55), for branches with current flow less than 70% of the branch limit. The size of the model is thus reduced considerably and the computation time is also significantly less than that of the full model. In particular, computation time of the 39-bus system is reduced from 19 minutes to only 2 minutes and for the 118-bus system, it is reduced from 28 minutes to 6 minutes.

5.7.6 Comparison of both approaches

In this part, tests on both approaches, combined GA and cumulant-based POPF and two-stage stochastic programming approach, are carried out with modified IEEE 14-bus system (in Section 5.7.1.1), and comparison is made for solutions of both approaches. Wind data at the only wind farm present are taken from 3-year historical data as those described in Section 5.4.1 and scaled up to an installed capacity of 350 MW (see Fig. 5.39), accounting for 47.8% of wind penetration, while 3-year load data, for the sake of simplicity, are assumed to have a normal distribution with a standard deviation of 10% (see Fig. 5.40). 3-year wind and load data are clustered and representative scenarios of wind and load are obtained as described in Section 5.5.1.1. The resulting clusters and representative scenarios of wind and load data as input of the two-stage stochastic model are shown in figures 5.41 and 5.42.

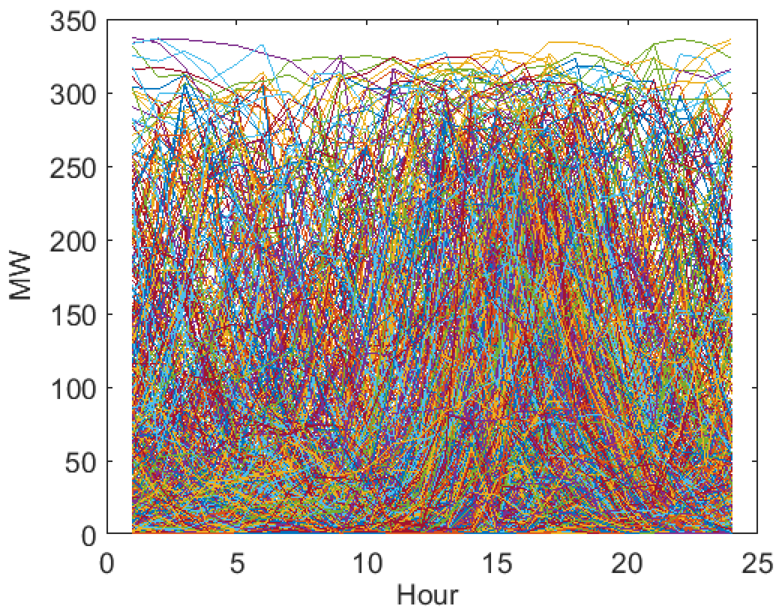

Figure 5.39: *Wind power data*

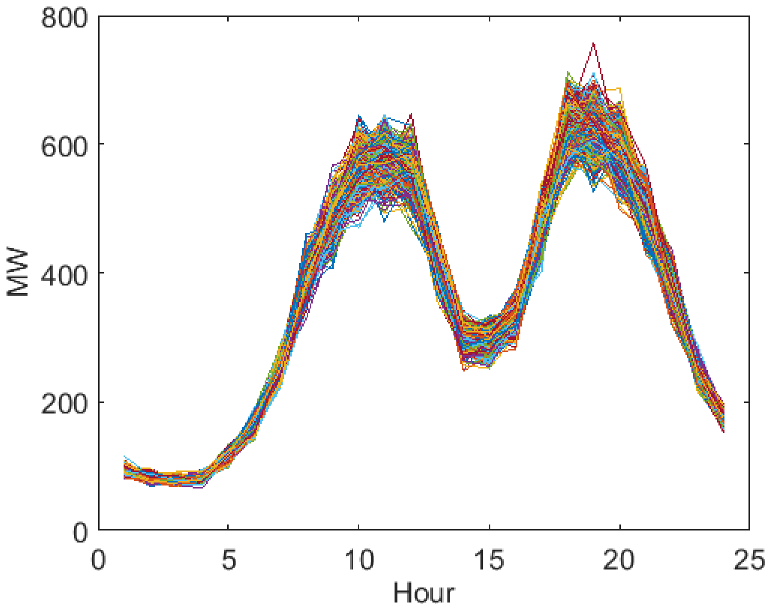

Figure 5.40: *Load data*

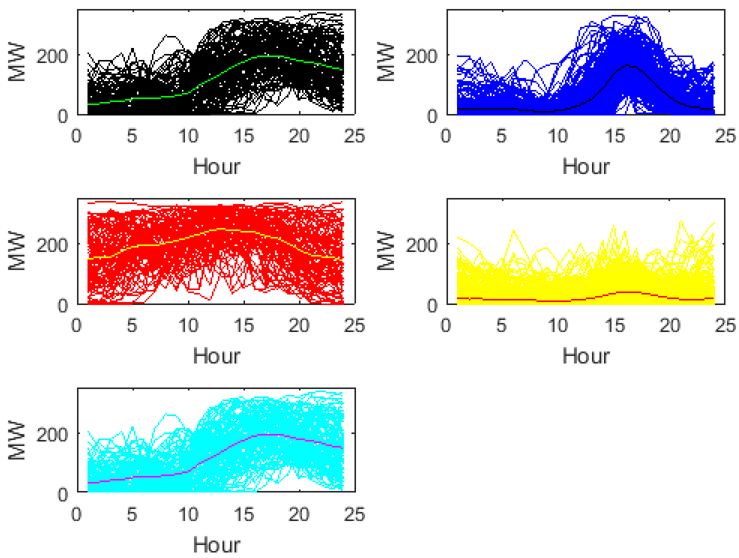

Figure 5.41: *Wind clusters with representative scenarios*

Tests are performed following the final procedure presented in Section 5.6. Specifically, a base case deterministic multi-period OPF is run first and the parameter df_i is determined. The best candidate buses for ESS installation are then identified based on values of df_i, which include buses 14, 10, 9, 13 and 7. These candidate buses are used as the search space for GA, instead of all 14 buses, in the combined GA and cumulant-based probabilistic approach. In the two-stage stochastic approach, 5 ESSs are allowed to be installed at these 5 candidate locations.

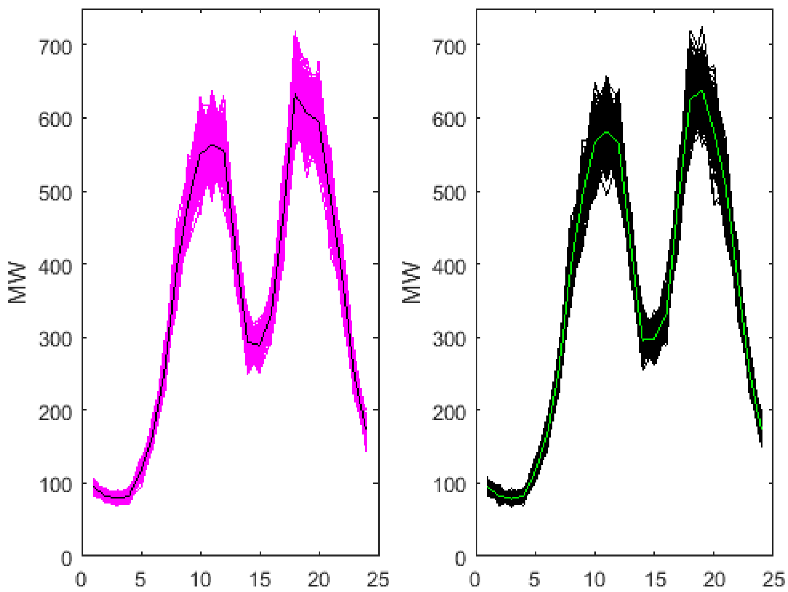

Figure 5.42: *Load clusters with representative scenarios*

From computation point of view, computing time in the combined GA and cumulant-based approach lies mainly in the GA part, which depends on the search space for optimal location. Thus, larger systems will result in higher computing time. In this case, preliminary identification of candidate ESS locations can help to significantly reduce the search space for GA and subsequently reduce computing time. Computing time in the two-stage stochastic approach also depends on the size of the system. The determination of candidate buses for ESS installation helps to identify locations for installing ESSs before determining their capacities. This also means the size of the system is reduced if locations of the ESSs have to be decided along with their capacities, since otherwise the ESSs could be installed in all buses.

Solutions obtained in both approaches are shown in tables 5.22 and 5.23, which are very different. This is not completely surprising, as the methodologies and the objective functions are actually different. The first difference is the number of ESSs selected. The combined GA and cumulant-based probabilistic approach decides to install only 1 ESS at the best candidate bus, i.e., bus 14 while in the two-stage stochastic approach, 2 ESSs out of 5 are used: a bigger one at bus 14 and a smaller one at bus 10 (optimal values of capacities of 3 ESSs installed at the remaining candidate buses are all zeros). The second difference is in the optimal capacities of the ESSs. Capacity of the ESS, installed at bus 14, in the first approach, is much smaller than ESS capacity at bus 14 in the second one. This difference is understandable since at this point, solution of the combined GA and cummulant-based approach is based on GA combined with a deterministic OPF, using expected wind and load data. In solution of the two-stage stochastic approach, on the contrary, wind and load uncertainties are already taken into account, i.e., using wind and load scenarios. This demonstrates that capacities of the ESSs, in case uncertainty is not included, are noticeably smaller than those in case uncertainty is taken into account, i.e., 12.8 MW and 38.2 MWh (in Table 5.22) compared to a total of 55.4 MW and 249.6 MWh (in Table 5.23).

Table 5.22: *Locations and expected value of ESS capacities in GA + cumulant-based approach*

Bus	$B^{max}[MWh]$	$R^{max}[MW]$
14	38.2	12.8

Table 5.23: *ESS capacities in two-stage stochastic approach*

Bus	$B^{max}[MWh]$	$R^{max}[MW]$
14	198.6	43.4
10	51.0	12.0
9	0.0	0.0
13	0.0	0.0
7	0.0	0.0

Now, the probabilistic part of the combined GA and cumulant-based probabilistic approach is carried out. CDFs of ESS capacities are shown in figures 5.43 and 5.44.

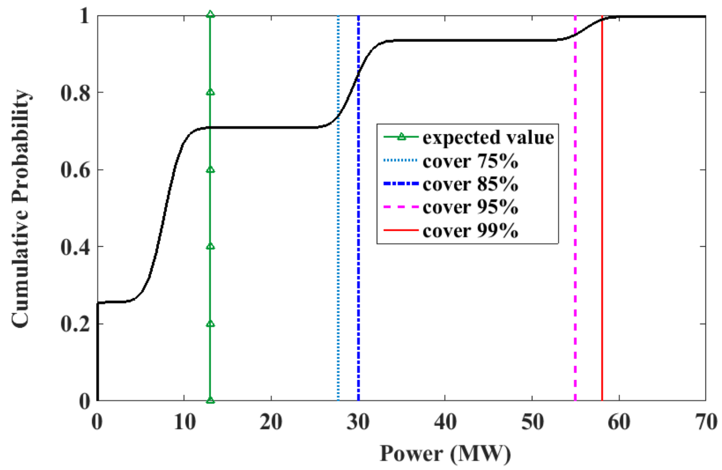

Figure 5.43: *CDF of ESS power capacity*

As noticed from these figures, with the expected value of ESS power capacity (in Table 5.22), only approximately 70% of wind and load uncertainties is covered and with the expected value of ESS energy capacity, only about 60% of the uncertainty is covered. In order to cover 100%, 99%, 95%, 85% and 75% of the uncertainty, power capacity of the ESS should be respectively 86.8 MW, 58 MW, 54.9 MW, 30 MW and 27.7 MW. Similarly, to cover 100%, 99%, 95%, 85% and 75% of the uncertainty, energy capacity of the ESS has to be 195.5 MWh, 175.2 MWh, 106.9 MWh, 99.3 MWh and 91.7 MWh, respectively. This approach results in a higher power capacity and smaller energy capacity of the ESS compared to total capacities optimal for the two-stage stochastic programming approach. For example, in this approach,

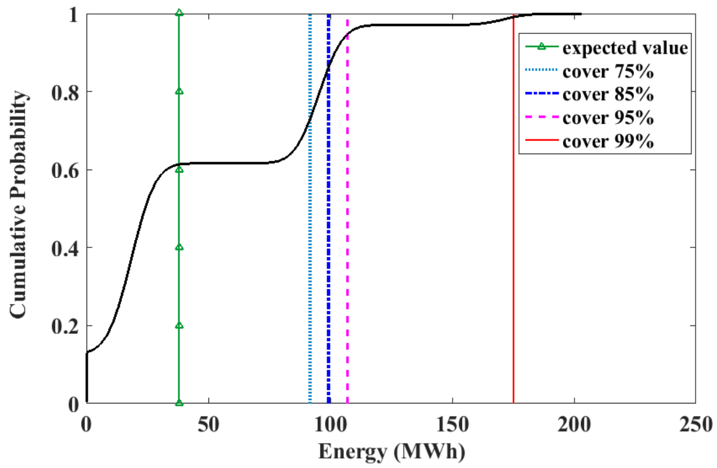

Figure 5.44: *CDF of ESS energy capacity*

capacities of the ESS in case 100% of uncertainty is covered are 86.8 MW and 195.5 MWh while in the other approach, total capacities of the ESSs are 55.4 MW and 249.6 MWh.

To examine operational costs of the system in both configurations, further simulation is performed by installing the ESS capacities and locations obtained above and running the OPF model with all 3-year wind and load data. The resulting operational costs and curtailed wind energy of 3-year operation and fixed costs of each case are shown in Table 5.24. As observed

Table 5.24: *Costs and amounts of curtailed wind energy in 3 year operation of the system with the obtained capacities and locations of the ESSs*

Approach	Bus	B^{max} [MWh]	R^{max} [MW]	Operational cost [M€]	Fixed cost [M€]	Curtailed wind [MWh]
Two-stage stochastic	14	198.6	43.4	639	10.07	2.71e+4
	10	51.0	12.0			
Combined GA and cumulant based POPF	14	38.2	12.8	642	1.71	6.29e+4
		expected value				
	14	99.3	30.0	641	4.31	4.83e+4
		cover 85%				
	14	106.9	54.9	640	5.51	4.50e+4
		cover 95%				
	14	195.5	86.8	639	9.56	2.88e+4
		cover 100%				

from this table, basically, the two-stage stochastic approach yields the same operational cost (the first row in the table) as the combined GA and cumulant-based POPF approach with 100% of uncertainty covering (the last row in the table). The amount of wind energy to be curtailed in the first approach is slightly lower than that in the second one, i.e., 2.71e+4 MWh compared to 2.88e+4 MWh whereas the fixed cost is a little bit higher, i.e., 10.07 M€ compared to 9.56 M€. Accordingly, if decision makers prefer a solution with a lower amount of wind curtailment, the two-stage stochastic approach can be an option. On the contrary, if a solution with lower capital cost is preferred, the combined GA and cumulant-based POPF approach can be adopted. Moreover, if decision makers want to further reduce the capital cost with some acceptable amount of wind curtailment, they can choose different levels of uncertainty covering in the solution of the combined GA and cumulant-based POPF approach. In general, the two-stage stochastic approach provides only one optimal solution while the combined GA and cumulant-based POPF approach provides a more flexible one, which allows decision makers to choose according to their desire.

Computing time for both approaches are shown in Fig. 5.45. In this figure, computing time in case there are candidate buses identified (Case 1) is shown along with the time when there is no candidate bus (Case 2), i.e., the search space of GA in the combined GA and POPF approach includes all 14 buses and in the two-stage stochastic approach, ESSs are installed at all buses. Obviously, with candidate buses preliminarily determined, computing time for both approaches are considerably reduced. In this case, time for the combined GA and POPF approach is lightly smaller than that of the two-stage stochastic approach.

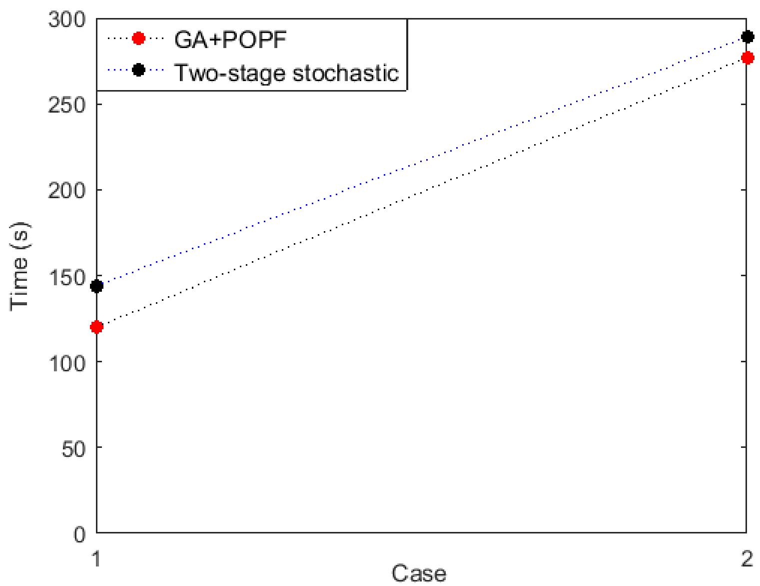

Figure 5.45: *Computing time for both approaches*

In Fig. 5.46, computing time of the two-stage stochastic programming approach with different numbers of scenarios of input random parameters are shown. Clearly, the higher the number of scenarios, the longer it takes to run the model. The time is not linearly increased with the number of scenarios but it is exponentially increased. Thus, scenario reduction is necessary to make this approach tractable.

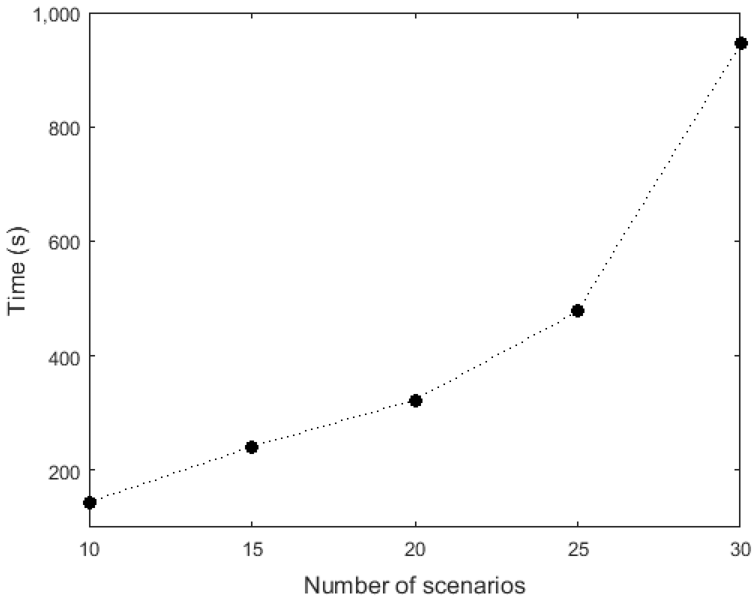

Figure 5.46: *Computing time of two-stage stochastic approach with different numbers of input scenarios*

5.8 Summary

This chapter presents methodologies and tests on the planning problems with ESSs. Two main approaches, i.e., combined GA and cumulant-based probabilistic approach and two-stage stochastic programming approach, are presented and discussed. In the cumulant-based probabilistic approach, the optimal capacities corresponding to average wind and load, and CDF of ESS power and energy content in each hour are obtained, which provides useful information for the operation of the ESSs. From this information, capacities of the ESSs can be determined by decision makers depending on the willingness to cover a certain level of uncertainty. This sizing approach can explicitly address system uncertainty while allowing a reasonable computation time. The stochastic approach, on the other hand, directly provides ESS capacities in the first stage (or planning stage) while considering all possible realizations of random parameters in the second stage (or operational stage). However, this approach is relatively computationally expensive and requires an efficient scenario reduction technique.

With the goal of reducing computational burden for ESS siting problems, the problem of selecting the best location for ESS installation is faced in Section 5.7.3. The sensitivities necessary to identify the buses, in case of installation of ESSs, allows the maximum benefit for power systems from several points of view: the minimum overall cost, the minimum curtailment of wind power (that could also lead to minimum CO_2 emissions), the maximum mitigation of congestions, and the maximum benefit, in terms of energy process.

The final procedure for ESS planning under uncertainties has also been summarized. An initial and necessary step is to preliminarily select candidate locations for ESS installation. This helps significantly reduce computing time in both developed approaches for ESS planning.

An extensive comparison is made between both approaches. Generally, the two-stage stochastic approach yields one optimal solution while the other approach results in a range of solutions for decision makers to choose. In solution of the two-stage stochastic approach, the fixed cost is higher while the amount of wind curtailment is slightly lower as compared to that in the solution of the combined GA and cumulant-based POPF approach with 100% of uncertainty covering.

CHAPTER 6

Conclusions and Future Work

6.1 Conclusions

In this thesis, the planning problems with ESSs to face uncertainties are investigated. A multi-period deterministic AC OPF model is formulated to incorporate ESSs and wind generation. The ESSs are employed for time-shifting wind generation, thus increases the value of wind energy and reduces wind curtailment. This multi-period formulation allows to take into account inter-temporal constraints of the ESSs. In addition, the AC OPF formulation can capture realistic physical power flows of the system better than the DC one. It is also much more accurate and reliable when issues such as congestion and voltage constraints are concerned. Two approaches are proposed for optimal planning of ESSs considering wind and load uncertainties, i.e., combined GA and cumulant-based POPF approach and two-stage stochastic programming approach. A methodology to define candidate buses for ESS installation is also proposed. A sensitivity analysis is then carried out to assess the impacts of ESS locations on system operation.

The AC OPF problem with ESSs and wind integration is formulated into single-period model and operation of the ESSs in both models, single-period and multi-period, are compared. Theoretically, multi-period model is a more suitable approach to deal with storage devices. From the tests carried out, multi-period model is shown to provide more economically optimal solution over single-period one in terms of production cost and amount of wind curtailment. Moreover, in single-period model, ESSs are only operated based on variations of wind power while in multi-period model, it is operated based on both wind and LMP variations. Therefore, the multi-period formulation is applied for planning problems with ESSs in this research.

In order to incorporate wind and load uncertainties into the planning of ESSs, an approach which combines GA and cumulant-based POPF is first proposed. In this approach, optimal placement and sizing of ESSs is implemented in two steps: in the first step, optimal ESS location and the expected value of ESS capacities are determined by GA and deterministic multi-period AC OPF with the goal of minimizing ESS investment cost and total expected generation cost while maximizing the generation of wind and storage; in the second step, probabilistic assessment is carried out on the obtained ESS locations and capacities. Probability distributions of ESS power and energy capacities are obtained, which can be used by decision makers to finally choose the size of ESSs to be installed. This approach, specifically the cumulant-based POPF approach, represents uncertain system inputs with probability distributions, but it retains the deterministic formulation of the OPF. Thus, the expected value of control variables is not influenced by the randomness of uncertain system inputs, but only the probability distributions of control variables are determined by them. Test results show that system uncertainty can be effectively captured in this approach with a reasonable computing time.

Another approach, namely two-stage stochastic programming, is developed for optimal sizing of ESSs. Wind and load scenarios as input of the problem are clustered and reduced into smaller sets of wind and load scenarios by adopting PCA-guided search for K-means clustering technique. This approach not only treats system inputs as random variables but also establishes stochastic formulation for the problem. Therefore, the uncertainty of random parameter inputs directly influences the optimization result. Test results show that this approach can explicitly incorporate wind and load uncertainties in the optimal sizing of ESSs.

A methodology to define the best candidate buses for ESS installation is also proposed in this research. The identification of candidate buses is performed based on the Lagrangian multiplier, which represents the variation of total production cost with respect to the variation of real injected power at a bus. A sensitivity analysis is performed, using this methodology, to assess the impacts of ESS locations on system operation. Two different applications of the ESSs are investigated, i.e., time-shifting wind generation to meet demand and mitigating transmission congestion to avoid wind curtailment and allow an efficient utilization of transmission capacity. Results show that installing ESSs at the best candidate buses allows the maximum benefit for power systems from several points of view: the minimum overall cost, the minimum curtailment of wind power (that could also lead to minimum CO_2 emissions), the maximum mitigation of congestions, and the maximum benefit, in terms of energy process.

Finally, a procedure for optimal siting and sizing of ESSs under uncertainty is proposed. First, to reduce computation burden for the planning problem, it is necessary to preliminarily identify candidate locations for the ESSs. Next, to take into account wind and load uncertainties in ESS planning, either the combined GA and POPF approach or two-stage stochastic programming approach, can be applied. At the output of the combined GA and POPF approach, ESS locations and probability distributions of ESS power and energy capacity are provided. Output of the two-stage stochastic programming approach provides an optimal ESS power and energy capacity.

Tests are performed on IEEE 14-bus system following the proposed final procedure: they show that the identification of candidate buses significantly reduce computing time for the siting of ESSs in both approach, i.e., the combined GA and cumulant-based POPF and the two-stage stochastic approach. In the first approach, it helps to reduce the search space for GA while in the second approach, it helps to identify locations for the ESSs before determining their capacities. Results are encouraging for both approaches and their comparison is presented and discussed in the thesis.

6.2 Future Work

A number of interesting and promising research topics arising from this work is as follows:

- **Incorporating uncertainty into the siting step of the combined GA and cumulant-based POPF approach**
  At this point, the siting of ESS in this approach is determined by GA based on a deterministic OPF. The POPF is performed afterwards for the sizing only. Thus, to explicitly address uncertainty in the planning of ESSs, it is necessary to consider uncertainty in the siting step as well.

- **Applying robust optimization approach for the planning of ESSs**
  Information on stochastic input data is not always available. It is, therefore, difficult to model uncertainty by employing PDFs. In this case, robust optimization, which becomes attractive to many researchers in recent years, can be a promising optimization technique to deal with uncertainty.

- **Dealing with different applications of ESSs**
  For wind generation applications, ESSs are not only employed to time-shift wind energy, but also used for a variety of other applications such as forecast hedging, frequency support, energy arbitrage, etc. This work can be extended to investigate on these applications of ESSs with wind generation.

- **Including technology selection into the planning problem**
  There are many different ESS technologies that can be employed for applications with wind. It is necessary to choose the right technology of ESSs before determining their locations and sizes. This can be an extension of the work in this thesis.

- **Applying the proposed approaches for large systems**
  The main challenge for planning problems with large systems lies in the tractability and computing time. This work can also be applied for optimal planning of ESSs in large systems. Such a large-scale problem should involve efficient techniques to reduce problem size, thus make it tractable.

- **Investigating on ESS operation**
  The focus of this thesis is on the planning of ESSs, which is carried out based on their optimal operation. Therefore, a direct extension of this work is incorporating uncertainty into the operation of ESSs.

APPENDIX A

ESS Cost and Technology Description

Table A.1: *Characteristics of bulk energy storage technologies used in cost analysis [15, 107, 108]*

Technology	Power Subsystem Cost ($/kW)	Energy Storage Subsystem Cost ($/kWh)	Efficiency (AC to DC)	Replacement Cost ($/kWh)	Replacement Frequency (year)	Fixed O&M ($/kW-year)
Lead-acid Batteries (Flooded Cell)	400	330	0.85	150	6	15
Lead-acid Batteries (VRLA)	400	330	0.85	200	5	5
Ni/Cd	600	125	0.65	600	10	5
Regenesys	100	275	0.65	150	10	15
High Temp Na/S	250	150	0.7	230	10	20
Compressed Air Energy Storage (CAES)	700	5	0.79	0	None	2.5
Pumped Hydro	1000	14	0.87	0	None	2.5
Pumped Hydro Variable Speed	1000	14	0.87	0	None	2.5

Table A.2: *Energy storage technologies suitable for wind power integration [7]*

Technology	Advantages	Disadvantages	Manufacturers
Vented Lead-Acid Batteries (Default)	Mature and well-known Low initial cost Long calendar life	Short cycle life Relatively intolerant of temperature extremes	Enersys GNB (Exide)
Valve-Regulated Lead-Acid	Low maintenance Low initial cost	Intolerant of temperature extremes Short cycle and calendar life	C&D Technologies Hawker Energy (Enersys)
Vented Nickel-Cadmium	Mature and well-known Long life Relatively intolerant to temperature extremes	Low cell voltage Float effect makes capacity testing difficult	Saft
Vanadium Redox (VRB)	Relatively high efficiency Power and energy rating are independent	Not yet proven for cycle life or maintenance costs High initial cost (at present)	VRB Power Systems
Compressed Air Energy Storage (CAES)	Mature technology High efficiency Long life Low cost for large scale	Requires suitable site geology May have ramp rate limit Large scale requires large capital investment and collaborations	Alstom Dresser-Rand Suizer
Pumped Hydro	Mature technology High efficiency Long life Low cost for large scale Power and energy independent	Requires suitable site geology Difficult environmental issues Large scale requires large capital investment and collaborations	Gugler GmbH Suizer North American Hydro Water Alchemy Harris
Sodium sulfur batteries (NAS)	High energy density High efficiency Long cycle and calendar life	Relatively new and untested High initial cost (at present)	NGK Insulator
Zinc-bromine batteries	High energy density Flat voltage profile	Relatively unknown and untested Many require occasional stripping cycles High initial cost (at present)	ZBB Energy
Superconducting Magnetic Energy Storage (SMES)	High power density High cycle life	Very high initial cost (at present) Low energy density	American Superconductor
Ultracapacitors	High power density High cycle life	High initial cost (at present) Low energy density	Maxwell NESS Capacitor ESMA
Flywheels	High power density High cycle life	Relatively high initial cost per kWh Low energy density	Active Power Beacon Piller
Regenerative	Hydrogen production	Short life (at present) Poor storage density Poor efficiency	

Bibliography

[1] International Energy Agency, Paris, France, *Energy technology perspectives 2010 - scenarios and strategies to 2050*, `https://www.iea.org/publications/freepublications/publication/etp2010.pdf`, 2010 (cit. on p. i).

[2] International Renewable Energy Agency (IRENA), *Rethinking energy: Towards a new power system*, `http://www.irena.org/rethinking/rethinking_fullreport_web.pdf`, 2014 (cit. on p. 1).

[3] Electric Power Research Institute (EPRI), Palo Alto, CA, and the US Department of Energy, Washington, DC, EPRI-DOE *handbook supplement of energy storage for grid connected wind generation applications*, `http://www.epri.com/abstracts/Pages/ProductAbstract.aspx?ProductId=000000000001008703`, 2004 (cit. on pp. 1, 3, 4, 23).

[4] The European Wind Energy Association (EWEA), *Large scale integration of wind energy in the euroupean power supply: Analysis, issues and recommendations*, `http://www.uwig.org/eweastudy/051215_grid_report.pdf`, 2005 (cit. on p. 2).

[5] DG ENER Working Paper, *The future role and challenges of Energy Storage*, `https://ec.europa.eu/energy/sites/ener/files/energy_storage.pdf`, Accessed: 2016-08-04 (cit. on p. 3).

[6] International Electrotechnical Commission (IEC), *Electrical energy storage*, `http://www.iec.ch/whitepaper/pdf/iecWP-energystorage-LR-en.pdf`, 2011 (cit. on pp. 3, 10).

[7] Electric Power Research Institute (EPRI), *Wind power integration: Energy storage for firming and shaping*, `http://www.epri.com/abstracts/Pages/ProductAbstract.aspx?ProductId=000000000001008388`, 2005 (cit. on pp. 4, 10–16, 23, 24, 122).

[8] A. F. Zobaa, *Energy storage - technologies and applications*. InTech, 2013 (cit. on pp. 5, 13–15, 18, 19, 21).

[9] National Renewable Energy Laboratory (NREL), *The role of energy storage with renewable electricity generation*, `http://www.nrel.gov/docs/fy10osti/47187.pdf`, 2010 (cit. on pp. 9, 12).

[10] H. Zhao, Q. Wu, S. Hu, H. Xu, and C. N. Rasmussen, "Review of energy storage system for wind power integration support," *Applied Energy*, vol. 137, pp. 545 –553, 2015, ISSN: 0306-2619. DOI: `http://dx.doi.org/10.1016/j.apenergy.2014.04.103`. [Online]. Available: `http://www.sciencedirect.com/science/article/pii/S0306261914004668` (cit. on pp. 10, 12, 18, 20, 21).

[11] C. Brivio, S. Mandelli, and M. Merlo, "Battery energy storage system for primary control reserve and energy arbitrage," *Sustainable Energy, Grids and Networks*, vol. 6, pp. 152 –165, 2016, ISSN: 2352-4677. DOI: `http://dx.doi.org/10.1016/j.segan.2016.03.004`. [Online]. Available: `http://www.sciencedirect.com/science/article/pii/S2352467716300017` (cit. on p. 12).

[12] Ecofys, *Energy storage opportunities and challenges - a west coast perspective white paper*, `http://www.ecofys.com/files/files/ecofys-2014-energy-storage-white-paper.pdf`, 2014 (cit. on pp. 12, 18, 21–25).

[13] State Utility Forecasting Group, *Utility scale energy storage systems - benefits, applications, and technologies*, `http://assets.fiercemarkets.net/public/sites/energy/reports/batterystoragereport.pdf`, 2013 (cit. on pp. 13, 14, 16).

[14] Sandia National Laboratories, *Energy storage for the electricity grid: Benefits and market potential assessment guide*, `http://www.sandia.gov/ess/publications/SAND2010-0815.pdf`, 2010 (cit. on p. 13).

[15] Sandia National Laboratories, Albuquerque, NewMexico 87185 and Livermore, California, *Characteristics and technologies for long-vs. short-term energy storage*, `http://prod.sandia.gov/techlib/access-control.cgi/2001/010765.pdf`, 2001 (cit. on pp. 14, 16, 101, 105, 121).

[16] Service BEAMS groupe Energie, Faculte des Sciences Appliquees, Universite Libre de Bruxelles, *Energy storage technologies for wind power integration*, 2010 (cit. on pp. 16, 20–22).

[17] Solar Magazine, *Energy Storage and Solar Power*, http://www.solarserver.com/solar-magazine/solar-report/solar-report/energy-storage-and-solar-power.html (cit. on p. 17).

[18] BRUSH, *Compressed Air Energy Storage (CAES)*, http://www.brush.eu/en/31/BRUSH-Group/Markets/Renewables/Compressed-Air-Energy-Storage-CAES (cit. on p. 20).

[19] Sandia National Laboratories, Albuquerque, New Mexico 87185 and Livermore, California 94550, DOE/EPRI *electricity storage handbook in collaboration with* NRECA, http://www.sandia.gov/ess/publications/SAND2015-1002.pdf, 2013 (cit. on p. 25).

[20] Mary B. Cain, Richard P. O'Neill and Anya Castillo, *History of optimal power flow and formulations optimal power flow paper 1*, http://www.ferc.gov/industries/electric/indus-act/market-planning/opf-papers/acopf-1-history-formulation-testing.pdf (cit. on p. 27).

[21] S. Frank, I. Steponavice, and S. Rebennack, "Optimal power flow: A bibliographic survey I - formulations and deterministic methods," *Energy Systems*, vol. 3, no. 3, pp. 221 –258, 2012 (cit. on p. 28).

[22] A. Castillo and D. F. Gayme, "Profit maximizing storage allocation in power grids," in 52^{nd} *IEEE Conference on Decision and Control*, 2013, pp. 429–435. DOI: 10.1109/CDC.2013.6759919 (cit. on pp. 33, 88).

[23] T. Wu, Z. Alaywan, and A. D. Papalexopoulos, "Locational marginal price calculations using the distributed-slack power-flow formulation," *IEEE Transactions on Power Systems*, vol. 20, no. 2, pp. 1188–1190, 2005, ISSN: 0885-8950. DOI: 10.1109/TPWRS.2005.846156 (cit. on p. 34).

[24] C. E. Murillo-Sánchez, R. D. Zimmerman, C. L. Anderson, and R. J. Thomas, "Secure planning and operations of systems with stochastic sources, energy storage, and active demand," *IEEE Transactions on Smart Grid*, vol. 4, no. 4, pp. 2220–2229, 2013, ISSN: 1949-3053. DOI: 10.1109/TSG.2013.2281001 (cit. on p. 36).

[25] M. Milligan, P. Donohoo, and M. OḾalley, "Stochastic methods for planning and operating power systems with large amounts of wind and solar power," in 11^{th} *Annual International Workshop on Large-Scale Integration of Wind Power into Power Systems as well as on Transmission Networks for Offshore Wind Power Plants*, 2012. [Online]. Available: http://www.ourenergypolicy.org/wp-content/uploads/2012/09/56208.pdf (cit. on p. 36).

[26] C. Skar, G. Doorman, and A. Tomasgard, "Large-scale power system planning using enhanced Benders decomposition," in *Power Systems Computation Conference (PSCC)*, 2014, pp. 1–7. DOI: 10.1109/PSCC.2014.7038297 (cit. on p. 37).

[27] L. Roald, M. Vrakopoulou, F. Oldewurtel, and G. Andersson, "Risk-constrained optimal power flow with probabilistic guarantees," in *Power Systems Computation Conference (PSCC)*, 2014, pp. 1–7. DOI: 10.1109/PSCC.2014.7038342 (cit. on p. 37).

[28] I. A. Sajjad, G. Chicco, and R. Napoli, "A probabilistic approach to study the load variations in aggregated residential load patterns," in *Power Systems Computation Conference (PSCC)*, 2014, pp. 1–7. DOI: 10.1109/PSCC.2014.7038105 (cit. on p. 37).

[29] R. Wiget, M. Vrakopoulou, and G. Andersson, "Probabilistic security constrained optimal power flow for a mixed HVAC and HVDC grid with stochastic infeed," in *Power Systems Computation Conference (PSCC)*, 2014, pp. 1–7. DOI: 10.1109/PSCC.2014.7038408 (cit. on p. 37).

[30] W. C. Conceição, T. P. Ramos, A. L. M. Marcato, J. A. P. Filho, R. B. da Silva Brandi, and P. A.M. S. David, "Stochastic dynamic programming with discretization of energy interchange between hydrothermal systems in the operation planning problem," in *Power Systems Computation Conference (PSCC)*, 2014, pp. 1–7. DOI: 10.1109/PSCC.2014.7038351 (cit. on p. 37).

[31] Q. Lambert, C. Sandels, and L. Nordström, "Stochastic evaluation of aggregator business models - optimizing wind power integration in distribution networks," in *Power Systems Computation Conference (PSCC)*, 2014, pp. 1–8. DOI: 10.1109/PSCC.2014.7038104 (cit. on p. 37).

[32] T. Summers, J. Warrington, M. Morari, and J. Lygeros, "Stochastic optimal power flow based on convex approximations of chance constraints," in *Power Systems Computation Conference (PSCC)*, 2014, pp. 1–7. DOI: 10.1109/PSCC.2014.7038376 (cit. on p. 37).

[33] M. Negnevitsky, N. Tomin, D. Panasetsky, N. Voropai, V. Kurbatsky, U. Hager, and C. Rehtanz, "Preventing large-scale blackouts in power systems under uncertainty," in *Power Systems Computation Conference (PSCC)*, 2014, pp. 1–7. DOI: 10.1109/PSCC.2014.7038340 (cit. on p. 37).

[34] A. Moreira, A. Street, and J. M. Arroyo, "Energy and reserve scheduling under correlated nodal demand uncertainty: An adjustable robust optimization approach," in *Power Systems Computation Conference (PSCC)*, 2014, pp. 1–8. DOI: 10.1109/PSCC.2014.7038415 (cit. on p. 37).

[35] P. Panciatici, M. C. Campi, S. Garatti, S. H. Low, D. K. Molzahn, A. X. Sun, and L. Wehenkel, "Advanced optimization methods for power systems," in *Power Systems Computation Conference (PSCC)*, 2014, pp. 1–18. DOI: 10.1109/PSCC.2014.7038504 (cit. on p. 37).

[36] W. Zhang, Y. Xu, Z. Y. Dong, Y. Wang, and R. Zhang, "An efficient approach for robust SCOPF considering load and renewable power uncertainties," in *Power Systems Computation Conference (PSCC)*, 2016, pp. 1–7. DOI: 10.1109/PSCC.2016.7540823 (cit. on p. 37).

[37] F. M. Mele, Á Ortega, R. Zárate-Miñano, and F. Milano, "Impact of variability, uncertainty and frequency regulation on power system frequency distribution," in *Power Systems Computation Conference (PSCC)*, 2016, pp. 1–8. DOI: 10.1109/PSCC.2016.7540970 (cit. on p. 37).

[38] Y. Lin, J. L. Mathieu, and J. X. Johnson, "Stochastic optimal power flow formulation to achieve emissions objectives with energy storage," in *Power Systems Computation Conference (PSCC)*, 2016, pp. 1–7. DOI: 10.1109/PSCC.2016.7540817 (cit. on p. 37).

[39] M. E. P. Maceira, A. C. G. Melo, and M. P. Zimmermann, "Application of stochastic programming and probabilistic analyses as key parameters for real decision making regarding implementing or not energy rationing - a case study for the Brazilian hydrothermal interconnected system," in *Power Systems Computation Conference (PSCC)*, 2016, pp. 1–7. DOI: 10.1109/PSCC.2016.7541014 (cit. on p. 37).

[40] O. Mégel, G. Andersson, and J. L. Mathieu, "Reducing the computational effort of stochastic multi-period DC optimal power flow with storage," in *Power Systems Computation Conference (PSCC)*, 2016, pp. 1–7. DOI: 10.1109/PSCC.2016.7541033 (cit. on p. 37).

[41] G. G. Moshi, C. Bovo, A. Berizzi, and L. Taccari, "Optimization of integrated design and operation of microgrids under uncertainty," in *Power Systems Computation Conference (PSCC)*, 2016, pp. 1–7. DOI: 10.1109/PSCC.2016.7540870 (cit. on p. 37).

[42] S. Karagiannopoulos, A. Rigas, N. Hatziargyriou, G. Hug, and A. Oudalov, "Battery energy storage capacity fading and control strategies for deterministic and stochastic power profiles," in *Power Systems Computation Conference (PSCC)*, 2016, pp. 1–7. DOI: 10.1109/PSCC.2016.7540956 (cit. on p. 37).

[43] A. Sauhats, R. Petrichenko, K. Baltputnis, Z. Broka, and R. Varfolomejeva, "A multi-objective stochastic approach to hydroelectric power generation scheduling," in *Power Systems Computation Conference (PSCC)*, 2016, pp. 1–7. DOI: 10.1109/PSCC.2016.7540821 (cit. on p. 37).

[44] J. E. R. Baptista, A. B. Rodrigues, and M. d. G. da Silva, "Two probabilistic methods for voltage sag estimation in distribution systems," in *Power Systems Computation Conference (PSCC)*, 2016, pp. 1–7. DOI: 10.1109/PSCC.2016.7540905 (cit. on p. 37).

[45] M. Sun, I. Konstantelos, S. Tindemans, and G. Strbac, "Evaluating composite approaches to modelling high-dimensional stochastic variables in power systems," in *Power Systems Computation Conference (PSCC)*, 2016, pp. 1–8. DOI: 10.1109/PSCC.2016.7540837 (cit. on p. 37).

[46] Alberta Electric System Operator (AESO), *10 Min Historical Data for Total Wind Power and Alberta Internal Load*, http://www.aeso.ca/gridoperations/20544.html (cit. on pp. 37, 38, 71).

[47] J. Zhu, *Optimization of power system operation*. John Wiley & Sons, Inc., Hoboken, New Jersey, 2009 (cit. on pp. 38, 39).

[48] M. Kendall and A. Stuart, *The advanced theory of statistics*. London, U.K.: C. Griffin, 4th edition, 1977 (cit. on pp. 41, 42).

[49] W. D. Tian, D. Sutanto, Y. B. Lee, and H. R. Outhred, "Cumulant based probabilistic power system simulation using laguerre polynomials," *IEEE Transactions on Energy Conversion*, vol. 4, no. 4, pp. 567–574, 1989, ISSN: 0885-8969. DOI: 10.1109/60.41715 (cit. on p. 42).

[50] D. D. Le, *Impact of wind power penetration on power system security by a probabilistic approach*, PhD Dissertation, Department of Energy, Politecnico di Milano, 2013 (cit. on pp. 42, 45, 47).

[51] H. Cramer, *Mathematical methods of statistics*. Princeton University Press, 1945 (cit. on pp. 43, 44).

[52] P. McCullagh, *Tensor methods in statistics*. London, U.K.: Chapman & Hall, 1987 (cit. on p. 44).

[53] D. D. Le, N. T. A. Nguyen, V. D. Ngo, and A. Berizzi, "Advanced probabilistic power flow methodology for power systems with renewable resources," *Turk J Elec Eng & Comp Sci*, 2016. DOI: 10.3906/elk-1511-302 (cit. on pp. 45, 47).

[54] L. Sanabria and T. Dillon, "Stochastic power flow using cumulants and von mises functions," *International Journal of Electrical Power & Energy Systems*, vol. 8, no. 1, pp. 47 –60, 1986, ISSN: 0142-0615. DOI: http://dx.doi.org/10.1016/0142-0615(86)90025-6. [Online]. Available: http://www.sciencedirect.com/science/article/pii/0142061586900256 (cit. on pp. 45, 46).

[55] Z. Hu and X. Wang, "A probabilistic load flow method considering branch outages," *IEEE Transactions on Power Systems*, vol. 21, no. 2, pp. 507–514, 2006, ISSN: 0885-8950. DOI: 10.1109/TPWRS.2006.873118 (cit. on pp. 45, 48).

[56] R. V. Mises, *Mathematical theory of probability and statistics*. New York: Academic, 5th edition, 1964 (cit. on p. 45).

[57] P. Zhang and S. T. Lee, "Probabilistic load flow computation using the method of combined cumulants and Gram-Charlier expansion," *IEEE Transactions on Power Systems*, vol. 19, no. 1, pp. 676–682, 2004, ISSN: 0885-8950. DOI: `10.1109/TPWRS.2003.818743` (cit. on p. 47).

[58] G. Li and X. P. Zhang, "Comparison between two probabilistic load flow methods for reliability assessment," in *IEEE Power Energy Society General Meeting*, 2009, pp. 1–7. DOI: `10.1109/PES.2009.5275534` (cit. on p. 47).

[59] A. Schellenberg, W. Rosehart, and J. Aguado, "Cumulant-based probabilistic optimal power flow (P-OPF) with Gaussian and Gamma distributions," *IEEE Transactions on Power Systems*, vol. 20, no. 2, pp. 773–781, 2005, ISSN: 0885-8950. DOI: `10.1109/TPWRS.2005.846184` (cit. on pp. 48, 50).

[60] J. F. Lawless, *Truncated distributions - claims distributions - encyclopedia of actuarial science*. John Wiley & Sons, Ltd, 2004 (cit. on p. 50).

[61] F. Bastin, *Trust-region algorithms for nonlinear stochastic programming and mixed logit models*. Facultes Universitaires Notre-Dame De La Paix Namur - Faculte Des Sciences, 2004. [Online]. Available: `http://dial.uclouvain.be/pr/boreal/object/boreal:4153` (cit. on pp. 51, 53, 54).

[62] B. L. Gorissen, I. Yanikoglu, and D. den Hertog, "A practical guide to robust optimization," *Omega*, vol. 53, pp. 124 –137, 2015, ISSN: 0305-0483. DOI: `http://dx.doi.org/10.1016/j.omega.2014.12.006`. [Online]. Available: `http://www.sciencedirect.com/science/article/pii/S0305048314001698` (cit. on p. 51).

[63] G. Li and X. P. Zhang, "Stochastic optimal power flow approach considering correlated probabilistic load and wind farm generation," in *IET Conference on Reliability of Transmission and Distribution Networks (RTDN)*, 2011, pp. 1–7. DOI: `10.1049/cp.2011.0514` (cit. on p. 52).

[64] G. B. Dantzig, "Linear programming under uncertainty," *Management Science*, vol. 1, no. 3-4, pp. 197 –206, 1955. [Online]. Available: `http://prof.if.ktu.lt/~jonas.mockus/dantzig.pdf` (cit. on p. 52).

[65] A. Charnes and W. W. Cooper, "Chance-constrained programming," *Management Science*, vol. 6, no. 1, pp. 73 –79, 1959. [Online]. Available: `http://pubsonline.informs.org/doi/pdf/10.1287/mnsc.6.1.73` (cit. on p. 52).

[66] J. R. Birge and F. Louveaux, *Introduction to stochastic programming*. Springer, 2011 (cit. on p. 52).

[67] "Optimization under uncertainty: State-of-the-art and opportunities," *Computers & Chemical Engineering*, vol. 28, no. 6 - 7, pp. 971 –983, 2004 (cit. on p. 52).

[68] A. Shapiro, D. Dentcheva, and A. Ruszczynski, *Lectures on stochastic programming: Modeling and theory*. The society for Industrial, Applied Mathematics, and the Mathematical Programming Society, 2009 (cit. on p. 53).

[69] P. Popela, J. Novotny, J. Roupec, D. Hrabec, and A. Olstad, "Two stage stochastic programming for engineering problems," *Engineering Mechanics*, vol. 21, no. 5, pp. 335 –353, 2014. [Online]. Available: `http://www.engineeringmechanics.cz/pdf/21_5_335.pdf` (cit. on p. 55).

[70] Q. Xu, C. Ding, J. Liu, and B. Luo, "PCA-guided search for K-means," *Pattern Recognition Letters*, vol. 54, pp. 50 –55, 2015, ISSN: 0167-8655. DOI: `http://dx.doi.org/10.1016/j.patrec.2014.11.017`. [Online]. Available: `http://www.sciencedirect.com/science/article/pii/S0167865514003675` (cit. on pp. 56, 58).

[71] A. K. Jain, "Data clustering: 50 years beyond k-means," *Pattern Recognition Letters*, vol. 31, no. 8, pp. 651 –666, 2010, ISSN: 0167-8655. DOI: `http://dx.doi.org/10.1016/j.patrec.2009.09.011`. [Online]. Available: `http://www.sciencedirect.com/science/article/pii/S0167865509002323` (cit. on pp. 56, 57).

[72] I. T. Jolliffe, *Principal component analysis*. Springer, New York, 2002 (cit. on p. 56).

[73] H. Cho, Y. Goude, X. Brossat, and Q. Yao, "Modelling and forecasting daily electricity load curves: A hybrid approach," *Journal of the American Statistical Association*, vol. 108, no. 501, pp. 7 –21, 2013 (cit. on p. 57).

[74] Statistical tools for high-throughput data analysis (STHDA), *Determining the optimal number of clusters: 3 must known methods - Unsupervised Machine Learning*, `http://www.sthda.com/english/wiki/determining-the-optimal-number-of-clusters-3-must-known-methods-unsupervised-machine-learning` (cit. on p. 58).

[75] W. Z. Chen, Q. B. Li, L. Shi, Y. Luo, D. D. Zhan, N. Shi, and K. Liu, "Energy storage sizing for dispatchability of wind farm," in 11^{th} *International Conference on Environment and Electrical Engineering (EEEIC)*, 2012, pp. 382–387. DOI: `10.1109/EEEIC.2012.6221407` (cit. on p. 61).

[76] T. Boutsika and S. Santoso, "Sizing an energy storage system to minimize wind power imbalances from the hourly average," in *IEEE Power and Energy Society General Meeting*, 2012, pp. 1 –8. DOI: `10.1109/PESGM.2012.6345551` (cit. on p. 61).

[77] M. Khalid and A. V. Savkin, "Optimization and control of a distributed battery energy storage system for wind power smoothing," in 19^{th} *Mediterranean Conference on Control Automation (MED)*, 2011, pp. 39 –43. DOI: `10.1109/MED.2011.5983095` (cit. on p. 61).

[78] Z. Y. Gao, P. Wang, L. Bertling, and J. H. Wang, "Sizing of energy storage for power systems with wind farms based on reliability cost and wroth analysis," in *IEEE Power and Energy Society General Meeting*, 2011, pp. 1 –7. DOI: 10.1109/PES.2011.6039468 (cit. on p. 61).

[79] Y. V. Makarov, P. Du, M. C. W. Kintner-Meyer, C. Jin, and H. F. Illian, "Sizing energy storage to accommodate high penetration of variable energy resources," *IEEE Transactions on Sustainable Energy*, vol. 3, no. 1, pp. 34 –40, 2012. DOI: 10.1109/TSTE.2011.2164101 (cit. on p. 61).

[80] Y. M. Atwa and E. F. El-Saadany, "Optimal allocation of ess in distribution systems with a high penetration of wind energy," *IEEE Transactions on Power Systems*, vol. 25, no. 4, pp. 1815 –1822, 2010. DOI: 10.1109/TPWRS.2010.2045663 (cit. on p. 62).

[81] K. Dvijotham, M. Chertkov, and S. Backhaus, "Storage sizing and placement through operational and uncertainty-aware simulations," in 47^{th} *Hawaii International Conference on System Sciences*, 2014, pp. 2408 –2416. DOI: 10.1109/HICSS.2014.302 (cit. on p. 62).

[82] H. Pandzic, Y. Wang, T. Qiu, Y. Dvorkin, and D. S. Kirschen, "Near-optimal method for siting and sizing of distributed storage in a transmission network," *IEEE Transactions on Power Systems*, vol. 30, no. 5, pp. 2288 –2300, 2015. DOI: 10.1109/TPWRS.2014.2364257 (cit. on p. 62).

[83] H. T. Le and T. Q. Nguyen, "Sizing energy storage systems for wind power firming: An analytical approach and a cost-benefit analysis," in *IEEE Power and Energy Society General Meeting - Conversion and Delivery of Electrical Energy in the* 21^{st} *Century*, 2008, pp. 1 –8. DOI: 10.1109/PES.2008.4596223 (cit. on p. 62).

[84] S. Wogrin and D. F. Gayme, "Optimizing storage siting, sizing, and technology portfolios in transmission-constrained networks," *IEEE Transactions on Power Systems*, vol. 30, no. 6, pp. 3304 –3313, 2015. DOI: 10.1109/TPWRS.2014.2379931 (cit. on p. 62).

[85] H. Bludszuweit and J. A. Dominguez-Navarro, "A probabilistic method for energy storage sizing based on wind power forecast uncertainty," *IEEE Transactions on Power Systems*, vol. 26, no. 3, pp. 1651 –1658, 2011. DOI: 10.1109/TPWRS.2010.2089541 (cit. on p. 62).

[86] P. Pinson, G. Papaefthymiou, B. Klockl, and J. Verboomen, "Dynamic sizing of energy storage for hedging wind power forecast uncertainty," in *IEEE Power Energy Society General Meeting*, 2009, pp. 1 –8. DOI: 10.1109/PES.2009.5275816 (cit. on p. 62).

[87] L. Li and L. Yang, “A chance-constrained programming based energy storage system sizing model considering uncertainty of wind power,” in *International Conference on Sustainable Power Generation and Supply (SUPERGEN)*, 2012, pp. 1 –6. DOI: 10.1049/cp.2012.1772 (cit. on p. 62).

[88] X. Wang, M. Yue, E. Muljadi, and W. Gao, “Probabilistic approach for power capacity specification of wind energy storage systems,” *IEEE Transactions on Industry Applications*, vol. 50, no. 2, pp. 1215 –1224, 2014. DOI: 10.1109/TIA.2013.2272753 (cit. on p. 62).

[89] M. Ghofrani, A. Arabali, M. Etezadi-Amoli, and M. S. Fadali, “A framework for optimal placement of energy storage units within a power system with high wind penetration,” *IEEE Transactions on Sustainable Energy*, vol. 4, no. 2, pp. 434 –442, 2013. DOI: 10.1109/TSTE.2012.2227343 (cit. on p. 62).

[90] K. Baker, G. Hug, and X. Li, “Optimal storage sizing using two-stage stochastic optimization for intra-hourly dispatch,” in *North American Power Symposium (NAPS)*, 2014, pp. 1 –6. DOI: 10.1109/NAPS.2014.6965384 (cit. on pp. 62, 63).

[91] C. Abbey and G. Joos, “A stochastic optimization approach to rating of energy storage systems in wind-diesel isolated grids,” *IEEE Transactions on Power Systems*, vol. 24, no. 1, pp. 418 –426, 2009. DOI: 10.1109/TPWRS.2008.2004840 (cit. on pp. 62, 63).

[92] P. Xiong and C. Singh, “Optimal planning of storage in power systems integrated with wind power generation,” *IEEE Transactions on Sustainable Energy*, vol. 7, no. 1, pp. 232 –240, 2016. DOI: 10.1109/TSTE.2015.2482939 (cit. on pp. 62, 63).

[93] R. A. Jabr, I. Dzafic, and B. C. Pal, “Robust optimization of storage investment on transmission networks,” *IEEE Transactions on Power Systems*, vol. 30, no. 1, pp. 531 –539, 2015. DOI: 10.1109/TPWRS.2014.2326557 (cit. on pp. 62, 63).

[94] L. Semeraro, E. Crisostomi, A. Franco, A. Landi, M. Raugi, M. Tucci, and G. Giunta, “Electrical load clustering: The Italian case,” in *IEEE PES on Innovative Smart Grid Technologies Conference Europe (ISGT-Europe)*, 2014, pp. 1–6. DOI: 10.1109/ISGTEurope.2014.7028919 (cit. on p. 63).

[95] A. Fabbri, T. G. S. Roman, J. R. Abbad, and V. H. M. Quezada, “Assessment of the cost associated with wind generation prediction errors in a liberalized electricity market,” *IEEE Trans. Power Syst.*, vol. 20, no. 3, pp. 1440 –1446, 2005. DOI: 10.1109/TPWRS.2005.852148 (cit. on p. 63).

[96] C. S. Park, *Fundamentals of engineering economics*. Pearson Education, Inc., New Jersey, 2004 (cit. on p. 65).

[97] V. A. Evangelopoulos and P. S. Georgilakis, "Optimal distributed generation placement under uncertainties based on point estimate method embedded genetic algorithm," *IET Generation, Transmission and Distribution*, vol. 8, no. 3, pp. 389 –400, 2014. DOI: 10.1049/iet-gtd.2013.0442 (cit. on p. 66).

[98] G. Celli, E. Ghiani, S. Mocci, and F. Pilo, "A multiobjective evolutionary algorithm for the sizing and siting of distributed generation," *IEEE Transaction on Power Systems*, vol. 20, no. 2, pp. 750 –757, 2005. DOI: 10.1109/TPWRS.2005.846219 (cit. on p. 66).

[99] N. Yang and F. Wen, "A chance constrained programming approach to transmission system expansion planning," *Electric Power Systems Research*, vol. 75, no. 2 - 3, pp. 171 –177, 2005. DOI: http://dx.doi.org/10.1016/j.epsr.2005.02.002 (cit. on p. 66).

[100] A. G. Bakirtzis, P. N. Biskas, C. E. Zoumas, and V. Petridis, "Optimal power flow by enhanced genetic algorithm," *IEEE Transaction on Power Systems*, vol. 17, no. 2, pp. 229 –236, 2002. DOI: 10.1109/TPWRS.2002.1007886 (cit. on p. 66).

[101] M. Ghofrani, A. Arabali, M. Etezadi-Amoli, and M. Fadali, "Energy storage application for performance enhancement of wind integration," *IEEE Trans. Power Syst.*, vol. 28, no. 4, pp. 4803 –4811, 2013. DOI: 10.1109/TPWRS.2013.2274076 (cit. on p. 66).

[102] T. Numnonda and U. D. Annakkage, "Optimal power dispatch in multinode electricity market using genetic algorithm," *Electric Power Systems Research*, vol. 49, no. 3, pp. 211 –220, 1999. DOI: http://dx.doi.org/10.1016/S0378-7796(98)00139-4 (cit. on p. 67).

[103] A. M. S. Zalzala, *Genetic algorithms in engineering systems*. Technology & Engineering, 1997 (cit. on p. 67).

[104] University of Washington, *Power system test case archive*, https://www.ee.washington.edu/research/pstca (cit. on pp. 79–82).

[105] S. Dutta and R. Sharma, "Optimal storage sizing for integrating wind and load forecast uncertainties," in *IEEE PES Innovative Smart Grid Technologies (ISGT)*, 2012, pp. 1–7. DOI: 10.1109/ISGT.2012.6175721 (cit. on p. 80).

[106] A. Kumar and W. Gao, "Optimal distributed generation location using mixed integer non-linear programming in hybrid electricity markets," *Generation, Transmission Distribution, IET*, vol. 4, no. 2, pp. 281 –298, 2010. DOI: 10.1049/iet-gtd.2009.0026 (cit. on p. 88).

[107] Sandia National Laboratories, Albuquerque, NewMexico 87185 and Livermore, California, *Long- vs. short-term energy storage technologies analysis*, `http://prod.sandia.gov/techlib/access-control.cgi/2003/032783.pdf`, 2003 (cit. on pp. 105, 121).

[108] Sandia National Laboratories, Albuquerque, NewMexico 87185 and Livermore, California, *Energy storage systems cost update*, `http://prod.sandia.gov/techlib/access-control.cgi/2011/112730.pdf`, 2011 (cit. on pp. 105, 121).